JPRS L/10709

4 August 1982

USSR Report

PHYSICS AND MATHEMATICS

(FOUO 6/82)

FBIS FOREIGN BROADCAST INFORMATION SERVICE

FOR OFFICIAL USE ONLY

APPROVED FOR RELEASE: 2007/02/09: CIA-RDP82-00850R000500090006-1

NOTE

JPRS publications contain information primarily from foreign newspapers, periodicals and books, but also from news agency transmissions and broadcasts. Materials from foreign-language sources are translated; those from English-language sources are transcribed or reprinted, with the original phrasing and other characteristics retained.

Headlines, editorial reports, and material enclosed in brackets [] are supplied by JPRS. Processing indicators such as [Text] or [Excerpt] in the first line of each item, or following the last line of a brief, indicate how the original information was processed. Where no processing indicator is given, the information was summarized or extracted.

Unfamiliar names rendered phonetically or transliterated are enclosed in parentheses. Words or names preceded by a question mark and enclosed in parentheses were not clear in the original but have been supplied as appropriate in context. Other unattributed parenthetical notes within the body of an item originate with the source. Times within items are as given by source.

The contents of this publication in no way represent the policies, views or attitudes of the U.S. Government.

APPROVED FOR RELEASE: 2007/02/09: CIA-RDP82-00850R000500090006-1

JPRS L/10709

4 August 1982

USSR REPORT

PHYSICS AND MATHEMATICS

(FOUO 6/82)

CONTENTS

APPROVED FOR RELEASE: 2007/02/09: CIA-RDP82-00850R000500090006-1

LASERS AND MASERS

UDC 537.525

KINETICS OF CHEMICAL PROCESSES IN PLASMA OF MOLECULAR GAS-DISCHARGE LASERS

Moscow KHIMIYA VYSOKIKH ENERGIY in Russian Vol 16, No 3, May-Jun 82 (manuscript received 5 May 81) pp 267-272

[Article by V. I. Volchenok, V. N. Komarov, V. N. Ochkin and N. I. Sobolev, Scientific Research Physicochemical Institute imeni L. Ya. Karpov]

[Text] Molecular plasma systems are classified within the framework of simplified three-component plasmochemical kinetics from the viewpoint of their operating life. The classification is made according to the ratio of the rates of reversible and irreversible (homogeneous and heterogeneous) interactions. It is shown that the active media of molecular lasers (CO_2, CO and N_2O) investigated earlier can be described by this scheme. The role of catalysts in extending the lifetime of the systems is determined.

A low-temperature molecular plasma is now used to implement a wide range of processes. All the devices in which these processes are realized can be divided from the viewpoint of application into two main groups: 1) devices that utilize the plasma as an active medium of a chemical reactor, in which the initial materials are reprocessed; it is desirable that these devices guarantee high rates and degree of transformation of the initial materials to the required reaction products; and 2) devices that utilize the plasma as an object with retained properties, for example, in light sources or active media of electric-discharge lasers. In this case, unlike the first case, it is necessary that the concentration of initial (working) molecules be maintained at a level that exceeds some minimum concentration required for operation of the devices for as long a time as possible. We will consider the second case in the given paper. The most detailed investigations of chemical processes in a molecular plasma have now apparently been conducted for active media of continuous infrafred electric-discharge lasers (see, for example, survey [1]). It is feasible in this regard to attempt to classify the main types of these systems from the viewpoint of the chemical kinetics of the gas-phase and heterogeneous processes occurring in them.

If laser transitions occur on molecules A present in the initial working mixture of gases, then the dependence of their concentration on time (t) can be represented in the general case as

$$[A](t)=[A](t=0)/(t). \quad (1)$$

The form of function f(t) can be found from solving a system of nonlinear differential equations of the type of Pauli equations that describe the total kinetics of homogeneous and heterogeneous chemical processes with participation of all particles formed in the discharge at different energy states. However, solution or analysis of this system in general form is impossible. Therefore, the problem can be simplified for qualitative analysis and classification of the main cases. We will consider a plasma in which chemically different components A, B and C undergo mutual conversion and interact with the surface.

Let us also suggest that the presence of particles of other kinds in the plasma, including charged and excited particles, is taken into account by effective rate constants of reactions A, B and C and therefore the kinetics is formally described by first-order equations.

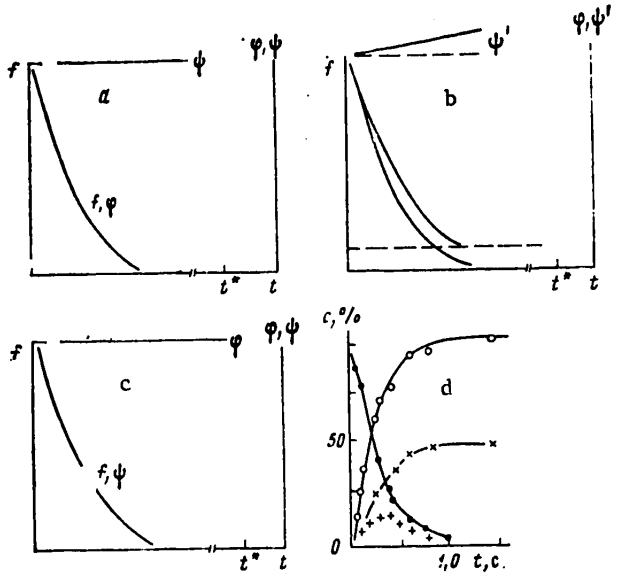

Figure 1. First Case of Classification of System (a-c) (see text): a--$r_A = 0$, $k_A^W = 0$; b--$r_A = 0$, $k_A^W = 0$, $k_A > k_A^W$; c--$r_A = 0$, $k_A = 0$. The dependence (d) of the concentration of N_2O, N_2, O_2 and NO molecules on the time the mixture is in the discharge, the initial N_2O-He mixture (1:4) at pressure of 0.532 kPa, current density of 31.8 A/m^2 and mass spectrometric measurements; ●--N_2O, O--N_2, X--O_2 and +--NO

If molecules A further break down in the plasma into particles B and C: $[A] = \alpha[B] + \beta[C]$ $(\alpha+\beta=1)$, then

$$[A] = -k_A[A]+k_B^A[B]+k_C^A[C]-k_A^W[A]+r_A \quad (2a)$$

$$[B] = -k_B[B] + \alpha k_A[A] - k_B^A[B] - k_B^W[B] + r_B \quad (2b)$$

$$[C] = -k_C[C] + \beta k_A[A] - k_C^A[C] - k_C^W[C] + r_C, \quad (2c)$$

where k_A is the rate constant of breakdown of A into B and C, k_B and k_C are the rate constants of breakdown of B and C into subsequent fragments, k_B^A and k_C^A are the rate constants of reversible processes B → A and C → A, k_A^W, k_B^W and k_C^W are the rate constants of irreversible heterogeneous binding processes of molecules A, B and C and r_A, r_B and r_C are the rates of appearance of molecules A, B and C from external sources (separation of molecules from the surface of the discharge elements, from special getters, from a ballast tank and so on).

By combining equations (2a)-(2c), let us write

$$[A] = -(k_A + k_A^W)[A] + \frac{k_B^A(\alpha k_A[A] - [B] + r_B)}{k_B + k_B^A + k_B^W} + \frac{k_C^A(\beta k_A[A] - [C] + r_C)}{k_C + k_C^A + k_C^W} + r_A \quad (3)$$

and let us consider typical limiting cases, having first noted the obvious circumstance that the cases when $[A](t^* - t) \approx [A]$, where $[A]^*$ is the density of the working molecules similar to the optimum with regard to laser parameters and t^* is the desirable operating time of the system, are of practical interest among them.

1. The working molecules A break down in a plasma at considerable rate, while the reversible reactions are hardly effective: $k_A[A] \gg k_B^A[B]$ and $k_C^A[C]$. Solution of equations (2) and (3) yields

$$[A] = [A]_0 \exp(-k_A t)\left\{\exp(-k_A^W t)\left[1 + \frac{r_A}{[A]_0(k_A + k_A^W)} \times (\exp(k_A t + k_A^W t) - 1)\right]\right\}, \quad (4)$$

where $[A]_0 = [A]\ (t=0)$. Equation (4) can be represented in the form $[A] = [A]_0\varphi(t)\psi(t)$, where $\varphi(t) = \exp(-k_A t)$ describes the gas-phase process of direct breakdown of molecules A in the plasma. In the simplest case of the absence of external sources ($r_A = 0$), function $\psi(t) = \exp(-k_A^W t)$ describes the absorption of the working molecules by surfaces. If $r_A \neq 0$, then separation into two functional dependencies for homogeneous and heterogeneous processes is unjustified, $\psi'(t)$ (the expression in brackets) becomes dependent on the rates of the gas-phase processes and with long times $[A]_\infty = r_A(k_A + k_A^W)^{-1}$. The relationship between k_A, k_A^W and r_A determines the process that limits the presence of molecules A in the system. Two limiting cases are possible in this case.

1-a. The gas-phase process of breakdown of working molecules is faster than heterogeneous processes. Some examples are presented in Figure 1a, b. If $r_A = 0$, then on the time scale corresponding to Figure 1a, $\psi = \text{const} = 1$ and elimination of A is determined by gas-phase breakdown $f = \phi$. If $r_A \neq 0$ (Figure 1b), then ψ' is an increasing function and $F > \phi$, reaching an asymptotic value of $[A]_\infty/[A]_0$. The situation corresponding to Figure 1a is typical, for example, for an N_2O laser [2]. The corresponding data of mass spectrometer measurements are presented on Figure 1d, showing how the densities of N_2O, N_2, O_2 and NO molecules (in % with respect to N_2O in the initial mixture) depend on the time that the discharge (with current density of 31.8 A/m^2 and pressure of 95.32 kPa) acts on the initial N_2O-He mixture (1.4). The working N_2 molecules are transformed (with fulfillment of the nitrogen and oxygen balance in the gaseous phase) to O_2 and N_2 with formation of NO at the intermediate stage. If the active medium of an N2O laser is connected to the ballast gas tank containing N_2O, then this corresponds to the situation shown in Figure 1b.

1-b. Irreversible heterogeneous binding processes of working molecules are faster than the gas-phase process of their breakdown, $f = \psi$, and $\phi = \text{const} = 1$. An example is presented in Figure 1c. This situation is typical, let us say, for CO_2 or N_2O lasers cooled by liquid nitrogen, where the rate of elimination of working molecules is determined by diffusion with subsequent concentration on the walls and $k_A^W \sim D/R^2$ (D is the diffusion coefficient and R is the radius of the tube).

2. Irreversible heterogeneous processes occur with high rate for transformation products of working molecules without affecting the working molecules themselves. Thus, $k_B^W \gg k_B^A$; $k_A^W \ll k_A$ and $k_C^W \ll k_C^A$. Let us assume for certainty that this occurs with regard to molecules B. Also let $r_A = r_B = r_C = 0$ (consideration of the effect of external sources leads to results similar to those illustrated by Figure 1b). The particles C are intermediate in the cycle $A \rightarrow C \rightarrow A$ and at sufficiently large value of $k_C^A \gg k_A$, according to the principle of quasi-stability,[1] $[C] = 0$.

With regard to these relations, integration of equation (3) yields

$$[A] = [A]_0 \exp\left\{-k_A\left(1-\beta\frac{k_C^A}{k_C^A+k_C}\right)t\right\}. \qquad (5)$$

If $k_C^A \gg k_C$, then the typical time of the exponential loss of working molecules is $\tau = (k_A\alpha)^{-1}$ (Figure 2a). In the given case the separation $f(t) = \phi(t)\psi(t)$ is unfeasible since gas-phase decomposition A is a limiting stage of the heterogeneous reaction B.

[1] This is a rather general principle of chemical kinetics [3], easily fulfilled for the systems being investigated. It follows from mass spectrometer measurements [4] that the density of oxygen atoms is constant over the entire investigated time interval ([O] = 0).

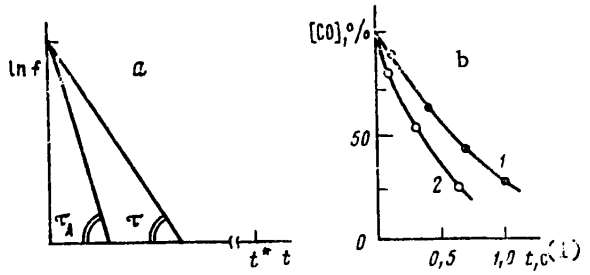

Figure 2. Second Case of Classification (a) (see text): $\tau = \tau_A \alpha^{-1}$ and $\tau_A = k_A^{-1}$. The dependence (b) of variation of the density of CO molecules in the initial CO-He mixture (1:10) on the time of the effective discharge; pressure of the mixture is 0.798 kPa; j = 95 (1) and 130 A/m^2 (2)

Key:
1. Seconds

An example that illustrates the given case may be a nitrogen cooled CO laser. One of the products of decomposition of carbon monoxide is CO_2 molecules that condense rapidly on the walls. With regard to the fact that decomposition of carbon monoxide occurs mainly through two channels [5] ($CO + e \rightarrow C + O + e$ and $CO + CO^* \rightarrow CO_2 + C$) and taking the ratio of the rates of the processes into account, we assume that $\alpha = \beta = 1/2$. Thus, the typical time of loss of working molecules τ in the given case is approximately twice as high as the typical time τ_A of homogeneous transformations of carbon monoxide. Examples of the experimental dependence of variation of density of CO molecules in the initial CO-He mixture on the time of effective discharge with cooling by liquid nitrogen is shown in Figure 2b. The data were found by the infrared absorption method [6]. It is obvious that the loss of working CO molecules occurs by a law close to exponential and the typical time of this process, although dependent on the discharge conditions, is short, on the order of seconds.

3. The rate of expenditure of initial and intermediate products in irreversible heterogeneous processes is less than the rate of reactions of the reversible cycle. It is obvious that in this case, due to the difference of typical times, the separation $f(t) = \phi(t)\psi(t)$ is feasible.

In this case the system initially arrives at a state of dynamic quasi-equilibrium and the kinetics of this process is described by the function $\phi(t)$. By analogy with the case of dynamic equilibrium considered in [5] in a water-cooled CO laser, this dependence can be written in the form

$$\varphi(t) = 1 - C_1(1 - \exp(-C_2 t)), \qquad (6)$$

where C_1 and C_2 are constants that are combinations of the rate constants of gas-phase processes. At long times $t \sim t_1$, where $t_1 >> C_2^{-1}$, $\phi(t) \rightarrow \phi_s = 1 - C_1$. To find $\psi(t)$, it is sufficient to consider equation (3) at times $t > t_1$, taking the initial suggestion on slow variation of $\psi(t)$ into account, i.e., $\psi(0) - \psi(t_1) << \psi(0)$. On this assumption $k_B^A >> k_B^W$ and in view of the principle of

quasi-stability $k_A[A] >> [B], [C]$. Let us denote $[A]_0\phi_s \equiv [A]_s$ and solution of equation (3) at $t > t_1$ can be written in the form

$$[A] = [A]_s \exp(-k^* t) + (\mu_r/k^*)(1-\exp(-k^* t)), \tag{7}$$

where $k^* = k_A\eta + k_A^W$, $\eta = 1-\alpha z_B - \beta z_C$, $\mu = r_A + r_B z_B + r_C z_C$, $z_B \equiv k_B^A(k_B^A + k_B + k_B^W)^{-1}$, $z_C \equiv k_C^A(k_C^A + k_C + k_C^W)^{-1}$.

Assuming for demonstration that breakdown of B and C into subsequent fragments does not occur (k_B, k_C = 0) and that there are no external sources, for $t > t_1$, disregarding the terms of second order of smallness, we find: $[A] = [A]_s\psi(t)$,

$$\psi(t) = \exp\left\{-k_A\left[1-\alpha\left(1-\frac{k_B^W}{k_B^A}\right)-\beta\left(1-\frac{k_C^W}{k_C^A}\right)\right]t - k_A^W t\right\}. \tag{8}$$

One can note that the expression in brackets in (8) is close to zero, but, if $k_A^W = 0$, then this expression also determines the time of displacement of equilibrium. This case is illustrated by Figure 3 and, unlike the two previous figures, is of practical interest in creation of sealed systems. It is obvious from Figure 3 that at short times $t << t_1$, the loss of working molecules is determined mainly by gas-phase processes and $f \approx \phi$. On the contrary, the loss is determined mainly in the range $t_1 < t \sim t^*$ by irreversible heterogeneous interactions.

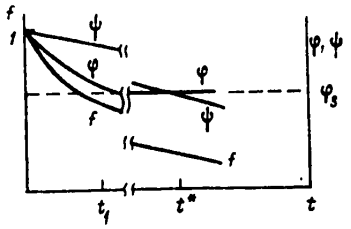

Figure 3. Third Case of Classification of System (see text)

Despite a number of simplifications related to finding it, expression (8) permits one to make some practically important conclusions. To extend the service life of sealed systems, one should bear in mind two possibilities. 1. A decrease of the initial "quasi-stable" ($t \sim t_1$) dissociation of working molecules. This can be achieved either by reducing the rates of decomposition reactions of molecules (for example, due to operation at lesser values of E/N with introduction of easily ionized Xe, Hg and other additives) or by acceleration of reversible reduction reactions, for example, by means of catalysts. 2. Reduction of the rates of irreversible heterogeneous processes by selection of the corresponding materials during design of active components and the technology of treating them. Expression (8) also permits one to make the not-too-obvious conclusion that the use of catalysts that accelerate reversible reactions affects not only the initial decomposition ($t \sim t_1$) described by the value of ϕ_s, but also the rate of irreversible heterogeneous processes, since the values of ratios k_B^W/k_B^A and k_C^W/k_C^A are included in expression (8) for $\psi(t)$. This means

with respect to physics that acceleration of reversible processes reduces the density of the reaction-capable particles of intermediate products, which are most active in interactions with surfaces. Apparently the true mechanism of the effect of catalysts of reversible processes on extension of the service life of sealed system is included in this (rather than in a decrease of the initial dissociation of working molecules).

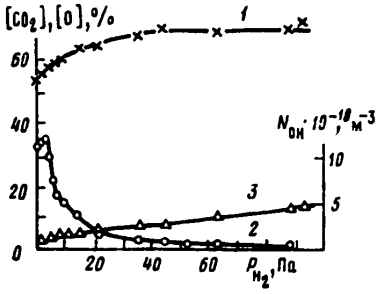

Figure 4. Dependence of Concentration (in percent of quantity of CO_2 in initial mixture) of some products of decomposition in CO_2-He mixture (1:6) on pressure p_{H_2} of hydrogen additive; pressure of the initial mixture is 0.266 kPa; density of discharge current is 64 A/m^2; 1--CO_2, 2 = O, 3--OH

Key:
1. Pa

The dependence of the densities of CO_2 molecules and oxygen atoms on the amount of hydrogen additive is presented in Figure 4 in percent with respect to CO_2 content in the initial CO_2-He mixture (1:6). The pressure of the initial mixture is 0.266 kPa and the density of discharge current is 64 A/m^2. The data were found by the mass spectrometer method. More detailed data on investigation of the effect of hydrogen additives on the chemical composition of a plasma under conditions typical for a CO_2 laser are contained in [7]. The density of hydroxyl radicals (in absolute units), found by the linear absorption method described in [8, 9], is presented in Figure 4 as well. A sharp decrease of the density of oxygen atoms when hydrogen is added is noteworthy. Since the process that limits the service life of sealed CO_2 lasers is one of binding the oxygen to surfaces [10, 11], the effect of hydrogen additives or water vapor on the service life of the system is explained in a natural manner [10, 12]. The role of hydroxyl radicals is reduced in this case to compensation for the decrease of the effectiveness of CO_2 regeneration upon recombination of $CO + O \rightarrow CO_2$ due to the reaction $CO + OH \rightarrow CO_2 + H$.

Thus, the simple scheme of chemical transformations which we considered and that takes into account only a limited number of components (three in the given case) in explicit form, permits one to describe in sufficient detail the nature of variation of the working substance in a plasma according to presently available experimental data, at least with regard to laser systems.

BIBLIOGRAPHY

1. Volchenok, V. I., V. N. Komarov, S. Ye. Kupriyanov and V. I. Stukanog, in "Khimiya plazmy" [Plasma Chemistry], edited by B. M. Smirnov, No 7, Moscow, Atomizdat, 1980.

2. Volchenok, V. I., N. P. Yegorov, V. N. Komarov, S. Ye. Kupriyanov, V. N. Ochkin and N. N. Sobolev, KHIMIYA VYSOKIKH ENERGIY, Vol 11, No 4, 1977.

3. Emanuel', N. M. and D. G. Knorre, "Kurs khimicheskoy kinetiki" [A Course in Chemical Kinetics], Moscow, Vysshaya shkola, 1974.

4. Volchenok, V. I., V. N. Komarov and S. Ye. Kupriyanov, FIZIKA PLAZMY, Vol 4, No 4, 1978.

5. Volchenok, V. I., N. P. Yegorov, V. N. Komarov, S. Ye. Kupriyanov, V. N. Ochkin, N. N. Sobolev and E. A. Trubacheyev, ZHURNAL TEKHNICHESKOY FIZIKI, Vol 42, No 12, 1976.

6. Mikaberidze, A. A., V. N. Ochkin and N. N. Sobolev, ZHURNAL TEKHNICHESKOY FIZIKI, Vol 42, No 7, 1972.

7. Baranova, O. D., V. I. Volchenok, V. N. Komarov, S. Ye. Kupriyanov and A. M. Novosel'tsev, KHIMIYA VYSOKIKH ENERGIY, Vol 13, No 4, 1979.

8. Ochkin, V. N. and N. A. Shubina, KHIMIYA VYSOKIKH ENERGIY, Vol 6, No 1, 1972.

9. Ochkin, V. N., S. Yu. Savinov and N. N. Sobolev, ZHURNAL TEKHNICHESKOY FIZIKI, Vol 47, No 6, 1977.

10. Ochkin, V. N., in "Trudy fizicheskogo instituta imeni P. N. Lebedeva AN SSSR" [Transactions of the Physics Institute imeni P. N. Lebedev, USSR Academy of Sciences], Vol 78, Moscow, 1974.

11. Aleynikov, V. S. and V. V. Karpetskiy, ELEKTRONNAYA TEKHNIKA, Vol 12, No 1, 1969.

12. Witteman, W. J., IEEE TRANSACTIONS, QF-4, No 11, 1968.

6521
CSO: 1862/195

UDC 621

ABSTRACTS OF PAPERS ON QUANTUM ELECTRONICS

Leningrad KVANTOVAYA ELEKTRONIKA (TRUDY LENINGRADSKOGO POLITEKHNICHESKOGO INSTITUTA) in Russian No 366, 1979 (signed to press 27 Dec 79) pp 114-119

UDC 621.373.826

SINGLE-FREQUENCY Nd:YAG LASER WITH ELEVATED POWER

[Abstract of article by Zaytsev, G. F., Kruzhalov, S. V. and Pakhomov, L. N.]

[Text] The paper gives the results of a theoretical and experimental study of a single-frequency Nd:YAG laser optimized with respect to output power. The output power attained in the one-frequency steady state was 800 mW. Figures 3, references 4.

UDC 621.373.826

SOLID-STATE RING LASER WITH LONGITUDINAL MODE LOCKING

[Abstract of article by Astakhov, A. V., Galkin, S. L. and Nikolayev, V. M.]

[Text] Experimental results are given on a YAG laser with longitudinal mode locking. A nonreciprocal phase-shifting device based on the Faraday effect was used to get beats of opposed waves. The lock-in band of opposed waves was measured at about 200-300 Hz. This low value is attributed to spatial separation of opposed waves in the phase-synchronous multimode state. Figures 3, references 4.

UDC 621.373.826

BEAT FREQUENCY OF OPPOSED WAVES OF MULTIMODE GAS LASER IN LONGITUDINAL MODE-LOCKED STATES

[Abstract of article by Galkin, S. L., L'vov, B. V., Nikolayev, V. M. and Samusev, K. B.]

[Text] A method of successive approximations is proposed for calculating the characteristics of ring gas lasers. This technique is used for calculating the way that the beat frequency of opposed waves in a helium-neon ring laser

depends on small alterations in cavity length in self-mode locking and forced longitudinal mode locking. It is shown that forced longitudinal mode locking reduces the dependence of beat frequency on cavity length compared with self-mode locking. Calculated results are confirmed by experiment. Figures 2, references 6.

UDC 621.373.826:535.417

MATRIX METHOD OF CALCULATING SPHERICAL CAVITIES WITH INHOMOGENEOUS POLARIZATION ANISOTROPY OVER THE CROSS SECTION

[Abstract of article by Petrun'kin, V. Yu. and Kozhevnikov, N. M.]

[Text] A matrix method is proposed for analyzing optical cavities with cross sectionally inhomogeneous polarization anisotropy generalizing the Jones method and the method of calculating isotropic spherical cavities. This method is used to calculate a confocal cavity with weak axisymmetric anisotropy. Figures 4, references 8.

UDC 621.373.826

MODE INTERACTION IN WEAKLY ANISOTROPIC GAS LASER

[Abstract of article by L'vov, B. V. and Mel'tsin, A. L.]

[Text] An analysis is made of mode interaction in a weakly anisotropic two-mode helium-neon laser with wavelength of 0.63 μm in the realistic range of pressures, intermode distances and cavity Q differences for orthogonal polarizations. The width of the zone of competition of generated modes is studied along with the addition to the frequency of intermode beats as a function of the lasing frequency mismatch relative to the center of the line of the equi-isotopic mixture in the working pressure range for different intermode intervals. Figures 3, references 12.

UDC 621.373.826

FREQUENCY SPLITTING OF OPPOSED WAVE LASING IN HELIUM-NEON RING LASER

[Abstract of article by Okunev, R. I. and Stepanyants, A. L.]

[Text] The paper gives the results of an experimental study of additional splitting of the frequencies of opposed waves when the beam is irised in a ring laser cavity and the active element is misaligned. It is shown that frequency splitting of opposed waves is due to deviation of the laser tube capillary from the cavity axis. Figures 3, references 6.

UDC 621.373.826

PHASE RELATIONS BETWEEN MODES IN TYPE-2 SELF-MODE LOCKED LINEAR GAS LASERS

[Abstract of article by Kotov, O. I. and Nikolayev, V. M.]

[Text] A spectral-time model is used to analyze phase distribution in multi-mode laser operation. A relation is established between steady-state phases

of longitudinal modes and the characteristics of both the optical spectrum and the emission pulses. The results of calculation agree with experimental data on a linear helium-neon laser. Figures 4, references 7.

UDC 621.373.826

SOME OPERATING FEATURES OF CATAPHORETIC HELIUM-CADMIUM LASER

[Abstract of article by Andreyeva, Ye. Yu., Yelagin, V. V., Terekhin, D. K. (deceased), Fotiadi, A. E. and Fridrikhov, S. A.]

[Text] By simultaneous measurement of lasing power and discharge plasma parameters of a cataphoretic He-Cd laser it is established that as the discharge current changes, the cadmium vapor pressure in the working part of the tube does not remain constant despite the fact that the temperature of the cadmium vapor source is held constant within ±0.5°C. Superposition of an axial magnetic field on the active medium in the single-frequency lasing mode leads to an increase in lasing power. Figures 3, references 9.

UDC 621.373.826

INVESTIGATING PARTICULARS OF OPPOSED WAVE COMPETITION IN RING LASER ON 3.39 μm LINE

[Abstract of article by Andreyeva, Ye. Yu., Kirina, M. Yu., Terekhin, D. K. (deceased)]

[Text] An experimental study is done on the influence that gas mixture pressure and an external axial magnetic field have on conditions of competition of opposed waves. It is established that a reduction in pressure with consideration of coupling through scattering narrows the region of competition of opposed waves. The longitudinal magnetic field removes the competition of opposed waves. The results enable us to calculate the coefficient of coupling through scattering between opposed waves, and can be used in selecting modes of operation of laser gyroscopes. Figure 1.

UDC 621.373.826

COMBINED LASER DISCHARGE WITH MICROWAVE PREIONIZATION

[Abstract of article by Golovitskiy, A. P., Kruzhaolv, V. A., Perchanok, T. M., Terekhin, D. K. (deceased) and Fridrikhov, S. A.]

[Text] It is proposed that a microwave discharge be used to preionize the medium of a CO_2 laser. The microwave discharge is excited in a slit cut in the narrow wall of a waveguide. Opposite the slit is an electrode to which pulsed voltage is applied. The gain of the active medium on a wavelength of 10.6 μm is studied as a function of pumping parameters. It is established that the microwave discharge sets up inversion in the medium only in direct proximity to the slit, but is conducive to development of discharge in the main volume. High gain that is uniform throughout the volume can be obtained by appropriate selection of pumping parameters. Figures 2, references 5.

UDC 535.853

ACOUSTO-OPTIC SPECTROGRAPH FOR RADIO ASTRONOMICAL STUDIES

[Abstract of article by Yesepkina, N. A., Kotov, B. A., Mikhaylov, A. V., Petrun'kin, V. Yu., Pruss-Zhukovskiy, S. V., Ryzhkov, N. F. and Shishkin, A. I.]

[Text] An examination is made of the principle of action, and results of an experimental study are given on a model of a radio astronomical spectrograph based on an acousto-optical spectrum analyzer, a CCD bit line and the Elektronika-100 computer. The authors determine the parameters (frequency band, resolution and radiometric gain) of such a spectrograph when operated in the modulation mode. Figures 3, references 13.

UDC 621.385.832.5

OPTICAL-TO-ELECTRICAL DATA CONVERSION BASED ON CHARGE-TRANSFER DEVICES

[Abstract of article by Karinskiy, S. S., Kotov, B. A. and Kotov, Yu. A.]

[Text] The paper presents the working principles of new semiconductor devices with charge transfer. It is shown that this class of new photoelectric converters has a group of parameters enabling optimum realization of the capability of optical computer systems, and development of optico-digital hybrid data processing systems with flexible structure and extensive capabilities. Limiting values are given for errors, noises and speed of these devices, and major characteristics of CTD's are compared with those of analogous devices (vidicons, dissectors, etc.). Figures 3, references 7.

UDC 621.327.8

DEVICE FOR INTERFACING OPTICAL AND DIGITAL DATA PROCESSING SYSTEMS USING LINEAR AND MATRIX CHARGE-TRANSFER DEVICES

[Abstract of article by Kotov, Yu. A., Mikhaylov, A. V. and Novitskiy, A. P.]

[Text] An examination is made of the principles of design of an interface for programmed control of linear and matrix charge-transfer devices (CTD's) for data input to the Elektronika-100 computer. Estimates are made of the data input time for various interface design structures using off-the-shelf peripheral equipment. Figures 2, references 5.

UDC 535.241.13:534

MULTICHANNEL HIGH-FREQUENCY ACOUSTO-OPTICAL MOCULATORS

[Abstract of article by Aksenov, Ye. T., Bukharin, N. A., Rogov, S. A. and Sayenko, I. I.]

[Text] The authors consider problems of making solid-state multichannel acousto-optical modulators (AOM's) for frequencies of 100-300 MHz. The paper

gives a descripcion of the technology of manufacturing the modulators and methods of matching input impedances of channels. Results of an experimental study of multichannel AOM's are presented. Figures 4, references 13.

UDC 535.241.13:534

INVESTIGATION OF ACOUSTO-OPTICAL SPECTRUM ANALYZERS OF RADIO SIGNALS BASED ON BRAGG MULTIPHASE LIGHT SCATTERING

[Abstract of article by Yesepkina, N. A., Lipovskiy, A. A., Chkalova, V. V. and Shcherbakov, A. S.]

[Text] An investigation is made of the feasibility of increasing resolution of an acousto-optical spectrum analyzer of radio signals by using multiphase scattering of light in crystals with a large coefficient of acousto-optic quality. It is experimentally shown that selection of the scattering geometry can remove the forbidenness of multiphase processes in the Bragg mode and give effective scattering of light to the second and third orders. The authors describe working models of acousto-optical spectrum analyzers based on the TeO_2 crystal that have double or triple the frequency resolution of analogous devices based on single-phase scattering for the same dimensions of the acoustic line. Figures 3, references 8.

UDC 535.241.13:534

CALCULATING PARAMETERS OF ACOUSTO-OPTIC INTERACTION IN CRYSTALS BY PERTURBATION METHOD

[Abstract of article by Shcherbakov, A. S.]

[Text] An examination is made of one of the possible methods of determining parameters of acousto-optic interaction in crystals for arbitrary scattering configuration. Covariant relations are found for the band of acousto-optic interaction, the index of phase modulation and effective photoelastic constants in the case of an anisotropic medium, and expressions are derived that describe the efficiency of Bragg multiphase light scattering. The author uses the method of expanding a single-frequency wave function in an infinite series of the theory of perturbations and calculating sample sums of this series using elements of the Feynman diagram method. Figures 2, references 16.

UDC 621.396.67:535.241.13.534-8

EXPERIMENTAL STUDY OF OPTICAL SIGNAL PROCESSING SYSTEM IN ANNULAR ARRAYS

[Abstract of article by Vodovatov, I. A., Vysotskiy, M. G., Yesepkina, N. A. and Rogov, S. A.]

[Text] An experimental investigation is done on an optical signal processing system in annular antenna arrays. Operation of the processing system is considered both in the static mode (with static transparency as input signal) and in real time with the use of an ultrasonic light modulator. The paper

gives results on signal processing with amplitude weighting. A discrete multichannel reference raster is used for recording the holographic filter. Figures 4, references 4.

UDC 621.396.67:522.59:535

OPTICAL SIMULATION OF ANTENNA APERTURE FIELDS

[Abstract of article by Vinogradov, G. K., Vodovatov, I. A., Vysotskiy, M. G. and Zubkova, T. I.]

[Text] Similarity conditions of fields in optical and radio systems are considered for some specific optical modeling arrangements. On the basis of these conditions, estimates are made of the accuracy of placing individual components in optical simulation schemes. Figure 1, references 4.

UDC 621.372.82:621.383.8

DIFFUSION OPTICAL WAVEGUIDES IN LITHIUM NIOBATE

[Abstract of article by Aksenov, Ye. T. and Lipovskiy, A. A.]

[Text] An experimental study is done on the feasibility of making optical waveguides in Y+36° and X-cut $LiNbO_3$ plates by exodiffusion in atmosphere and diffusion of Na^+ ions. It is shown that the characteristics of the resultant optical waveguides are close to the characteristics of waveguides formed by exodiffusion in vacuum and diffusion of Ag^+ ions. The investigated methods of optical waveguide formation are technologically simple and economic. Figure 1, references 6.

UDC 621.373.826:621.397.22

USING WIDE-BAND ACOUSTO-OPTIC COMPONENTS IN LASER VISUALIZATION OF TV IMAGE

[Abstract of article by Aksenov, Ye. T., Bukharin, N. A., Ignatov, A. B., Kiseleva, N. V., Maron, N. F., Seysyan, R. P., Uman, S. D. Shapiro, L. P. and Shustarev, D. Yu.]

[Text] The paper gives experimental results of investigation of a system for laser visualization of TV images in which the laser beam is controlled by an acousto-optical modulator and deflector with complex sectionalized piezoelectric converters that enable scanning of an acoustic beam. It is shown that such systems can be used to get television images with better quality than in conventional electronic television systems. Figures 3, references 10.

UDC 535.421

LIGHT DIFFRACTION BY RELIEF GRATINGS IN TOTAL INTERNAL REFLECTION REGION

[Abstract of article by Bobrov, S. T., Butusov, M. M., Ovchinnikov, V. A., Turkevich, Yu. G. and Udoyev, Yu. P.]

[Text] The authors study angular dependences of diffraction efficiency of relief gratings with spatial frequencies of 900-1700 lines/mm and relief depth

of 0.02-0.4 μm. The measurements were done on $\lambda = 0.6$ μm with the grating illuminated from the backing side. It was established that near the critical angle of total internal reflection the angular dependences contain a structure with form that depends on the polarization of the incident wave, period and depth of grating relief. Possible mechanisms that give rise to this structure are discussed. Figures 3, table 1, references 15.

UDC 778.38

METHODS OF GETTING HIGH-RESOLUTION HOLOGRAPHIC IMAGES OF MICROSCOPIC OBJECTS

[Abstract of article by Sokolov, A. V. and Bykov, V. N.]

[Text] An investigation is made of the feasibility of using methods of optical holography for direct registration of microscopic objects, their microstructure and spatial placement are studied, and also the dynamics of processes in systems of microscopic objects. Microscopic objects are classified on the basis of their light-scattering properties, conditions of image formation in Lippmann holography and Fraunhofer lensless holography are considered, and recommendations are made on choosing the holographing arrangement as a function of types of microscopic objects and their placement in the investigated volume. Figure 1.

UDC 533.9

THE 'SLOW BURNING' OPTICAL DISCHARGE MODE

[Abstract of article by Pakhomov, L. N., Petrun'kin, V. Yu. and Podlevskiy, V. A.]

[Text] Two versions are suggested for maintaining plasma combustion of an extended optical discharge, based on the particulars of cavity design and Q-switch. Experimental results are given. Figures 3, references 2.

UDC 681.121:539.143.43

AMPLITUDE-TAGGED NMR FLOWMETER

[Abstract of article by Dudkin, V. I., Semenov, V. V. and Uspenskiy, L. I.]

[Text] The paper describes an amplitude-tagged NMR flowmeter using the effect of parametric resonance in a flowing liquid. It is shown that introducing modulation of the magnetic field in the sensor of the nutation magnet characteristically changes the shape of the nutation line and extends the functional capabilities of the device. Figures 2, references 6.

UDC 621.373. 823:621.317.444

NUCLEAR MAGNETOMETER WITH AUTOMATIC ADJUSTMENT BASED ON MASER WITH FLOWING FLUID

[Abstract of article by Dudkin, V. I., Kravtsov, I. A. and Filimonov, V. I.]

[Text] The authors consider problems of designing an automatic magnetometer by using the effect of nuclear magnetic resonance in a running fluid. An

experimental study is done on a maser-based self-generating magnetometer model. The model device was used for measuring variations in a magnetic field with intensity of 600 ± 30 oersteds [$4.8 \cdot 10^5 \pm 2387$ A/m]. Relative measurement error is no more than 10^{-6} for the case of magnetic field variation with frequency $\omega \geqslant 1$ rad/s and amplitude of 30 oersteds [2387 A/m]. Figures 2, references 8.

UDC 539.184:535.21

COMBINED EXCITATION OF SPIN PRECESSION IN A GROUP OF OPTICALLY ORIENTED ATOMS

[Abstract of article by Semenov, V. V. and Sergeyeva, I. V.]

[Text] A theoretical and experimental study is done on excitation of spin precession in a group of optically oriented cesium atoms in magnetic resonance under conditions of intensity-modulated resonant detecting radiation. Observable signals are calculated for combined action of an intensity-modulated detecting light beam and rf field on the system of optically oriented atoms. The results are experimentally evaluated. Figures 3, references 3.

UDC 621.373.8

ABSORBED POWER OF OPTICAL RADIATION IN QUANTUM FREQUENCY STANDARDS

[Abstract of article by Matisov, B. G. and Toptygin, I. N.]

[Text] Constant populations of a three-level system interacting with resonant rf and optical pumping fields are calculated in the first nonvanishing approximation with respect to the small parameter μ/ν. This extends the previously developed theory of absorption by an optical power system in the presence of an rf field to vanishingly small amplitudes of the rf field. Figure 1, references 4.

UDC 539.183.184

CALCULATING ADIABATIC AND NONADIABATIC COLLISIONAL BROADENING OF HFS LINES FOR ALKALI ATOMS IN BUFFER GAS

[Abstract of article by Batygin, Vl. V., Gornyy, M. B., Gurevich, B. M. and Sokolov, I. M.]

[Text] The authors calculate adiabatic broadening of hfs lines of atoms of hydrogen, Rb and Cs due to collisions with He, Ne, Ar, Kr and Se. New formulas for matrix elements of transition with and without spin flip are derived on the basis of the mechanism of nonadiabatic spin relaxation suggested by Hermann, considering angular dependence. The relation between the computed cross sections and experimentally measured values is discussed. Tables 2, references 15.

UDC 539.183.184

HYPERFINE TRANSITION LINE COLLISIONAL SHIFTS AND DIFFUSION COEFFICIENTS OF ALKALI ATOMS IN BUFFER GAS

[Abstract of article by Batygin, Vit. V., Batygin, Vl. V., Gornyy, M. B. and Gurevich, B. M.]

[Text] The frequency shift is plotted as a function of the ratio of ionization potentials (I_b/I_a) from results of measurements of shifts of the hyperfine transition line of alkali atoms (A) in buffer gas (B). The values of the shifts do not differ strongly from experimental measurements. Based on the correlation theory of line shape, an estimation formula is derived for calculating shifts in the frequency of the hyperfine transition. The dependence of shifts on the ionization potential ratio as calculated by this formula gives a good description of the experimental curves. The calculated values of the shifts agree satisfactorily with the experimental data. Shifts are predicted for some A-B pairs. An approximate formula is suggested for the potential of interatomic interaction of A-B pairs. The diffusion coefficients for an extensive set of A-B pairs calculated by this potential are approximately half the experimental values. Figures 3, tables 3, references 18.

UDC 778.38

RECORDING HOLOGRAMS IN BICHROMATED GELATIN LAYERS WITH LATENT IMAGE MONITORING

[Abstract of article by Yerko, A. I. and Malov, A. N.]

[Text] The authors study the characteristics of latent image formation in bichromated gelatin layers as a function of the energy of exposure and the intensity of radiation during recording. Experiments demonstrate the presence of a mechanism of charged ion diffusion from the exposed region, which is a cause of decay of the latent image. An experimental curve is found for the diffraction efficiency of the developed bichromated gelatin layer as a function of the diffraction efficiency of the latent image. Figures 2, references 5.

UDC 621.373.826

MINIATURE HELIUM-NEON LASER FOR OPTICAL DATA PROCESSING SYSTEMS

[Abstract of article by Pruss-Zhukovskiy, S. V., Senyukov, A. I. and Shishkin, A. I.]

[Text] The paper gives the results of calculations and an experimental study of characteristics of a miniature helium-neon laser for optical data processing systems. Tests of the laser as part of the acousto-optical spectrograph on the RATAN-600 radio telescope showed that the proposed laser satisfies major requirements for output power, stability and reliability. References 6.

6610
CSO: 1862/174

UDC 621.378.3

CHEMICAL-GASDYNAMIC CO_2 LASER USING CO+O+M RECOMBINATION REACTION PRODUCTS

Novosibirsk FIZIKA GORENIYA I VZRYVA in Russian Vol 18, No 1, Jan-Feb 82 (manuscript received 15 Sep 81) pp 88-96

[Article by V. V. Kovtun, S. S. Novikov and I. B. Svetlichnyy, Moscow]

[Text] According to Ref. 1, there may be considerable excitation of vibrational degrees of freedom of CO_2 molecules formed in the exothermal reaction ($\Delta E \cong 125$ kcal/mole) of CO+O+M recombination. In the calculation done in Ref. 2, an examination is made of the feasibility of realizing inverse populations in the system of levels of CO_2 molecules that are products of the recombination reaction taking place under conditions of gasdynamic laser (GDL) operation. The author assumes that all reaction energy ΔE is released to vibrational degrees of freedom, and that this energy is distributed uniformly with respect to the vibrational modes of the CO_2 molecules. This assumption about the dynamics of the reaction and the process of vibrational energy exchange in the system of levels of CO_2 molecules corresponds to most favorable conditions for realization of chemical pumping in the course of the CO+O+M recombination reaction.

In Ref. 3 in spectroscopic studies of a steady-state $CO+O_2$ flame (at pressure $p \cong 40$ mm Hg), nonequilibrium distribution of CO_2 molecules is observed with respect to vibrational degrees of freedom (with preferred population of the collective mode of CO_2). The complexity of calculations of dynamics of the three-particle CO+O+M reaction, absence of experimental data on the distribution of reaction energy with respect to internal degrees of freedom of CO_2 molecules require determination and substantiation of conditions under which recombination would lead to realization of population inversion of laser levels of CO_2 molecules.

To realize chemical pumping of laser levels of CO_2 molecules ($\lambda = 10.6$ μm), the conditions of the experiment must on the one hand ensure a sufficient rate of formation of vibrationally excited CO_2 molecules in the course of the three-particle CO+O+M recombination reaction, and on the other hand prevent their rapid deactivation during relaxation processes. Chemical pumping is possible if ratio $\tau_{chem}/\tau_{rel} \lesssim 1$ can be met, where $\tau_{chem} = (k[CO][M])^{-1}$ is the characteristic time of the reaction CO+O+M, τ_{rel} is the characteristic time of relaxation of vibrationally excited CO_2 molecules. The value of τ_{chem} in the reaction zone is $\tau_{chem} \sim 0.7$ μs at $p \cong 15$ atm and $T \cong 2000$ K. Estimates of τ_{rel} under

the same experimental conditions are made by using Anderson's relaxation scheme [Ref. 4]: $\tau_{rel} = \Delta E/\Theta \cdot \tau_1 \approx 2.3$ μs, where τ_1 is the characteristic time of relaxation of the collective mode of CO_2 molecules, ΔE is the energy released to vibrational degrees of freedom of CO_2 in the course of an elementary act of recombination of $CO+O+M$, Θ is the magnitude of a quantum of the deformation mode of CO_2.

The dependence of the rate of the three-particle recombination reaction on particle density in the reaction zone is determined by the relation $k \sim p^3$, and the relaxation rate is $k_{rel} \sim p^2$; therefore the relation $\tau_{chem}/\tau_{rel} \sim p^{-1}$ is met. It is clear from the given estimates that the ratio of characteristic times $\tau_{chem}/\tau_{rel} \lesssim 1$ will be satisfied if the pressure in the reaction zone is ≳15 atm. To retain vibrational excitation of the reaction products (CO_2 molecules), the drop in temperature and density must be made sufficiently rapid that deactivation processes in the system are "frozen".

The mixer GDL technique enables us to bring about thermodynamic conditions necessary for chemical pumping in the reaction zone, and in the flow of reaction products cooled during expansion through the nozzle. This technique also gives us the capability of monitoring the extent of the reaction zone, and hence the completeness of chemical and relaxation processes in the system.

In our research, we did experiments on a facility of pulsed GDL type based on a shock tube with flat nozzle on the end face (Fig. 1). The principal structural components of the facility: fast-action electromagnetic valve 4 similar to that used in Ref. 5, and nozzle-plug injector 3 of cylindrical shape with axis parallel to the nozzle slit. Atomic oxygen O was produced in region 2 behind the reflected shock wave by partial dissociation of O_2 molecules in a mixture of initial composition $0.4O_2 + 0.6$ Ar. The change of pressure in region 2 was monitored by piezoelectric sensor 21 installed close to the end face of the shock tube. After diaphragm 1 in front of the nozzle was broken, an equilibrium flow of $O+O_2+Ar$ entered the mixing zone, where it was mixed with the other reagent ($CO+He$ mixture) discharged from the cavity of valve 4 through injector 3. The configuration of the zone in which flow intermixing and chemical reactions occurred in the system was determined by the profile of the lateral surface of the cylindrical injector and the geometry of the subsonic part of the nozzle (Fig. 2). The configuration of the mixing zone and the positions of the injector orifices determined the duration of flow intermixing and the length of time that the gas stayed in this zone.

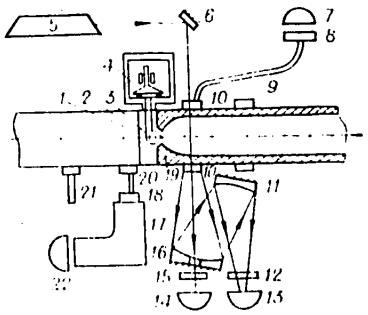

Fig. 1

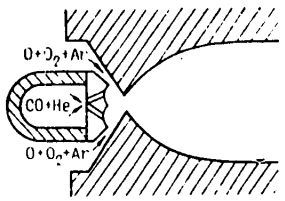

Fig. 2

Shaped nozzle 19 with profile described in Ref. 6 was used in the experiments. Nozzle parameters:

height of critical cross section $h_* \approx 1.0$ mm, vertex half-angle $\alpha \approx 42°$, degree of expansion of the flow $A/A_* \approx 23$. It is shown in Ref. 5 that the time during which the gas discharge from the nozzle is steady-state is ~0.2 s. The duration of existence of steady-state conditions in the "hot" plug behind the shock wave in the O_2 + Ar mixture is considerably shorter: $\tau_0 \approx 0.15$–0.30 ms. Therefore triggering of the electromagnetic valve was synchronized with the arrival of the shock wave at the end face of the shock tube in such a way that the flow injected from the channel cavity was formed with a lead of 200-300 μs before the instant when the diaphragm in front of the nozzle burst.

The physicochemical processes in our research were diagnosed on the basis of registration of intensities of spontaneous ($\lambda = 4.3$ μm) and stimulated ($\lambda = 10.6$ μm) infrared radiation in the working cross section of the gas flow, and also spontaneous recombination emission accompanying the reactions $O + O \rightarrow O_2 + h\nu$ (Schumann-Runge band, $\lambda = 401.0$ nm) and $O + CO \rightarrow CO_2 + h\nu$ (continuum 280-700 nm, $\lambda = 488$ nm). A diagram of the optical channels of the system is shown on Fig. 1. The course of the recombination reaction CO+O+M was monitored by measuring the concentration of oxygen atoms in the hot plug (see Fig. 1, 2) and in the supersonic flow of reaction products in the cross section situated at a distance of $x = 50$ mm from the plane of the critical cross section of the nozzle.

The concentrations of oxygen atoms in the hot plug were determined from measurements of intensity I_{401} of radiation of O_2 molecules on wavelength $\lambda = 401.0$ nm. Radiation from the pre-nozzle region 2 was coupled to photomultiplier 22 (FEU-39A) through fiber-optics guide 20, quartz lens 18 and monochromator 17. Luminescence intensity I_{401} is related to the concentration of oxygen atoms in the hot plug by the expression [Ref. 7]

$$I_{401} = C_{401}\Gamma_{401}(T_0')[O]^2, \qquad (1)$$

where $I_{401}(B)$ is the magnitude of the signal registered on the oscilloscope screen corresponding to radiation on wavelength $\lambda = 401.0$ nm, C_{401} is the calibration factor of the registration system in $V \cdot Å \cdot sr/(W \cdot cm^{-3})$, $\Gamma_{401}(T_0')$ in $W \cdot sr^{-1} \cdot cm^3)/(Å \cdot mole^2)$ is the value of function $\Gamma_\lambda(T_0')$ that describes the distribution of radiation intensity in the Schumann-Runge band at $\lambda = 401.0$ nm, T_0' is the temperature in kelvins in the hot plug after equilibrium dissociation of O_2 molecules is established in the mixture of initial composition $0.4O_2$ + 0.6Ar, and [O] is the density in mole/cm^3 of oxygen atoms in the hot plug.

The intensity of visible radiation in the supersonic flow of reaction products (at a distance of 50 mm from the plane of the critical cross section of the nozzle) is determined mainly by the cross section in the chemiluminescent reaction $O + CO \rightarrow CO_2 + h\nu$, and hence depends on the concentration of oxygen atoms. In this paper measurements were made of the radiation intensity in the spectral range of $\lambda = 488 \pm 7.5$ nm by using fiber-optics guide 9, interference filter 8 and photomultiplier 7 (FEU-39A). According to Ref. 8, the intensity of radiation in the given spectral interval is related the concentration of oxygen atoms by expression

$$I_{488} = C_{488}\Gamma_{488}(T)[O][CO]. \qquad (2)$$

Calibration factors C_{401}, C_{488} were experimentally determined. The values of $\Gamma_{488}(T)$ at T = 293 K are given in Ref. 8. To extrapolate function $\Gamma_{488}(T)$ to other values of T we used the temperature dependence of the rate constant of chemiluminescent reaction $CO + O + CO_2 + h\nu$ on temperature [sic] [Ref. 9].

At T_0^1 = 3500-3850 K in the hot plug, molecules of $O_2(B^3\Sigma_u^-, v' = 0,1)$ make the principal contribution to radiation ($\lambda = 401.0 \pm 7.0$ nm, Schumann-Runge band) of $O_2(B^3\Sigma_u^-) \rightarrow O_2(X^3\Sigma_g^-)$) [Ref. 7]. In accordance with the Franck-Condon principle this corresponds to excitation of vibrational levels $v'' \geqslant 18$ of the lower electron state of $O_2(X^3\Sigma_g^-)$ [Ref. 10]. The equilibrium population of vibrational levels $v'' \geqslant 18$ of molecules $O_2(X^3\Sigma_g^-)$ does not exceed 10^{-5} of the number of molecules of $O_2(X^3\Sigma_g^-, v'' = 0)$. Analogously in the course of chemiluminescent reaction $CO + O \rightarrow CO_2 + h\nu$ ($\lambda = 488.0 \pm 7.0$ nm) we get excitation of vibrational levels of the ground electron state of $CO_2(^1\Sigma_g^+)$ that are situated ~48 kcal/mole higher than the ground vibrational level $v_1 = v_2 = v_3 = 0$ of the $CO_2(^1\Sigma_g^+)$ molecule [Ref. 9]. These levels are also practically unpopulated under conditions of supersonic flow with translational temperature T = 150-300 K. Because of low population, the given levels of the O_2 and CO_2 molecules make no contribution to radiation transfer, and therefore in recording recombination radiation of $O + O \rightarrow O_2 + h\nu$ and $O + CO \rightarrow CO_2 + h\nu$ in the given system there is no need to account for reabsorption of radiation. This enables us to use relations (1) and (2) that are valid for conditions of an optically thin layer.

The systematic error in measuring oxygen atom concentration ξ_O^e in the hot plug is due to the error in determination of the quantity $\Gamma_{401}(T)$ given in Ref. 7, and also to the error in measurements of the calibration factor C_{401}. The overall error of measurements of the quantity ξ_O^e in the hot plug did not exceed 20%.

In the case of optical measurements in the supersonic flow (x = 50 mm), an error associated with the uncertainty of values of translational temperature is added to the above-mentioned sources of errors. Deviation of the actual values of T in the flow from those calculated in the approximation of uniform steady-state discharge through the nozzle is related to the possible increase in T due to V-T relaxation of excited reaction products in the flow. Without consideration of this factor, the calculated values of temperature T in the expression are understated, and consequently the measured values of concentration of oxygen atoms ξ_O^m are overstated. Therefore the systematic error in determination of ξ_O^m in the flow was from +30 to -70%.

Infrared diagnosis of the state of the nonequilibrium flow of reaction products in cross section x = 50 mm was based on measurements of intensity of spontaneous radiation $I_{4.3}$ of CO_2 molecules in the 4.3 μm band, as well as measurements of the small-signal gain (or absorption) K_0 of the probing CO_2 laser radiation ($\lambda = 10.6$ μm). The vibrational temperatures of asymmetric (T_3) and collective (T_2) modes of the CO_2 molecules that are reaction products were determined from the measured values of $I_{4.3}$ and K_0. The method of determining vibrational temperatures from characteristics of spontaneous and stimulated emission is given in detail in Ref. 11. In the given experiments, a beam from an LG-23 CO_2 electric-discharge laser ($\lambda = 10.6$ μm) (see Fig. 1, 5) after reflection from flat mirror 6 passed through BaF_2 windows 10 located in cross section

x = 50 mm and dispersion filter 15, and was incident on photoresistor 14 (FSG-22A). From the same cross section of the flow by means of spherical mirrors 11 and 16 and narrow-band filter 12 ($\lambda = 4.41 \pm 0.05$ μm) spontaneous radiation was measured in the band of the CO_2 molecules with center $\lambda = 4.3$ μm (photoresistor 13).

Calibration of the system for registration of infrared radiation is described in Ref. 11, according to which the accuracy of measurements of vibrational temperatures T_3 and T_2 is determined mainly by the random error and amounts to 10%.

The parameters of the gas behind the reflected shock wave in the mixture of initial composition $0.4O_2 + 0.6Ar$ were: $p_0 = 15 \pm 2.0$ atm, $T_0 = 3800 - 4820$ K. Results of calculation of the relative concentration of oxygen atoms in the hot plug (assuming establishment of equilibrium dissociation of O molecules) are shown on Fig. 3. Characteristic time of establishing conditions of equilibrium dissociation under the conditions of the experiment was ~12 μs. After establishment of equilibrium dissociation of O_2 molecules, the temperature in the hot plug according to theoretical calculation dropped to $T_\delta^1 = 3450$-3850 K. The experimentally measured concentrations of oxygen in the hot plug are shown on Fig. 3. The relative concentrations of oxygen atoms under the conditions of the given experiments were $\xi_O^e = 0.06$-0.15 depending on the equilibrium temperature behind the reflected shock wave T_δ^1. The measured values of ξ_O^e average 15% less than the calculated values.

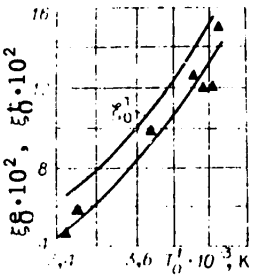

Fig. 3

On the basis of results of Ref. 12, estimates were made of the duration of the process of intermixing flows as a jet of CO + He is injected in a direction close to the normal with respect to the direction of the flow of $O + O_2 + Ar$ in the cross section where the Mach number of this flow is $M \approx 0.2$. These estimates showed that intermixing of flows is completed at distance τ_m ~2.5 mm from the injection point. The time of intermixing of flows ($\tau_m \sim 5$ μs) is $0.7\tau_2$, where τ_2 is the time interval from the instant of injection of gas CO + He into the mixing zone to the instant of arrival of the mixed flow in the critical cross section of the nozzle. Comparison of the characteristic time of the recombination reaction CO + O + M (τ_{chem}) and mixing time τ_m shows that these quantities are of the same order of magnitude.

For efficient chemical pumping ($\tau_{chem}/\tau_{rel} \lesssim 1$) under conditions of a mixing GDL, conditions must be favorable for the chemical reaction. This requires organization of rapid mixing of flows ($\tau_m \cong \tau_{chem}$) to produce a reaction mixture that is uniform with respect to component makeup.

The composition of the mixture in the mixing zone was calculated in the approximation of a model of instantaneous mixing of flows under initial conditions in the hot plug of $p_0 \cong 15$ atm, $T_0 \cong 4820$ K. The relative content of principal components in the mixing zone was: $0.07O + 0.21O_2 + 0.14CO + 0.37Ar + 0.21He$.

The kinetic scheme of processes that take place in the mixing zone is described by the following principal reactions:

$$O + CO + M \rightarrow CO_2 + M, \quad (3)$$
$$O + O + M \rightarrow O_2 + M, \quad (4)$$
$$O + O_2 + M \rightarrow O_3 + M, \quad (5)$$
$$O + O_3 \rightarrow 2O_2, \quad (6)$$
$$CO + O_2 \rightarrow CO_2 + O, \quad (7)$$

where M = O, O_2, CO, CO_2, Ar, He.

Calculation of the relative contribution γ made by side reactions (4)-(7) to the consumption of atomic oxygen showed that γ comprises about 20% of the overall consumption of atomic oxygen. The calculation used rate constants given in Ref. 13, 14. Thus it has been demonstrated that recombination reaction CO + O + M under the conditions of the xperiment makes the principal contribution to consumption of atomic oxygen formed in the hot plug.

As a consequence of the strong dependence of the rate of three-particle recombination on particle density in the flow $k \sim p^2$, the chemical reactions in the flow are practically frozen after passing a single diameter downstream from the critical cross section of the nozzle. Therefore, comparison of relative concentrations of oxygen atoms in the hot plug and in the supersonic flow (x = 50 mm) gives information on the completeness of chemical processes with participation of atomic oxygen. It has been experimentally shown that the relative concentration of oxygen atoms in the supersonic flow is $\xi_O^m = 0.005\text{-}0.008$, which is considerably less than the concentration of these atoms in the mixing zone ξ_O^c ($\xi_O^c \cong 0.07$ at $T_0^* \cong 4820$ K). This result shows the almost total completion of chemical processes with participation of atomic oxygen in the mixing zone.

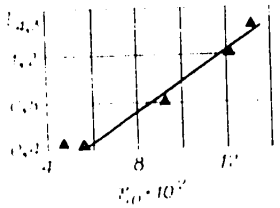

Fig. 4

Fig. 4 shows the way that radiation intensity in the 4.3 μm band of CO_2 molecules as recorded in a supersonic flow ($x \cong 50$ mm) of reaction products depends on relative concentration of oxygen atoms ξ_O^e in the hot plug. The quantity $I_{4.3}$ increases linearly with increasing ξ_O^e in the range from 0.08 to 0.13. The increase in relative concentration ξ_O^e in the given experiments was achieved by increasing the initial temperature behind the reflected shock wave in the mixture of $0.4O_2 + 0.6Ar$. This led correspondingly to an increase in translational temperature T in the supersonic flow; however, as shown in Ref. 15, changing T has little effect on the intensity of radiation in the 4.3 μm band of CO_2 molecules.

Probing the flow of reaction products with electric-discharge CO_2 laser radiation in cross section x = 50 mm revealed absorption of laser radiation (λ = 10.6 μm) with absorption coefficient $K_0 = 0.0\text{-}0.03$ m^{-1}. Vibrational temperatures that describe the populations of levels of asymmetric (T_3) and collective (T_2) modes of the CO_2 molecules that are reaction products were determined from the

measured values of K_0 and the intensity of spontaneous radiation in the 4.3 μm band of CO_2 molecules.

Vibrational temperatures were calculated for experimental conditions with maximum (in the given experiments) content of atomic oxygen in the mixing zone $\xi\delta \cong 0.07$ (at $T_0 \cong 4820$ K). The amount of energy stored in a unit volume of gas during recombination reaction $CO + O + M$ is proportional to the number of CO_2 molecules that are formed, and consequently to the initial concentration of atomic oxygen $\xi\delta$. Thus the conditions of calculation correspond to the maximum contribution of energy from recombination reaction $CO + O + M$ to the total amount of energy of the gas, and consequently to the vibrational degrees of freedom of CO_2 molecules.

The state of the gas in the cross section of the flow ($x = 50$ mm) to which the calculated values of vibrational temperatures T_3 and T_2 are referred corresponds to: $0.06CO_2 + 0.23O_2 + 0.09\ CO + 0.39Ar + 0.23He$, $T \cong 190$ K, $p \cong 2.5 \cdot 10^{-2}$ atm. The values of the vibrational temperatures of CO_2 molecules were: $T_3 \cong 2080$ K, $T_2 \cong 1100$ K.

The experimentally obtained high values of T_3 evidence appreciable excitation of vibrational levels of CO_2 as a result of reactions that occur in the mixing zone. We will show that excitation of the asymmetric mode of CO_2 molecules is due to the recombination reaction $CO + O + M$, and that the contribution of other chemical processes is minor. Consider the kinetic scheme of chemical processes with participation of hydrogen-containing impurities $H_2(H_2O)$. According to the technical specifications of the degree of purity for the gases used in the experiments (O_2, CO, Ar, He) the content of impurities $H_2(H_2O)$ does not exceed $6 \cdot 10^{-5}$ mole fraction. Additional purification of O_2 and CO was done by fractional distillation of the gases. Argon was dried in a trap with liquid nitrogen ($T \cong 77$ K). With low content of impurities $H_2(H_2O)$, the kinetic scheme of the reactions in the system $CO + O_2 + H_2(H_2O)$ in addition to reactions (3)-(7) includes the following processes:

$$O + H_2 \xrightarrow{k_8} OH + H, \tag{8}$$

$$H + O_2 \underset{k_{-9}}{\overset{k_9}{\rightleftarrows}} OH + O, \tag{9}$$

$$O + H_2O \underset{k_{-10}}{\overset{k_{10}}{\rightleftarrows}} 2OH, \tag{10}$$

$$H + H_2O \underset{k_{-11}}{\overset{k_{11}}{\rightleftarrows}} H_2 + OH, \tag{11}$$

$$CO + OH \underset{k_{-12}}{\overset{k_{12}}{\rightleftarrows}} CO_2 + H, \tag{12}$$

$$O + H + M \xrightarrow{k_{13}} OH + M, \tag{13}$$

$$O_2 + H + M \xrightarrow{k_{14}} HO_2 + M. \tag{14}$$

The values of reaction constants (8)-(14) are given in Ref. 13, 14. Under the conditions of the experiment we have the ratio of concentrations [O], $[O_2]>>[H_2]([H_2O])$.

Analysis of kinetic reaction scheme (8)-(14) can be conveniently divided into two cases: a) hydrogen H_2 is the predominant impurity in the initial mixture; b) the principal hydrogen-containing impurity is from H_2O molecules.

In case a), calculation in the approximation of rapid establishment of quasi-steady concentrations of atoms H and radicals OH ($d[H]/dt \approx d[OH]/dt \approx 0$) with consideration of conservation of the number of atoms H in a unit volume of the reacting mixture written as

$$[H] + [OH] + 2[H_2] = 2[H_2]_0, \tag{15}$$

leads to the relation

$$Z = \frac{[OH]}{[H_2]_0} = 2\frac{k_8}{k_{-9}}\frac{1}{k_8[O]/2k_{-9} + 1 + k_8/k_{-9}}. \tag{16}$$

With variation of the parameters in the mixing zone $T_c = 1660$-1820 K, $\xi_0^6 = 0.04$-0.07, the value of Z ranges from 0.16 to 0.18. Thus the content of OH radicals is practically constant in the formulated experiments (assuming the same initial content of H_2 impurities in the investigated mixtures).

Consideration of the other mechanism of formation of OH radicals with participation of water vapor impurities (case b) leads to the relation $[OH] \approx 2[H_2O]$ since chemical equilibrium in the main reaction (10) of this mechanism is strongly shifted to the right. Analysis of both mechnisms of formation of OH radicals shows that the OH content in the mixing zone remains constant with an appreciable change in conditions in the hot plug: $T_0 = 4000$-4820 K, $\xi_0^6 = 0.07$-0.13.

If the vibrationally excited molecules of $CO_2(\nu_3)$ were formed in reaction (12), the rate of formation of CO_2 molecules would be determined by the relation

$$\frac{d[CO_2(\nu_3)]}{dt} = k_{12}[CO][OH] - \frac{[CO_2(\nu_3)] - \overline{[CO_2(\nu_3)]}}{\tau_1}, \tag{17}$$

where τ_1 is the characteristic time of relaxation of molecules of $CO_2(\nu_3)$ in the reaction zone, $\overline{[CO_2(\nu_3)]}$ is the equilibrium content of $CO_2(\nu_3)$ in the reaction zone at $T_c = 1820$ K, $p_c \approx 15$ atm. Under conditions of dynamic equilibrium between processes of chemical pumping and deactivation of levels of $CO_2(\nu_3)$ (at $d[CO_2(\nu_3)]/dt \approx 0$) we have the condition

$$[CO_2(\nu_3)] = \overline{[CO_2(\nu_3)]} + k_{12}\tau_1[CO][OH]. \tag{18}$$

The time of establishing this mode is ~0.02 μs. From an examination of the quantities appearing in the right member of equation (18) we see that the values of τ_1, k_{12}, $\overline{[CO_2(\nu_3)]}$ vary weakly over a range of $T_c = 1660$-1820 K, $\xi_0^6 = 0.07$-0.13. The concentration of OH radicals, as shown by analysis of kinetic reaction scheme (8)-(14) with participation of impurities of H_2 (or H_2O) and CO molecules, remained almost constant in all experiments.

Expression (18) shows that the content of vibrationally excited molecules of $CO_2(\nu_3)$ should be unchanged in the mixing zone in the supersonic flow. The experiments showed linear dependence of $I_{4,3}(\xi_0^6)$ (see Fig. 4) at $\xi_0^6 = 0.07$-0.13. Since $I_{4,3} \sim [CO_2(\nu_3)]$, comparison of the experimental plot of $I_{4,3}(\xi_0^6)$ and expression (18) demonstrates the validity of the assumption of the insignificant contribution of reactions (8)-(14) with participation of $H_2(H_2O)$ to formation of $CO_2(\nu_3)$.

The concentration of molecules of $CO_2(\nu_3)$ under conditions of quasi-steadiness of reaction $CO + O + M \rightarrow CO_2 + M$ and processes of vibrational relaxation satisfies the relation

Equation (19) shows that $I_{4,3} \sim [CO_2(\nu_3)] \sim \xi_0^6$ (or ξ_0^6). Thus the assumption of chemical pumping of $CO_2(\nu_3)$ during recombination reaction $CO + O + M \rightarrow CO_2 + M$ is in agreement with the experimentally obtained plot of $I_{4,3}(\xi_0^6)$.

In the given analysis of the dependence $I_{4,3}(\xi_0^6)$, we used results of infrared diagnosis of vibrationally excited molecules of $CO_2(\nu_3)$; therefore the question of the possible contribution of reaction (12) to formation of CO_2 molecules in the ground vibrational state requires separate consideration. When the value of k_{12} from [Ref.] 14 is used, it is shown that the maximum content of CO_2 molecules formed in reaction (12) does not exceed 0.3% of the total concentration of particles in the reaction zone. Thus the given analysis of the kinetics of chemical processes in the system of reagents using equations (3)-(14) and analysis of the experimental dependence $I_{4,3}(\xi_0^6)$ indicate that the main reaction leading to formation of CO_2 molecules is recombination reaction $CO + O + M$.

The values of $T_3 \cong 2080$ K found in the experiments correspond to a much greater population of levels of the asymmetric mode of CO_2 molecules that are the reaction products of recombination (by a factor of 1.6) than when the levels of this mode are populated in the mixing GDL based on inert mixtures of $CO_2 + N_2 + He$ at initial temperature in the hot plug of $T_0 \cong 3850$ K. The considerable population ($T_2 \cong 1100$ K) of levels of the collective mode of CO_2 molecules is the reason for absorption of probing radiation ($\lambda = 10.6$ μm), despite the high values of vibrational temperature of the asymmetric mode T_3. Realization of conditions that favor relaxation of levels of the collective mode of CO_2 molecules that are reaction products should lead to population inversion in the system of vibrational levels of these molecules.

Experiments were done with displacement of the probing region downstream to the flow cross section situated at distance $x = 95$ mm from the plane of the critical cross section of the nozzle. In this case, amplification of the CO_2 probe laser radiation was observed in the stream of CO_2 molecules. The measured gains were $\cong 1.3\ m^{-1}$ (Fig. 5).

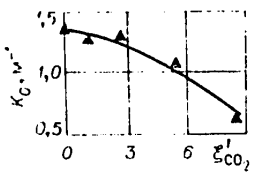

Fig. 5

In this research, experiments were done with partial replacement of the helium in the CO + He mixture by carbon dioxide injected from the valve cavity. These experiments enable estimation of the influence that CO_2 molecules

formed in the initial stage of mixing of streams of $O+O_2+Ar$ and $CO+He$, and possibly having lost a considerable part of the vibrational excitation, have on the gain in the expanding flow. The action of this mechanism was simulated by introducing "cool" CO_2 molecules into the $CO+He$ mixture.

The measured values of gain $K_0 \cong 1.3\ m^{-1}$ showed little change as ξ'_{CO_2} ranged from 0 to 0.03 (see Fig. 5) (ξ'_{CO_2} is the relative concentration of CO_2 molecules introduced into the $CO+He$ mixture as calculated in the approximation of the instantaneous mixing model for streams of $O+O_2+Ar$ and $CO+CO_2+He$). A further increase in concentration in a range of $\xi'_{CO_2}=0.03$–0.08 led to a reduction in gain from 1.3 to 0.6 m^{-1}. Since the rate of reaction $O+CO_2 \rightarrow CO+O_2$ is small, introducing "cool" molecules of CO_2 into the mixture injected from the valve cavity has little effect on chemical equilibrium in the system. The observed reduction in K_0 with increasing ξ'_{CO_2} is thus due to the participation of CO_2 molecules introduced into the $CO+He$ mixture in relaxational V-T and V-V' processes.

Thus in this research we have realized chemical pumping of levels of the asymmetric mode of CO_2 molecules populated in the course of recombination reaction $CO+O+M$. Population inversion was achieved in the system of levels ($00^0 1$–$10^0 0$) of CO_2 molecules formed in the course of this reaction under mixing GDL conditions.

REFERENCES

1. Biryukov, A. S., TRUDY FIZICHESKOGO INSTITUTA IMENI P. N. LEBEDEVA, Vol 83, Moscow, Nauka, 1975.

2. Carrington, T., Garvin, D., in "Vozbuzhdennyye chastitsy v khimicheskoy kinetike" [Excited Particles in Chemical Kinetics], Moscow, Mir, 1973.

3. Koopmann, R. K., Saunders, A.R., J. QUANT. SPECTR. RAD. TRANS., Vol 10, 1970, p 403.

4. Anderson, J. D., PHYS. FLUIDS, Vol 13, 1970, p 1983.

5. Kroshko, V. N., Soloukhin, R. I., Fomin, N. A., in: "Gazovyye lazery" [Gas Lasers], Moscow, Nauka, 1977.

6. Ktalkherman, M. G., Mal'kov, V. M. et al., FIZIKA GORENIYA I VZRYVA, Vol 15, 1979, p 6.

7. Myers, B. F., Burtle, E. R., J. CHEM. PHYS., Vol 48, No 9, 1968, p 3935.

8. Pravilov, A. P., ZHURNAL FIZICHESKOY KHIMII, Vol 52, No 8, 1978, p 1863.

9. Clyne, M. A., Thrush, B. A., PROC. ROY. SOC. LONDON, Vol A269, 1962, p 404.

10. Gilmoure, F., J. QUANT. SPECTR. RAD. TRANS., Vol 5, 1965, p 369.

11. Kudryavtsev, N. N., Novikov, S. S., Svetlichnyy, I. B., KVANTOVAYA ELEKTRONIKA, Vol 6, No 4, 1979, p 690.

12. Kompaniyets, V. Z., Ovsyannikov, A. A., Polak, L. S., "Khimicheskiye reaktsii v turbulentnykh potokakh gaza i plazmy" [Chemical Reactions in Turbulent Flows of Gas and Plasma], Moscow, Nauka, 1979.

13. Kondrat'yev, V. N., "Konstanty skorostey gazofaznykh reaktsiy" [Rate Constants of Gas-Phase Reactions], Moscow, Nauka, 1974.

14. Baulch, D. L., Drysdale, D. D., Horue, O. G., "Evaluated Kinetic Data for High-Temperature Reactions", Vol 1, 2, Butterworths, 1972.

15. Kudryavtsev, N. N., Novikov, S. S., in: "Materialy vtoroy Vsesoyuznoy konferentsii po metodam aerofizicheskikh issledovaniy" [Materials of the Second All-Union Conference on Methods of Aerophysical Research], Novosibirsk, 1979.

6610
CSO: 1862/184

OPTOELECTRONICS

THEORY OF DYNAMIC IMAGE SELECTION EFFECT IN PHOTOREFRACTIVE MEDIA

Leningrad FIZIKA TVERDOGO TELA in Russian Vol 24, No 2, Feb 82 (manuscript received 16 Jul 81) pp 337-343

[Article by V. V. Bryksin, L. I. Korovin, M. P. Petrov and A. V. Khomenko, Physicotechnical Institute imeni A. F. Ioffe, USSR Academy of Sciences, Leningrad]

[Text] A model of a photorefractive medium is proposed that leads to the phenomenon of dynamic selection of images --flashing of images in the recording light after it is switched off in the geometry of a PRIZ optical electromodulator. The results of the theory for diffraction efficiency of the medium as a function of the time of exposure of the recording beam and the frequency of its spatial modulation agree qualitatively with experiments done on $Bi_{12}SiO_{20}$ crystals.

Investigation of processes of optical data recording in photorefractive crystals has led to the detection of an unusual effect -- suppression of stationary parts of images being recorded, and isolation of the nonstationary parts [Ref. 1]. This phenomenon, which has been termed the effect of dynamic selection of images, may be treated under certain conditions as time differentiation of an unsteady pattern presented to the crystal, whereas the response of light-sensitive media is usually proportional to the integrated action of an optical input signal. Experimentally, the effect of dynamic selection of images has been observed in image recording on a thin ($\cong$0.5 mm) $Bi_{12}SiO_{20}$ single crystal plate cut in plane [111] or [110] when an electric field of $1\text{-}2\cdot10^4$ V/cm is applied to this plate by transparent electrodes applied to the faces of the plate parallel to the given planes. If an image in blue or green light is presented under these conditions to the given structure (which is called a PRIZ light modulator), with readout at the same time in polarized red light, the readout light will show mainly the nonstationary parts of the recording image. The principal characteristics of this experiment are readout light intensity of $\cong10^{-5}$-10^{-4} W, rate of change in input information $\cong$1-0.1 s, degree of suppression of stationary part of the image 10-20 dB.

Experiments done with the PRIZ modulator show that image recording arises due to excitation of photocarriers by the recording light, the charge

redistribution being proportional to the distribution of intensity of the recording light. The resultant charge distribution causes electric fields to appear in the crystal, giving rise to spatial modulation of birefringence. The polarized readout light undergoes a change in the state of polarization due to the transverse electro-optic effect. It has been experimentally established that with slow changes of input signal intensity J(x, y, t), the phase difference $\Delta\phi(x, y, t)$ between the ordinary and extraordinary readout beams at the output of the device is proportional to dJ/dt [Ref. 2]. Although at present the relation between the electro-optical characteristics of the crystal and the condition of image recording has been fairly well established both experimentally and theoretically [Ref. 3], and we also have some idea of the nature of charge distribution under steady-state conditions [Ref. 2], nonetheless the dynamic behavior of the system leading up to the effect of dynamic selection of images has not been studied, and there are not even any reliable qualitative ideas about the nature of this effect.

This paper is the first to present a theoretical analysis of a model picture that allows us to establish the major causes leading to the effect of dynamic selection of images.

1. Qualitative Picture of the Phenomenon

When the transverse electro-optic effect is used, the phase difference $\Delta\phi(x, y, t)$ is proportional to the integral characteristic I(x, y, t) of the transverse field $E_\perp$ that is set up in the specimen [Ref. 4]

$$I(x, y, t) = \int_0^{d_0} E_\perp(x, y, z, t)\, dz, \qquad (1)$$

where the z-axis is opposite to the direction of the external field E_0 applied to the specimen, and d_0 is the thickness of the specimen. An important characteristic of the photorefractive medium is diffraction efficiency η. In the case where $\Delta\phi < 1$, it can be considered with fair accuracy that $\eta \sim (\Delta\phi)^2$, and consequently η is proportional to the square of the amplitude of modulation of the quantity I(x, y, t).

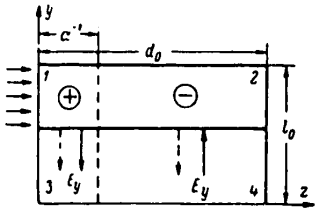

Fig. 1. Schematic picture of the change in direction of transverse fields E_y in time. Solid arrows in regions 3 and 4 indicate the direction of E_y under lighting, and the broken arrows indicate the direction of E_y after lighting is switched off. The direction of the light beam is shown to the left of the y-axis. It is assumed that light is completely absorbed at distance α^{-1}.

The qualitative picture of dependence of I on time t, which is what determines the effect of dynamic selection of images, can be explained in the following way. To simplify the discussion, let us assume that there are illuminated and unilluminated sections of the plate surface. In an illuminated section (region 1), after the light is switched on, photoelectrons and ionization donors appear (see Fig. 1). Charge separation begins in an external field E_0. If diffusion processes are disregarded, the space charge will extend over the illuminated regions along the z-axis (region 2). Assuming that diffusion takes place slowly compared with motion in the external field, the entire process of establishment of the steady state in the system can be broken down into two stages: establishment of a quasisteady state in regions 1 and 2, and spreading of the charge in direction y on the second stage (into regions 3 and 4). On the first stage the negative charge is balanced that consists of the electrons in the band and those captured by traps in regions 1 and 2. This balancing under conditions of electroneutrality of the specimen leads to charge separation. In the process of charge separation, region 1 is positively charged with respect to region 1; the transverse field is directed from 1 toward 3 (solid arrows on Fig. 1). In region 2, which is negatively charged, E_y takes the opposite direction. Conditions in an experiment are usually such that $\alpha d_0 > 1$ (α is the coefficient of absorption), and therefore region 1 is smaller than region 2. As a result, the shielding action of the metal electrodes (shielding length of the order of a period of spatial modulation l_0) reduces the total field E_y more strongly in region 1 than in region 2. Thus on the first stage the main contribution to I(t) is from the field between regions 2 and 4. This stage is characterized by an increase in image brightness.

On the second stage, the negative charge of electrons in the band and on traps is equalized by diffusion along y. In such equalization the contribution to I(t) from the negative charge gradually disappears. The quantity I(t) begins to decrease in absolute value, vanishes, and after sufficiently long times reaches a steady-state positive value that is determined by the contribution to field E_y from nonuniformly distributed positively charged donors. As we can see from the following, image storage takes place on this stage.

After lighting is switched off, the system arrives at the initial equilibrium state, and free electrons in region 1 recombine on donors. Recombination will continue due to electrons from region 2 that enter region 1 through the external circuit. And if diffusion in the transverse direction is the slowest process, no negative charge will remain in regions 1 and 2, whereas a positive charge will remain in region 1 since some of the electrons are distributed in regions 3 and 4. On this stage, a transverse field arises between regions 2 and 4 (broken arrows on Fig. 1) so that the directions of the field coincide between regions 2, 4 and 1, 3. This leads to a further increase in I(t) as compared with the steady-state value. Diffusion from regions 3, 4 into 1, 2 begins to reduce the field E_y, and the electrons entering region 1 recombine on donors. As a result this leads to total disappearance of the local charge and the internal field.

2. Description of Model and Principal Equations

Let us consider a dielectric (photoconductor) with two systems of discrete levels: donor levels with concentration n_d and trap levels with concentration n_t. Of all possible transitions between levels and the conduction band, in future we will consider transitions from donors in the conduction band under the action of light and recombinations from the conduction band on donors, and also capture of band electrons by traps and thermal ejection of electrons from trap levels into the band. With consideration of this, the system of equations studied below for determining electron concentration n in the band, the concentration of ionized donors n_+ and charged traps n_- can be written as

$$e\partial(n + n_- - n_+)/\partial t = e\mu E_0 \partial n/\partial z + \mu kT\partial^2 n/\partial y^2, \quad (2)$$

$$\partial n_+/\partial t = g\theta(t_0 - t)F(z, y)n_d - n_+/\tau_d, \quad (3)$$

$$\partial n_-/\partial t = nn_t/\vartheta_t - n_-/\tau_t. \quad (4)$$

Here e is the modulus of the electronic charge, μ is carrier mobility in the conduction band, gF(z, y) is the rate of generation of electrons from donor levels under conditions of nonuniform illumination. $\theta(t_0 - t)$ is the Heaviside function (step) that switches off the light at time t_0; light is switched on at time $t = 0$. It is assumed that the light is modulated along the y-axis.

Processes of recombination and capture in equations (3) and (4) that are nonlinear in nature are approximated by linear processes: recombination on donors is described by term n_+/τ_d, and capture on traps is described by term nn_t/ϑ_t (τ_d is the effective time of recombination on donors, ϑ_t is the constant of capture on traps). This approach disregards depletion of donor levels and the nonlinear term that limits filling of traps. These approximations are valid when conditions $n_+ \ll n_d$, $n_- \ll n_t$ are met (n_- is the concentration of charged traps), which corresponds to illumination levels that are not too high. After switching off the recording light, the system can be returned to the initial state only if the electrons are moving in a direction perpendicular to the external electric field $\vec{E}_0$. In this connection, equation (2) takes consideration of electron diffusion along the y-axis. Accounting for diffusion processes along the external field should not cause any qualitative change in the results. The right-hand part of equation (2) is the divergence of current density in which the term $n\nabla\phi$ is omitted, i. e. the influence of internal fields on electron motion is disregarded. Here ϕ is the potential of the internal fields, i. e. the fields that arise as a result of charge redistribution after discounting field $\vec{E}_0$. The distribution of electric fields is determined from Poisson's equation

$$\nabla^2\varphi = (4\pi e/\varepsilon)(n + n_- - n_+), \quad (5)$$

where ε is the permittivity of the crystal. Let us note that equations (2)-(4) are a linearized version of the general system of nonlinear equations that describe the way that internal fields in the crystal depend on time and coordinates in the presence of spatially modulated illumination and under conditions of current passing through the specimen [Ref. 5].

For further analysis it is convenient to convert to dimensionless variables

$$\left.\begin{array}{c} N=n/n_d,\quad N_\pm=n_\pm/n_d,\quad \zeta=\alpha z,\quad \xi=\alpha y,\\ \beta=\mu E_0\alpha\tau_d,\quad \delta=\mu kTa^2\tau_d/e,\quad \Omega=n_t\tau_d/\vartheta_t,\\ \omega=\tau_d/\tau_t,\quad \tau=t/\tau_d,\quad \Phi=\varepsilon\alpha^2\varphi/(4\pi e n_d), \end{array}\right\} \tag{6}$$

in which equations (2)-(5) take the form

$$\left.\begin{array}{c} \partial(N+N_--N_+)/\partial\tau=\beta\partial N/\partial\zeta+\delta\partial^2N/\partial\xi^2,\\ \partial N_+/\partial\tau=g\vartheta(\tau_0-\tau)\,\tau_dF(\zeta,\xi)-N_+,\\ \partial N_-/\partial\tau=\Omega N-\omega N_-,\quad \tau_0=t_0/\tau_d,\\ [(\partial^2/\partial\zeta^2)+(\partial^2/\partial\xi^2)]\,\Phi=N+N_--N_+. \end{array}\right\} \tag{7}$$

It is assumed below that lighting intensity is modulated by a cosine law, and damps out exponentially into the plate, so that $F(\zeta, \xi)$ is equal to

$$F(\zeta,\xi)=\exp(-\zeta)\,[1+b\cos(\varkappa,\xi)],\quad \varkappa=2\pi/(\alpha l_0). \tag{8}$$

3. Integral Characteristic of Transverse Field

In virtue of the linearity of equations (6) and the selected form of light modulation, all unknown quantities (concentrations of electrons, ionized donors and charged traps, and also the internal field potential) are representable as $A+B\cos\kappa\xi$, where A and B do not depend on ξ. Since a contribution proportional to A does not lead to a transverse field, we consider below only the contribution proportional to B, i. e. the first (and in this sense the only) Fourier component of the internal field. Therefore only the first harmonics of the concentrations and potential are considered below (without changing the symbols).

In the internal transverse electro-optic effect, the diffraction efficiency η of the light-sensitive medium is determined by modulation of the phase difference $\Delta\phi$. Therefore we investigate below the first harmonic of the dimensionless characteristic of the transverse field (see formula (1))

$$I(\tau)=\varkappa\int_0^d\Phi(\zeta,\tau)\,d\zeta,\quad d=\alpha d_0. \tag{9}$$

The solution of system of equations (7) is given in the Appendix. $I(\tau)$ takes the form

$$[I(\tau)/(bg\tau_d)]=S(1)\,\vartheta(\tau_0-\tau)-[W(\tau)-W(\tau-\tau_0)\,\vartheta(\tau-\tau_0)], \tag{10}$$

where W is the sum of the exponentials and of the oscillating part

$$W(\tau)=\tilde{W}(\tau)+C(p_0^+)\exp(-p_0^+\tau)+C(p_0^-)\exp(-p_0^-\tau)+C_1\exp(-\tau) \tag{11}$$

(analogously for $W(\tau-\tau_0)$). S(1) (see II, 6) corresponds to the steady-state value of I, i. e. when $\tau_0\to\infty$ and $\tau\to\infty$, and $\tilde{W}$ is the sum of the oscillating terms

$$\tilde{W}(\tau)=-\frac{4G}{d}\sum_{k=1}^{\infty}\mathrm{Re}\left\{\frac{\varkappa^2\delta+i\beta\vartheta_k)}{(1-i\vartheta_k)(\varkappa^2+\vartheta_k^2)}\left[\frac{\exp(-p_k^+\tau)}{f(p_k^+)}+\frac{\exp(-p_k^-\tau)}{f(p_k^-)}\right]\right\}, \tag{12}$$

$$\left.\begin{array}{c} f(p)=p(1-p)\,[1+\Omega\omega(\omega-p)^{-2}],\quad \vartheta_k=2\pi k/d,\\ G=[1-\exp(-d)]\,\mathrm{th}\,(\varkappa d/2). \end{array}\right\} \tag{13}$$

The period of oscillations and damping of exponentials in (12) is determined by quantities $p_k^{\pm}$

$$p_k^{\pm} = 2^{-1}\{\Omega + \omega + \varkappa^2\delta + i\beta\vartheta_k \pm \sqrt{(\Omega + \omega + \varkappa^2\delta + i\beta\vartheta_k)^2 - 4\omega(\varkappa^2\delta + i\beta\vartheta_k)}\}. \quad (14)$$

The nature of the oscillations of $I(\tau)$ is analogous to that described in Ref. 5. Coefficients C and C_1 are equal to

$$C(p) = \delta[(2G/d) - \varkappa(1 - \exp(-d))] f^{-1}(p), \quad (15)$$

$$C_1 = (1-q)^{-1}\{[G\,\mathrm{cth}(qd/2) - \varkappa q \quad (1 - \exp(-d))][q + \varkappa^2\delta/\beta][q^2 - \varkappa^2]^{-1} + (1 + \varkappa^2\delta/\beta) S(1)\}, \quad (16)$$

where $q = q(-1)$ is given in the Appendix (II, 1). Curves of the time dependence of I calculated by formulas (10)-(16) are given on Fig. 2 and 3.

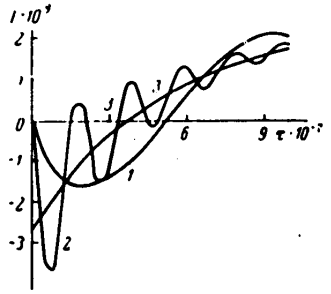

Fig. 2. Time dependence of integral characteristic of transverse field at different values of the external field E_0. Values--β: 1--10^{-4}, 2--$5\cdot10^{-4}$, 3--∞; $\omega = 10^{-5}$, $\Omega = 10^{-2}$, $\alpha l_0 = 100$, $d = 10$, $\delta = 5\cdot10^{-3}$, bg $\tau_d = 10^{-7}$. Curve 3 increases from 0 to the extremum value in time $\tau \sim \Omega^{-1}$ at the selected values of parameters in time $\tau \sim 100$

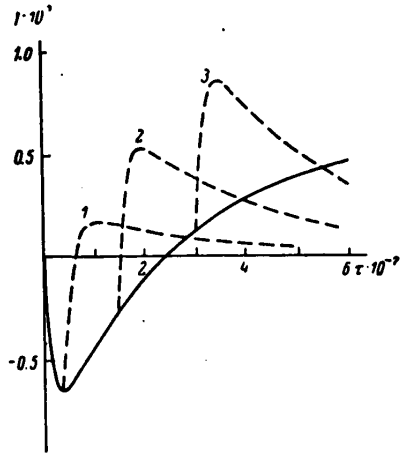

Fig. 3. Time dependence of integral characteristic of transverse field at different times of switching off the lighting. Values of τ_0: 1--$0.4\cdot10^7$, 2--$1.5\cdot10^7$, 3--$3.0\cdot10^7$. Solid curve corresponds to $\tau_0 \to \infty$. $\omega = 10^{-5}$, $\Omega = 10^{-2}$, $\alpha l_0 = 10$, $d \to \infty$, $\delta = 10^{-4}$, $\beta = -10^{-3}$, bg $\tau_d = 10^{-7}$

4. Discussion of Results and Comparison With Experiment

As can be seen from Fig. 2 and 3, the proposed model leads to a time dependence $I(\tau)$ that in general features coincides with that found in section 1 from qualitative considerations. If conditions are met that preclude oscillations of the quantity I, i. e. for the interval of fairly weak and fairly strong fields (Fig. 2), then the time dependence of I^2 behaves as follows. I^2 passes through a maximum, vanishes, and then settles to a steady value. The vanishing of the I^2 should show up in the experiment as a single flicker of the image. A rather significant property of this model is the appearance of a maximum in

the response of the medium to switching off illumination, i. e. one of the manifestations of dynamic selection of images. The maximun of the intensity of the flash in the readout light after switching off the lighting depends strongly on the switch-off time, and for small switch-off times practically disappears. For example the ratio of the maximum of I^2 for curve 3 to the maximum for curve 1 (shown by broken lines on Fig. 3) is 30.

Let us now turn to analysis of the dependence of I^2 on the frequency of spatial modulation of light $\kappa/2\pi$ (let us recall that I^2 determines the diffraction efficiency η of the medium). Since the function $I(\kappa)$ is parametrically dependent on time, it is convenient to study the dependence on κ at small τ, where $I(\tau)$ depends linearly on time. If we assume that $\omega \ll \Omega$, $\delta \ll 1$, then at sufficiently small times in formula (11) we can omit terms proportional to $\exp(-\tau)$, $\exp(-p_k^+\tau)$ and $\exp(-p_0^+\tau)$. Besides, if we disregard diffusion at small times, then term $\exp(-p_0^-\tau)$ is very weakly dependent on τ. Finally, if we assume that $\omega \gg p_k^-$ (i. e. $\Omega \gg \beta\theta_k$), then formula (10) is simplified,

$$I(\tau) = -\frac{4Gbg\tau_d\tau\beta\omega}{d\Omega}\sum_{k=1}^{\infty}\frac{\vartheta_k^2}{(1+\vartheta_k^2)(\varkappa^2+\vartheta_k^2)}. \qquad (17)$$

Summing the series, we finally get for I^2

$$I^2(\varkappa) = \left(\frac{b\tau_d g\omega\tau\beta}{\Omega}\right)^2\left\{\frac{[1+\exp(-d)]}{(1-\varkappa^2)}\left[\varkappa\,\mathrm{th}\,\frac{d}{2} - \mathrm{th}\,\frac{\varkappa d}{2}\right]\right\}^2. \qquad (18)$$

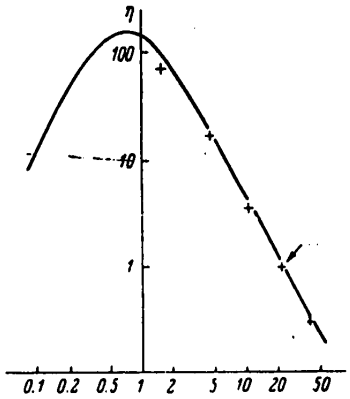

Fig. 4. Diffraction efficiency in relative units as a function of spatial frequency of lighting modulation. The crosses denote experimental values. The arros shows the point of coincidence of the experimental and theoretical curves; $d = 0.72$ ($d_0 = 400$ μm, $\alpha = 18$ cm^{-1})

We see from (18) that at small κ, $I^2 \sim \kappa$, and then I^2 passes through a maximum (at $\kappa_{max} \cong d$), and as $\kappa \to \infty$, $I^2 \sim \kappa^{-2}$ (Fig. 4). The dependence of η on κ has been experimentally observed on a PRIZ modulator in which the active element

was a $Bi_{12}SiO_{20}$ single crystal plate 400 μm thick. The recording was done in AG laser light ($\lambda = 476$ μm, $\alpha = 18$ cm^{-1}). The experimental points are shown on Fig. 4. At small values of spatial frequencies ($l_0^{-1} < 1$ line/mm), the linear section of the dependence $\sqrt{\eta}(t)$ was not experimentally observed, which precludes measurement of $\eta(\kappa)$ in this frequency region. However, the experimental curve for dependence of η on the spatial frequency measured in the region of nonlinear time dependence of $\sqrt{\eta}$ has a maximum at l_0^{-1} of about 1 line/mm [Ref. 4], which agrees with the conclusions of the theory.

Comparison of the results of the theory presented in this paper with the available experimental data [Ref. 1-4] shows that the proposed model qualitatively explains the principal observed effects: the presence of dynamic selection of iamges, the presence of a maximum in $\eta(\kappa)$, dependence $\eta(\kappa) \sim \kappa^{-2}$ as $\kappa \to \infty$. However, quantitative comparison on the given stage is extremely difficult in view of the absence of reliable experimental values of the relaxation characteristics of photostimulated centers and charges (τ_d, θ_t, τ_t). Therefore, the proposed mechanism at present cannot be considered the only possible or predominant mechanism for the specific conditions under which the experimental studies were done ($Bi_{12}SiO_{20}$ crystal, type of contacts, range of applied fields and lighting intensities and so on).

Appendix

After Laplace transformation of equations (7) with respect to time under zero initial conditions for all concentrations, and elimination of $N_{\pm}$, we get an equation for electron concentration

$$\frac{dN}{d\zeta} + q(p)\,N + \frac{b g \tau_d \exp(-\zeta)\,[1 - \exp(-p\tau_0)]}{(p+1)\,\beta} = 0, \qquad (\Pi, 1)$$

$$q(p) = -(\varkappa^2 \delta/\beta) - (p/\beta)\,[1 + \Omega\,(p+\omega)^{-1}]$$

(p is the Laplace variable, $\tau_0 = t_0/\tau_d$). Equation (П, 1) was solved under the condition of electroneutrality of the specimen

$$\int_0^d d\zeta\,(N + N_- - N_+) = 0. \qquad (\Pi, 2)$$

Setting up the combination $N + N_- - N_+$, we get the Poisson equation for the first harmonic of the potential

$$\frac{d^2\Phi}{d\zeta^2} - \varkappa^2\Phi = V_1 \exp(-q\zeta) + V_2 \exp(-\zeta), \qquad (\Pi, 3)$$

$$V_1 = b g \tau_d\,[\exp(-d) - 1]\,[1 - \exp(-p\tau_0)]\,p^{-1}\,(p+1)^{-1}\,(q-1)^{-1},$$
$$V_2 = b g \tau_d\,(1 - \delta\varkappa^2/\beta)\,[1 - \exp(-p\tau_0)]\,p^{-1}\,(p+1)^{-1}\,(q-1)^{-1}.$$

Solving equation (П, 3) with boundary conditions $\Phi(0) = \Phi(d) = 0$, we get the potential in the Laplace representation

$$\Phi = V_1 Q(q) + V_2 Q(1), \qquad (\Pi, 4)$$
$$Q(q) = (q^2 - \varkappa^2)^{-1}\,(\operatorname{sh} \varkappa d)^{-1}\,[e^{-q\zeta} \operatorname{sh}(\varkappa d) - e^{-qd} \operatorname{sh}(\varkappa\zeta) - \operatorname{sh} \varkappa\,(d - \zeta)].$$

Integrating Φ with respect to ζ from 0 to d, and multiplying by κ, we get I(p)

$$I(p) = -V_1 S(q) - V_2 S(1), \qquad (\Pi, 5)$$

$$S(q) = (q^2 - \varkappa^2)^{-1} [1 + \exp(-qd)] [\mathrm{th}(\varkappa d/2) - (\varkappa/q)\,\mathrm{th}(qd/2)]. \qquad (\Pi, 6)$$

Inverse Laplace transformation of quantity I(p) leads to formula (10), which gives the exact expression for $I(\tau)$ in the given model.

REFERENCES

1. Petrov, M. P., Khomenko, A. V., Marakhonov, V. I., Shlyagin, M. G., PIS'MA V ZHURNAL TEKHNICHESKOY FIZIKI, Vol 6, 1980, p 385.

2. Petrov, M. P., "Primeneniye metodov opticheskoy obrabotki informatsii v golografii" [Using Methods of Optical Data Processing in Holography], collection edited by S. B. Gurevich V. I. Sokolov, Leningrad, Physico-technical Institute, 1980, p 203.

3. Petrov, M. P., Khomenko, A. V., FIZIKA TVERDOGO TELA, Vol 23, 1981, p 1350.

4. Petrov, M. P., Khomenko, A. V., Shlyagin, M. G., Marakhonov, V. I., Krasin'kova, M. V., ZHURNAL TEKHNICHESKOY FIZIKI, Vol 51, 1981, p 1422.

5. Bryksin, V. V., Korovin, L. I., Petrov, M. P., Khomenko, A. V., FIZIKA TVERDOGO TELA, Vol 24, No 1, 1982.

6610
CSO: 1862/162

UDC 537.533.001

USING OPTICAL DATA PROCESSING

Moscow OPTICHESKAYA I OPTOELEKTRONNAYA OBRABOTKA INFORMATSII in Russian 1976 (signed to press 30 Aug 76) pp 155-214

[Chapter 6 from book "Optical and Optoelectronic Data Processing", by Valeriy Konstantinovich Ablekov, Petr Ivanovich Zubkov and Aleksandr Viktorovich Frolov, Izdatel'stvo "Mashinostroyeniye", 6000 copies, 255 pages]

[Text] The field of optical data processing includes various methods of measuring and transmitting optical signals. The purpose of optical processing is to separate the signal from noise, to measure its individual parameters, to filter the spatial frequencies of the signal, and also to synthesize individual optical systems.

6.1. Optical Systems for Filtering and Isolating Signals Against a Noise Background

One of the important jobs of filtration is that of producing an optical system with transfer function H(u) = 1 [Ref. 64, 166]. Let us assume that there are n linear systems connected in series. The spectrum of the signal at the output of the last system is defined by the expression

$$F_{out}(u)=H_1(u)H_2(u)...H_n(u)F_{in}(u),$$

where $H_n(u)$ is the transfer function of the n-th system. Theoretically, we can create such a system in which

$$H_k(u)=1\Big/\prod_{1}^{k-1}\prod_{k+1}^{n}H_n(u). \qquad (6.1)$$

In this case, the overall transfer function is equal to 1. In practice, condition (6.1) cannot be satisfied since any optical system has a limited entrance pupil. If $\prod_{1}^{k-1}\prod_{k+1}^{n}H_n(u)$ has a series of zeros or approaches zero for high spatial frequencies, then transfer function $H_k(u)$ must have a large value for frequencies corresponding to these zeros. This cannot be done for passive filters. However, for a limited frequency band in a small region near the optical axis condition (6.1) can be satisfied.

The problem of determining the transfer function can be approached from another standpoint, viz. as a problem in reconstructing the initial function when it is transmitted by a discrete set of arbitrarily shaped pulses [Ref. 66]. Let us isolate a function f(x) that is limited with respect to spectrum ($-u_0$, $+u_0$) from a sequence of equidistant pulses (Fig. 6.1):

$$f_1(x)=\sum_{n=-\infty}^{\infty} f(x)\delta(x-nx_0),$$

where the readout interval is $x_0 \leqslant \pi/u_0$.

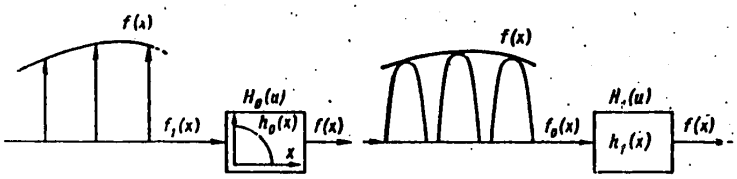

Fig. 6.1. On determining the ideal optical system

If $F_1(u) = \Phi\{f_1(x)\}$, then

$$F_1(u)=\sum_{n=-\infty}^{n=+\infty} f(nx_0)\,e^{-inx_0u}=\sum_{n=-\infty}^{n=\infty} F\left(u+\frac{2\pi n}{x_0}\right)=\sum_{n=-\infty}^{n=\infty} F(u+2u_0n).$$

Passing such a signal through a filter with transfer function

$$H(u)=\begin{cases}1, & |u|\leqslant u_0\\ 0, & |u|>u_0,\end{cases} \qquad (6.2)$$

we get a signal at the output in the form of the Fourier spectrum $F_1(u)H(u) = F(u)$ of initial function f(x).

Now let us assume that to reconstruct the distribution of f(x), rather than taking the sequence of pulses $f_1(x)$, we use the signal

$$f_0(x)=\sum_{n=-\infty}^{\infty} f(x)h_0(x_0-nx_0),$$

where $h_0(x)$ is an arbitrary function selected from considerations of simplicity in obtaining it. Obviously $f_0(x)$ can be treated as the output signal of a hypothetical filter with input signal $f_0(x)$ and response function $h_0(x)$. If

$$H(u)=H_0(u)H_1(u) \qquad (6.3)$$

is a function defined by expression (6.2), then the system will be ideal. This method appreciably improves optical imaging systems.

Another important job of filtration is signal detection against a noise background. If the useful signal at the input to the system is f(x), and noise or interference is n(x), then to maximize the signal/noise power ratio, the

transfer function of the optimum system is [Ref. 19, 184]

$$H_{opt}(u) \sim \frac{F^*(u)}{N(u)}, \qquad (6.4)$$

where N(u) is the noise spectrum.

For the case of white noise, where the spectrum is constant, the resultant expression takes the form $H_{opt} = F^*(u)$.

Thus for the simplest cases the system is a matched or complex-conjugate filter.

The matched filtration technique also enables solution of the pattern recognition problem. Let a signal $f = f_1 + f_2 + f_3 + \ldots + f_n$ go to the input of a system, and let the system perform the operation of matched filtration. We pass the signal simultaneously or sequentially through n filters with transfer functions $H_1^*(u)$, $H_2^*(u)$,..., $H_n^*(u)$.

The corresponding response functions of these filters are normalized relative to the energy contained in each component of the input signal. Under this condition, the signal at the output of the system is maximum for the channel where the corresponding component is filtered by its own matched filter. The intensity for the k-th component is defined as

$$I_k = \frac{\left|\int_{-\infty}^{\infty} |H_k|^2\, du\right|^2}{\int_{-\infty}^{\infty} |H_k|^2 du} = \int_{-\infty}^{\infty} |H_k|^2\, du.$$

For all other signals the intensity is

$$I_n = \frac{\left|\int_{-\infty}^{\infty} H_k F_n^*\, du\right|^2}{\int_{-\infty}^{\infty} |F_n|^2 du}, \quad n \neq k.$$

Using the Schwarz inequality, we get

$$\left|\int_{-\infty}^{\infty} H_k F_n^*\, du\right|^2 \leqslant \int_{-\infty}^{\infty} |H_k|^2\, du \int_{-\infty}^{\infty} |F_n|^2 du.$$

which implies that $I_n \leqslant \int_{-\infty}^{\infty} |H_k|^2\, du = I_k$.

If the signals are different in scale, we can write $I_n = CI_k$, where $C < 1$, i. e. slight differences in scale lead only to a reduction of signal intensity. Thus matched filters can be used to detect any signal of a set that is known beforehand.

Optical filtration of a signal is most easily accomplished in coherent systems of sequential Fourier transformation (Fig. 6.2).

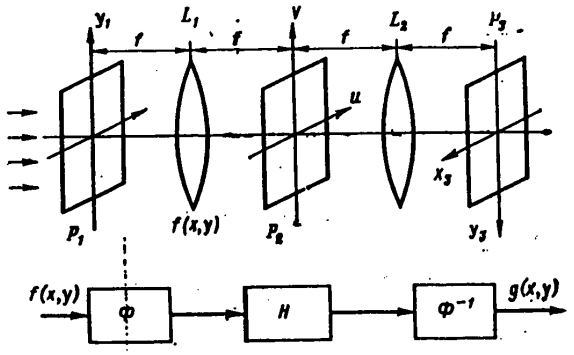

Fig. 6.2. Diagram of optical filtration

Having the spectrum of spatial frequencies of input signal f(x, y) in plane P_2, we acquire the capability of changing the amplitude and phase of each component F(u, v) individually, i. e. we can perform the operation of filtration. Let us assume that a transparency is placed in plane P_2 with complex amplitude of transmission $H(u, v) = \Phi\{h(x, y)\}$. Field distribution immediately behind the transparency is $U_+(u, v) = F(u\ v)H(u, v)$. As a result of secondary Fourier transformation by lens L_2, we get signal g(x, y) in plane P_3, which is equal to

$$g(x, y) = C\int\limits_{-\infty}^{\infty} F(u, v) H(u, v) e^{-i(ux+vy)} du dv =$$

$$= -\int\limits_{-\infty}^{\infty} f(\xi, \eta) h(x-\xi, y-\eta) d\xi d\eta.$$

Thus a correlation signal is observed at the output.

In an analogous way we can perform the operation of filtration in all other systems of optical convolution. For example, for imaging systems with incoherent illumination that are linear relative to the input signal intensity, the operation of filtration is performed by placing the filter in the plane of the exit pupil since intensity distribution in this plane and the distribution in the image plane are related by a Fourier transform. Such a method (apodization) is used to reduce aberrations and for a posteriori correction of a photographic image [Ref. 57, 154].

Limitation of the spatial frequency band takes place in optical systems. For example in the arrangement represented in Fig. 6.2 the pupil of lens L_1 is such a limitation. The range of frequencies transmitted is increased if transparency f(x, y) is placed immediately in front of lens L_1. In this case, a quadratic phase coefficient will appear in the formula for Fourier transformation of the input signal. As a rule, this coefficient has no appreciable effect on the course of filtration. It should be recalled that the ratio between the product of Fourier transforms and the convolution formula is real only for spatially invariant systems. This fact imposes a condition of input

and observation of the signal in isoplanatic regions (paraxial region). Since we have explained the influence of these factors previously, we will assume for the sake of simplicity that the system is free of aberrations, spatially invariant and transmits all frequencies characterizing the input signal. As has already been pointed out, there are two mathematically equivalent approaches for analyzing optical systems. This fact dictates two methods as well for synthesizing the required filters.

For synthesis in the frequency region, a filter with a certain transfer characteristic H(u, v) is introduced in the Fourier transform plane of the signal, and acts directly on its spectral makeup. For synthesis in the spatial region, a filter with response function h(x, y) (reference mask) is placed in the image plane and changes the signal at the input to the system. Both methods give the same result; however, the display of the output signal is different. In the case of transformations in the frequency region, the resultant signal is detected in the form of intensity distribution in the plane of observation. For transformation in the spatial region, the signal manifests itself in a single point.

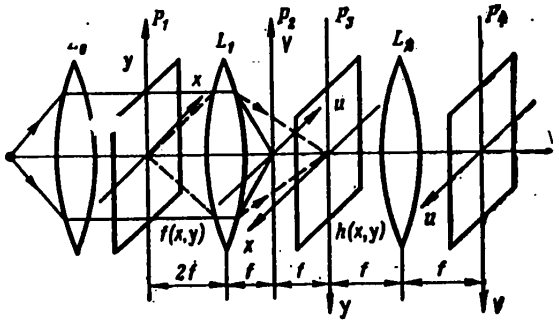

Fig. 6.3. Diagram of optical filtration in spatial region

Fig. 6.3 depicts an optical system using filtration in the spatial region.

A plane monochromatic wave from a point source illuminates the transparency with function of transmission f(x, y) located in plane P_1. Lens L_1 forms an image of the transparency in plane P_3 while forming spectrum F(u, v) simultaneously in plane P_2. Reference filter mask h(x, y) is located in plane P_3. Thanks to signal transformation by lens L_2, field distribution corresponding to the Fourier transform of the product f(x, y)h(x, y) is observed in plane P_4. If the transparency at the input is shifted in the x and y directions, the signal at the output of the system takes the form

$$g(u, v, x, y)=C\int_{-\infty}^{\infty} f(x-\xi, y-\eta)\,h(\xi, \eta)\,e^{-i(u\xi+v\eta)}d\xi d\eta.$$

Thus, in order to get the transformation of convolution, it is necessary to have u = v = 0. In this case

$$g(x, y)=C\int_{-\infty}^{\infty} f(x-\xi, y-\eta)\,h(\xi, \eta)\,d\xi d\eta.$$

The technique of spatial transformations requires the operation of scanning, which is not needed for the technique of filtration in the frequency region. In most cases, the filter introduced into the optical system is recorded on photographic film as some transmission function. In the frequency region the filter transmission function has the form $H(u, v) = |H(u, v)|e^{i\phi(u,v)}$. Spatial filters are usually passive elements, and consequently $|H(u, v)| \leq 1$, i. e. the possible values of complex filters are in the limits of a unit circle with center at the coordinate origin of the complex plane (Fig. 6.4).

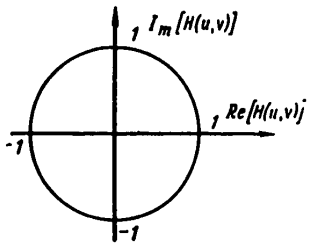

Fig. 6.4. On defining the parameters of a spatial filter

Let us now go on to examine some problems of synthesizing spatial filters. The simplest optical filter is a binary filter that has values equal to zero or unity. Such filters are simple to make as they are merely different limiting diaphragms. Despite the relative simplicity, They are used to handle some important jobs in optical filtration. Abbe was one of the first to describe the use of binary filters for filtering the spectral components of an optical image in his theory of image formation in the microscope [Ref. 96].

If an object of the grating type is placed in plane P_1 (see [Fig.] 6.2), the distribution of the spectrum in the rear focal plane of lens L_1 is a set of functions $\sin u/u$ localized in the vicinity of points corresponding to the principal spatial frequency of the grating and its multiple harmonics. Besides, a focused signal of the reference beam will be observed. By placing different binary filters in plane P_2 (holes, slits, limiting diaphragms) we can get different images at the output of the system. For example if we introduce a limiting diaphragm so that spatial harmonics u are transmitted, the image of a one-dimensional grating with rectangular line shape is transformed to a sine-wave grating with doubled spatial frequency [Ref. 166, 187].

Binary filters are used to increase the contrast of an ordinary photograph with partial or complete suppression of the spectral component of zero frequency. To do this, an opaque or partly transparent circle of definite size is placed on the axis in plane P_2 [Ref. 166, 187].

Binary filters have found extensive use for visualizing phase inhomogeneities in shadow methods [Ref. 20].

Binary filters are also used to solve the problem of optimum filtration in isolating a periodic signal against a noise background. It is known from communication theory that an ideal method for isolating a periodic signal in the presence of noise is formation of the function of cross-correlation of the input signal with a function that is a series of δ-functions with interval in space corresponding to the fundamental frequency of the signal. The optical equivalent of construction of the cross-correlation function is insertion of an opaque mask in spectral plane P_2 (see Fig. 6.2) with apertures

that filter the spectral orders of the periodic input signal. The transfer characteristic of such a filter is

$$H(u)=\sum_m \delta(u-mu_x).$$

Let the signal f(x) at the input be equal to the sum of the useful periodic signal $f_1(x)$ [and] noise n(x)

$$f(x)=f_1(x)+n(x),$$

where $f_1(x)=\sum_m Ce^{imu_x x}$.

As a result of filtration and double Fourier transformation, we get a distribution at the output equal to

$$g(x)=C_1\left[f(x)*\sum_m \delta(x-mx_0)\right],$$

where x_0 is the spatial period of the useful signal. Obviously the function of cross-correlation of the periodic signal with the sum of δ-functions of the same period is the sought signal except for a constant coefficient. The convolution of the function that describes the noise with the sum of δ-functions is equal to a constant quantity that is related to the average value of the spectrum of noise power. Consequently, the distribution of intensity at the output is

$$I(x)=|C_1 f_1(x)+C_2|^2.$$

Binary filters are used for optimum filtration of optical signals that have a sufficiently uniform spectrum. In this case, the filtration process is done with some approximation since complex filters are necessary in the general case. However, the problem is simplified by the fact that the binary filter can be calculated on a computer. Let the Fourier transform $A(u)e^{i\phi(u)}$ of the sought signal $f(x)=a(x)e^{i\phi(x)}$ be known. The approximate matched filter for such a signal has the transfer characteristic [Ref. 150]

$$H(u)=\frac{1}{2}+\frac{1}{2}\,\frac{A(u)\cos[au+\varphi(u)]}{|A(u)\cos[au+\varphi(u)]|}=\sum_{m=0}^{\infty} C(0,m)\cos[mau+m\varphi(u)],$$

where $C(0,m)=\dfrac{\Sigma_m}{2\Gamma\left(1-\frac{m}{2}\right)\Gamma\left(1+\frac{m}{2}\right)}$

$$\Sigma_m=\begin{cases}1, & m=0\\ 2, & m=1,2\ldots;\end{cases}$$

$\Gamma\left(1-\frac{m}{2}\right)$, $\Gamma\left(1+\frac{m}{2}\right)$ are gamma functions; α is the frequency of the spatial carrier.

Substituting the values of coefficients, we get

$$H(u)=\frac{1}{2}+\sum_{m=1,2,5}^{\infty}\frac{2(-1)^{(m-1)/2}}{m\pi}\cos[mau+m\varphi(u)]. \qquad (6.5)$$

If the filter is installed in the optical system shown in Fig. 6.2, we have a series of images at the output that are localized in orders of the spectrum. Under condition $\alpha \geqslant 2b$ (2b is the maximum linear dimension of the input signal), the m-image is shifted relative to the axis by distance $\geqslant 2mb$, and consequently the resultant images do not overlap and do not interfere. Let us rewrite expression (6.5) in the form

$$H(u)=\sum_{m=0,\pm 1,\pm 3} \frac{C(0,|m|)}{\Sigma_m} e^{i m|\omega+\varphi(u)|}.$$

From this we see that for a signal with spectrum $A(u)e^{i\phi(u)}$, the filter is phase-matched at m = -1. A pulse code signal is detected by such a filter.

The next class of filters are amplitude and phase filters with transfer characteristics that can take on any values between 0 and 1 on the real axis (see Fig. 6.4). These filters are usually recorded on photographic emulsions, the transmission function of the processed film also varying in a range of 0 to 1. Amplitude filters are quite useful for detecting or isolating a signal in the presence of noises with respect to the criterion of mean square error. This criterion postulates the minimum value of ε [Ref. 93]:

$$\varepsilon=\left|f(x, y)-\int_{-\infty}^{\infty} f(\xi, \eta) h(x-\xi, y-\eta)\, d\xi d\eta\right|^2.$$

Let us assume that signal f(x, y) with known autocorrelation function $R_f(x, y)$ is distorted by noise n(x, y) whose autocorrelation function $R_n(x, y)$ is also known. To carry out the operation of optimum filtration with respect to the criterion of the least mean square error, it is necessary that the transfer function of the filter have the form

$$H(u, v)=\frac{S_f(u, v)}{S_f(u, v)+S_n(u, v)},$$

where $S_f(u, v)$ and $S_n(u, v)$ are spectral densities of signal and noise

$$S_{f,n}(u, v)=\int_{-\infty}^{\infty} R_{f,n}(x, y) e^{-i(ux+vy)} dx\, dy.$$

Here H(u, v) is a real positive function, and therefore an amplitude filter can be used.

Amplitude filters are also used instead of binary filters if the presence of an abrupt transition at a boundary leads to undesirable interference effects.

The effect of phase spatial filtration consists in delaying individual spatial components without changing their amplitude. Phase filters take on a value between -i and +i on the imaginary axis of the complex plane. Such filters are made by applying a thin film on a plane-parallel plate, or in the form of specially shaped glass plates (cylindrical, conical lenses and so on). Phase filters have found wide application in phase-contrast microscopy [Ref. 3]

and for processing radar information [Ref. 119]. For example, a reflected radar signal obtained by a synthesized grating is recorded as a one-dimensional Fresnel diffraction structure (one-dimensional zone plate) with focus that depends on range coordinate. The corresponding range-matched filter for each channel is a combination of lenses. The filter includes conical lenses for compensating the change in focus and a set of cylindrical-spherical lenses for Fourier transformation of the signal with respect to azimuth, and construction of an image from the range coordinate. The effectiveness of such processing lies in the nature of the light signal and the matched filters that transmit light almost without losses.

Combined use of amplitude and phase filters enables image correction. Amplitude-phase control is realized directly on the entrance pupil of the optical system. This method is like apodization in that it utilizes control at the input (or output) of the system and incoherent lighting. The thing that essentially distinguishes it from apodization is correction in phase and amplitude. Amplitude and phase filters are also used for filtration in the frequency region (double diffraction method) with the system shown on Fig. 6.2.

If wavefront distortions on the exit pupil in the imaging system are equal to $W(\rho)$, the compensation filter mask installed on the pupil must have transmission function $H(\rho) = e^{-ikW(\rho)}$.

Obviously such a filter is complicated to make. Therefore most frequently a mask is made with transmission function

$$H(\rho) = \frac{1}{1+C}\{C + \cos[kW(\rho) + \delta]\},$$

where C is a parameter associated with the aberrations introduced by the system; δ is the coefficient of reduction of aberrations. If $C > 1$, the mask simply attenuates radiation. If $C < 1$, amplitude and phase filtration are accomplished with change in phase [by] 0 or π. For the case $C = 0$ we get the most favorable conditions.

The next important stage in development of the technique of optical data processing was the use of filters realized on the basis of methods of holography. The principle of optical filtration in combination with holography enables registration and processing of a wide class of complex optical signals.

Let us consider the procedure of realizing a filter for optimum isolation of a known signal against a noise background. The transmission function of the filter is described by expression (6.4). The denominator of $H_{opt}(u)$ is a positive function and is realized by conventional methods of photography. The function $F^*(u)$ in the general case is complex, and the technique of holography is used for recording it. Optical arrangements for formation of $F^*(u)$ are given on Fig. 6.5 [Ref. 188, 189]. They are modified versions of systems for recording Fourier holograms. The resultant function takes the form

$$T(u) = |U_0(u)|^2 + |F(u)|^2 \mp 2|U_0(u)||F(u)|\cos\varphi(u) - \theta(u)|,$$

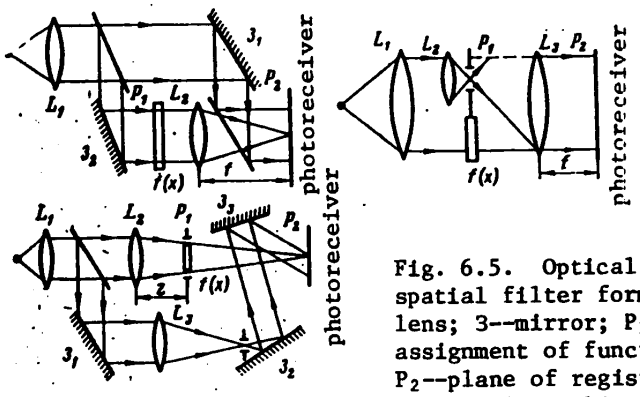

Fig. 6.5. Optical schemes of spatial filter formation: L--lens; 3--mirror; P_1--plane of assignment of function f(x); P_2--plane of registration of holographic filter

where $U_0(u) = |U_0(u)| \exp i\phi(u)$ is the field distribution in the reference beam; $F(u) = |F(u)|e^{i\theta(u)}$ is the spectrum of the sought signal. We can get the necessary value of F*(u) by varying the value of $|U_0(u)|$ and $\phi(u)$. By combining the resultant hologram with a positive that has transmission 1/N(u), we construct the filter

$$\frac{T(u)}{N(u)} = \frac{|U_0(u)|^2 + |F(u)|^2}{N(u)} + \frac{U_0^* F}{N} + \frac{U_0 F^*}{N}.$$

If $|U_0(u)| = C$ and $\varphi(u) = bu$, then

$$\frac{T(u)}{N(u)} = A(u) + H_1^*(u)\, e^{-ibu} + H_1 e^{+ibu},$$

where $A(u) = \frac{|U_0(u)|^2 + |F(u)|^2}{N(u)}$; $H(u) = \frac{CF^*(u)}{N(u)}$;

C and b are constant coefficients. The third term of this expression corresponds to the transfer function of the sought filter. The filter is set in plane P_2 of the coherent optical system (see Fig. 6.2), the signal to be analyzed being formed at the input of this system (plane P_1). In observation plane P_3 the field distribution g(x) is equal to the Fourier transform of the product of spectrum $F_1(u)$ of input signal $f_1(x)$ and the filter T(u)/N(u), i. e.

$$g(x) = \frac{1}{2\pi}\int_{-\infty}^{\infty} F_1(u) A(u) e^{iux} + \frac{1}{2\pi}\int_{-\infty}^{\infty} F_1(u) H_1^*(u) e^{i[(x-b)u} du +$$

$$+ \frac{1}{2\pi}\int_{-\infty}^{\infty} F_1(u) H_1(u) e^{i(x-b)u} du. \qquad (6.6)$$

The first term of expression (6.6) characterizes distribution localized near the optical axis of the system, and in the given analysis is of no interest. The second term characterizes the filtered signal, the field distribution being localized near a point that is displaced relative to the optical axis by an amount x = b. It will have the maximum value when the spectra $F_1(u)$ and

F(u) coincide. The field distribution characterized by the third term will be shifted relative to the axis by an amount x = -b. With appropriate selection of the values of b, all three patterns are separated in space relative to one another. In the simplest case of steady-state white noise N(u) = const we observe the function of cross-correlation and the function of convolution of the useful input signal with the signal recorded on the filter simultaneously in plane P_3:

$$\int_{-\infty}^{\infty} f_1(\xi) f^*(x+b+\xi)\,d\xi = [f_1(x+b) \ast f^*(x+b)]; \qquad (6.7)$$

$$\int_{-\infty}^{\infty} f_1(\xi) f(x-b-\xi)\,d\xi = [f_1(x-b) \ast f(x-b)]. \qquad (6.8)$$

If $f_1(x)$ contains a series of signals that are separated in space, then the maximum value is observed for the signal that is determined by the autocorrelation part of expression (6.7). In this way the problem of recognition and detection of the sought object is solved. When several filters are recorded on the same light-sensitive medium, several signals can be recognized simultaneously without using the operation of mechanical scanning or change of filters [Ref. 87].

Note should be taken of some peculiarities inherent in the given method. Translational displacement of the input signal leads to the same displacement of the signal of convolution or correlation in the observation plane. A change in scale of the signal without altering overall intensity leads to signal attenuation. In an analogous way, filtration is sensitive to rotations of the initial signal. The permissible displacements and rotations of filters depend to a considerable extent on the nature of the sought signal [Ref. 190]. Most often, the problem of optimum filter placement is resolved by changing the scale and angular orientation to maximize the signal at the output of the system. Unfortunately, such an operation consumes considerable time.

The given method has been used to recognize a known shape or part of a text against a background of a complicated transparency [Ref. 187]. It has been suggested that the method can be used with appropriate updating for high-speed recognition (reading) of printed symbols [Ref. 124, 131].

An interesting possibility has opened up with the use of matched optical filtration for correcting the direction of flight of an aircraft [Ref. 191]. In this technique, the signal coming from the radar screen of an aircraft flying at a certain altitude (radar map of the region) is compared with the signal recorded on a hologram filter (marker inside the given territory). The same method has been used for recognition of markers in spaceflight [Ref. 142]. An advantage of the method is simplicity of recognition. It is only required that the object to be recognized fall within the field of view of a telescope carried on the spacecraft.

The input optical image can be made in the form of an ordinary transparency that provides amplitude modulation of the radiation passing through it. An optoelectronic holographic device can be used in the same way with deformation of a reflecting surface, which enables phase modulation of the incident light.

The experiment used photographs taken on missions of the Gemini-4 and Gemini-5 spacecraft. The setup of the experiment was similar to that diagrammed on Fig. 6.2. The light source was a helium-neon laser.

Landmarks were recognized in eight regions characterized by different dimensions and terrain from photographs of the northeastern part of the Arabian Desert. In every case, recognition was successful. The signal/noise ratio was in a range of 100-250. It was established that high contrast of objects is not a mandatory requirement for reliable recognition.

Recognition of individual valleys and even sections of desert was completely satisfactory.

Recognition was possible even with photographs of poor quality. It was successful even when drawings and maps were used for making the spatial filters. It was established that recognition of an object is possible even with cloud cover of 90% of its surface area. This effect can be attributed to the fact that the intensity of luminescence of points in the plane of recognition depends nonlinearly on the area of the given object.

The dimensions of the optical image and the spatial filter may differ by 15% without destroying reliability of recognition. There are methods that can ensure recognition even if the dimensions of the corresponding images differ by a factor of ten. The same methods can be used for determining such navigational parameters as altitude and slant range. Spatial filters have been used for recognizing stellar objects, which are ideally suited for this purpose. In this case, the signal/noise ratio reached 400.

To guarantee a predetermined error, the focal length must be increased with increasing distance of the vehicle above the surface of the planet. For the described system, the error did not exceed 10^{-4}. A source of error is the limited resolution of the vidicon; the magnitude depends directly on the dimensions of the field of view of the telescope, and can be reduced by a corresponding increase in focal length. In the case of flight at an altitude of 160 km, the focal length can be taken as equal to 15.2 cm. Then the angle of view of the telescope is 6°, and the magnitude of the error in measuring the position of a landmark does not exceed 15 m. At higher altitudes, the same precision can be achieved by increasing the focal length.

Methods of optical filtration and holography are used to solve the problem of posterior correction of photographic images, which in principle is analogous to construction of an ideal linear system [Ref. 166]. To do this, it is necessary to know the scattering function of the forming system in the presence of distortions. It has been possible in practical cases to improve the images of objects such that each point has undergone aberrations that are the same in the statistical sense. This means that the distortions should not disrupt the spatial invariance of the forming system. From the expression characterizing the structure of the image on the photographic plate as recorded in the spatial region,

$$g(x) = I(x) * |h(x)|^2 \qquad (6.9)$$

and the corresponding expression for the frequency region

$$G(\mu)=I(u)L(u), \qquad (6.10)$$

where

$$L(u)=\Phi\{|h(x)|^2\},$$

we see that to isolate the sought image it is necessary to have a matched filter with transmission function $T=L^*/|L|^2$, since $GT=I$. Here $I(x)$ is the distribution of intensity of the undistorted image; $|h(x)|^2$ is the scattering function of the shaping system. The component L^* of the filter is made by recording the spectrum of a point source (positive) obtained in a system with aberrations on a Fourier hologram. Component $|L|^2$ is formed by recording the power spectrum of this image on a photographic plate placed in the focal plane of the corresponding lens. By installing filter T in plane P_2 (see Fig. 6.2), and the positive to be corrected in plane P_2, we get an improved image in one of the diffraction orders in plane P_3. It should be emphasized that the given method corrects images only within the limits of those spatial frequencies that have passed through the system. Thus at the output one observes a signal of the form

$$g_1(x)=I(x)\ast|h_1(x)|^2, \qquad (6.11)$$

where $|h_1(x)|^2$ is the scattering function (intensity-response function) of the corrected system. The difference between a system with transfer function $L_1(u)=\Phi\{|h_1(x)|^2\}$ and a system with transfer function $L(u)=\Phi\{|h(x)|^2\}$ consists in the fact that in the latter system the spatial frequencies are shifted in phase and have lower amplitude than those of system $L_1(u)$. The existence of a finite number of zeros in function $L(u)$ has no significant influence on the effect of filtration.

If the photographic image has been obtained in the presence of a steady-state turbulent medium and the exposure time is much greater than the time of fluctuations, the photographic emulsion fixes the average intensity distribution [Ref. 166]:

$$\langle g(x)\rangle=I(x)\ast\langle|h_1(x)|^2\rangle.$$

The scattering function of the system, assuming quasimonochromatic illumination, is written as

$$\langle|h_1(x)|^2\rangle=\langle\gamma(x)\rangle|h_0(x)|^2,$$

where $\langle\gamma\rangle$ is the averaged function of mutual intensity in the plane of the entrance pupil of the forming system as determined by the point source in the object plane; $h_0(x)$ is the response function of the forming system. In the frequency region we have

$$\langle G(u)\rangle=I(u)\langle\Gamma(u)\rangle|H(u)|^2$$

or, assuming that all spatial frequencies characterizing the object are recorded,

$$\langle G(u)\rangle = I(u)\langle \Gamma(u)\rangle.$$

It is clear from this that to realize the operation of matched filtration we must have a filter of the form

$$T(u)=C/\langle \Gamma(u)\rangle.$$

In the general case, its realization necessitates the use of holograms; however, for most cases, such as inhomogeneous steady-state media, $\gamma(x)$ is a real and even function. Consequently, conventional photography can be used for recording $\langle\Gamma(u)\rangle$.

The effectiveness of this method has been experimentally studied [Ref. 162]. A turbulent steady-state medium was modeled by heating air in the region situaced between the object and the shaping lens. The image of the object, and also an image of a point source located in the center of the object plane were fixed on photographic emulsion. The matched filter was made by photographing the spatial spectrum of the image of the point source and processing the photographic emulsion with contrast coefficient equal to unity. The image was corrected in the system diagrammed in Fig. 6.2. The experiments showed that the quality of the photographic images is considerably improved if the blurred scattering function is gaussian.

The idea of posterior correction of images was further developed in Ref. 178. Let the blurred image of an object be defined by expression (6.11). If signal $g(x)$ passes through a system with response function $h_1^*(x)$, where

$$|h_1(x)|^2 \ast h_1^*(x)=\int_{-\infty}^{\infty}|h(\xi)|^2 h^*(x+\xi)\,d\xi=\delta(x), \qquad (6.12)$$

then we get a deblurred image characterized by function $I(x)$. Condition (6.12) for the frequency region is written as $LH_1^* = 1$.

Realization of the proposed method is optically accomplished by two techniques. In the first case, the function $g(x)$ is recorded on a Fourier hologram. As a result, we get a transparency with transmission function

$$(u)=1+|G|^2+G+G^*=1+|G|^2+IL+I^*L^*. \qquad (6.13)$$

Placing this hologram in the original position and illuminating it with wave H_1, we isolate the field distribution characterized by the last term of equation (6.13): $I^*L^*H_1 = I^*$.

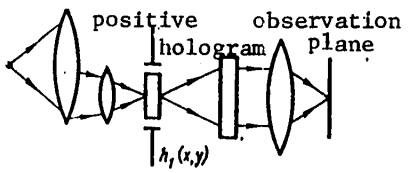

Fig. 6.6. Diagram of image deblurring using a positive

As a result, an improved image is reconstructed (Fig. 6.6). Wave $H_1(u)$ is formed by illuminating the (positive of) image of the function $h_1(x)$ placed at the location of the point source.

In the second case, a Fourier hologram of the image is recorded with an extended reference source $h_1(x)$. The transmission function of the holograms is

$$T(u)=(O+H_1)(O+H_1)^*=|O|^2+|H_1|^2+ILH_1^*+I^*L^*H_1.$$

If LH* = 1, the corrected image is formed in a beam of light characterized by the term ILH* = 1.

For this purpose, the resultant hologram is placed in the original position and illuminated by a wave from a point source situated in the location of the extended source $h_1(x)$ (Fig. 6.7).

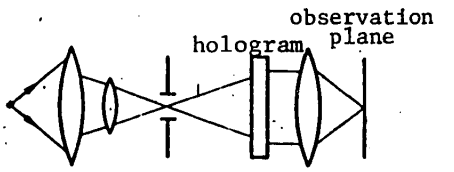

Fig. 6.7. Diagram of reconstructing deblurred image from a hologram

The given technique has been used to reconstruct lensless Fourier holograms, which were produced by using an extended object in the form of a frosted plate and a set of point sources (a two-dimensional grating of 9000 point diaphragms [Ref. 179]). Reconstruction was done by the arrangement diagrammed in Fig. 6.7 using the same reference sources. Since condition (6.12) was satisfied by using extended reference sources of the indicated type, an image of good quality was observed. The experiments showed that the setup is quite critical to exact placement of the $h_1(x)$ transparency. With a mismatch of ~8 μm, the reconstructed image was completely suppressed by noises [Ref. 719].

It should be emphasized that the effectiveness of the proposed techniques for image deblurring depends in large measure on the accuracy of measuring the scattering function of the system. Only in the case where $|h_1(x)|^2$ is known and does not vary from experiment to experiment (steady-state system) can a matched filter be formed or the function $h_1(x)$ be selected. In principle, the scattering function is calculated on the basis of certain assumptions relative to the statistical characteristics of introduced distortions. However, such an approach has so far had little success in practice [Ref. 143].

The methods considered above have applied to classical methods of optical filtration. The technique of holography has only appreciably simplified the formation of optimum filters. The principles lying at the basis of holography have led to the development of new methods of optical filtration that had not existed before. Let us consider a relatively simple method of compensating phase distortions based on the property of holograms to reconstruct both a real image and a complex-conjugate virtual image [Ref. 21, 148, 153].

An inhomogeneous optically transparent medium is described by the spatial variation of the index of refraction n(z). For inhomogeneities with geometric dimensions much greater than a wavelength, the scalar equation of propagation

takes the form

$$\nabla^2 u + k^2 n^2(z) u = 0, \qquad (6.14)$$

where $k = 2\pi/\lambda$, u is complex field amplitude. For waves propagating at a small angle to the z-axis, the solution of equation (6.14) is written as

$$u = f(z) e^{-i\beta z}. \qquad (6.15)$$

Here f(z) is a slowly varying function, β = const. The families of rays characterized by solution (6.15) and by the complex-conjugate solution have the same optical path, but propagate in opposite directions. Therefore if a wave front that has been scattered and distorted by the inhomogeneous medium is fixed on the hologram, and then during reconstruction a complex-conjugate wave front is passed through a system that introduces the same distortions, the phase aberrations of the wave front are compensated.

This property is extensively used for eliminating lens aberrations [Ref. 182], and for suppressing noise in interference studies [Ref. 132].

Investigations have been made of the effectiveness of using this method to compensate atmospheric distortions [Ref. 109].

An optical diagram of the facility is shown on Fig. 6.8. The reference beam was formed by objective lens O and collimator C, and directed by mirror M_2 to hologram Г. The working beam bassed through beam splitters B_1 and B_2, through a glass plate with thickness of 2 cm with inhomogeneous air pockets, and was incident on target T. A flat mirror was used as the target. Part of the radiation reflected by the target passed a second time through the distorting medium and beam splitter B_3 and was incident on hologram Г. In this way, the actual conditions of observation of objects through the atmosphere were simulated for illumination by a coherent light wave scattered by inhomogeneities. On the reconstruction stage, the hologram was illuminated by the wave reflected by mirror M_1. The complex-conjugate image of the distorting medium was projected in plate D. As a result, phase aberrations were compensated, and an image of the target illuminated by the scattered light wave was observed. To bring the directions of propagation of the working and reconstructing beams into register, a cyclic interferometer was used (the Hari-Haran interferometer [Ref. 127]). Alignment accuracy was checked by the interference pattern in plane F.

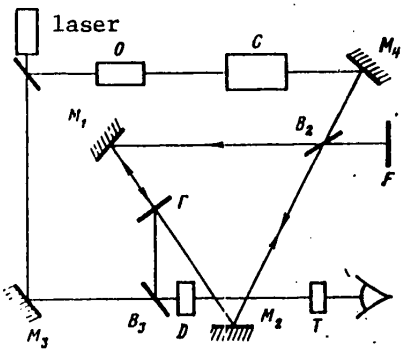

Fig. 6.8. Diagram of experimental setup for studying the method of compensating atmospheric distortions: O--objective lens; C--collimator; M--mirror; B--beam splitter; D--inhomogeneous glass plate; T--target; Г--hologram; F--plane of interference pattern observation

An advantage of this method is that it is not necessary to precalculate or measure the distortions that are introduced -- compensation for them is realized automatically. Among its disadvantages are the necessity of bringing the directions of propagation of the reference and reconstructing beams into exact registration, and also the need for good collimation. The slightest deviation from these conditions negates the effect of interference suppression. Let us also point out that practical implementation of the given scheme necessitates fast-acting light-sensitive media. The entire procedure of recording and reconstruction must be carried out in a shorter time than the characteristic period of oscillation of fluctuations.

To distinguish an optical signal against a background of steady-state noise, the technique of subtraction of optical signals has been suggested [Ref. 133, 105]. The operation of subtraction is accomplished by means of interference between the reconstructed signal recorded on the hologram and the signal arriving at the input of the system.

Let there be a hologram with transmission function

$$t(x)=C+\gamma T u^2(x)+\gamma T u_0 u(x)\left[e^{i[kax-\varphi(x)]}+\bar{e}^{i[kax-\varphi(x)]}\right], \quad (6.16$$

on which signal u(x) is recorded. Here T is exposure time; γ is the coefficient of contrast; u_0 is the field of the reference wave. By reconstructing the hologram with wave $u_0' e^{ik\alpha x}$, and simultaneously illuminating it with wave $ue^{i\phi(x)}$, we observe in one of the diffraction orders distributions of the field of form

$$\left[Cu'(x)+\gamma T u'(x)\,u^2(x)\right]e^{i\varphi(x)}-\gamma T u_0' u(x)\,e^{i[\varphi(x)+\varepsilon]}. \quad (6.17)$$

Considering

$$\gamma=-C/Tu^2,$$

we find from (6.17) that complete suppression of the signal in the given diffraction order requires satisfaction of the condition

$$\frac{u_0'}{u'(x)}=\frac{u_0}{u(x)}-\frac{u(x)}{u_0},$$

and since usually $u_0^2 >> [u(x)]_{max}$, it is sufficient that $u_0'/u'(x) \cong u_0/u(x)$.

Thus if there are two optical signals with certain differences in a small region of space, we can distinguish their difference, e. g. the image of an object or part of it included in this region.

This method was used for analyzing ordinary photographic images in Ref. 105. Holograms of different types were taken from a positive image (Fresnel, Fourier and focused-image holograms). After processing, they were placed in the original position in the corresponding optical system, and were then exposed with a reference wave and with a wave that had been diffracted by a transparency installed at the input of the system. Appearing in the plane of observation was an image of the part of the transparency recorded on the hologram.

Just as the preceding methods, this technique requires exact placement of the filter hologram in the proper position, and location of the intensity in the linear region of the characteristic curve of the light-sensitive media.

One of the effective ways to deal with random interference is signal averaging. In this case, the repeated addition of the regular useful signal intensifies it, and at the same time the random sign-alternating random signal is attenuated and suppressed.

It has been suggested that the averaging procedure be done by recording a definite number of uncorrelated realizations of the wave front and adding them on the reconstruction phase [Ref. 34]. To do this, the holograms are transilluminated sequentially so that the k-th wave front corresponding to the real image is the reconstructing wave for the (k+1)-th hologram. As a result of such a process and isolation of the component with the summary phase, we form a field distribution

$$u_{\Sigma_k} = u_0^n e^{i\sum_{k=1}^{n}\varphi_k(x)},$$

where u_0 is the field distribution in the plane of the hologram in the absence of a distorting medium; $\phi_k(x)$ is the phase distortion distribution function.

Using a calculator, we extract the n-th root and get the value of the field averaged with respect to n realizations

$$\langle u\rangle = u_0 e^{i\frac{1}{n}\sum_{k=1}^{n}\varphi_k(x)}.$$

The corresponding average value of intensity in the sought image under condition of isotropism of the random medium is determined by the correlation function of the entrance pupil of the system $K_p(x)$, the correlation function of field distribution without distortions $K_{u_0}(x)$ and the correlation function of distortions $K'_\phi(x)$:

$$\langle I(x)\rangle \; CK_{u_0}(x)K_p(x)K'_\varphi(x). \qquad (6.18)$$

For pure phase distortions distributed by normal law,

$$K'_{\varphi(x)} = e^{-\sigma^2/n} + \frac{K_{\varphi(x)}}{n}, \qquad (6.19)$$

where σ^2 is the dispersion of phase distribution function $\phi(x)$;

$$K_{\varphi(x)} = \varphi(x) \divideontimes \varphi^*(-x).$$

Expressions (6.18) and (6.19) imply that for sufficiently large n the influence of aberration can be considerably reduced. It has been shown by numerical calculation that distortions are practically totally suppressed by averaging 100 times [Ref. 37]. The averaging procedure can be modified if individual realizations of the wave front are accumulated on the stage of formation of the hologram. Technically, this is done by sequentially recording n exposures

on photographic emulsion or on a photoelectronic medium. Upon reconstruction of such a complex hologram, an image appears in the plane of observation with intensity determined by the average over the set of realizations of the wave front. For sufficiently large n, the fluctuations of intensity introduced by the inhomogeneous medium become insignificant [Ref. 27].

The given method of interference suppression has a serious disadvantage. This is due to the fact that it is necessary to record a certain number of statistically independent realizations of wave fronts. Practical implementation of such recording is complicated when observing moving objects through inhomogeneous media.

This flaw is eliminated by using a method proposed in Ref. 138. The hologram recording arrangement is shown in Fig. 6.9. The object is illuminated by a coherent light source (not shown on the diagram), and may be either two- or three-dimensional [Ref. 179]. Next to the object is a small reflector that forms a reference wave. If the reflector and object are sufficiently close together, the aberrations of the working and reference waves will be approximately equal. Distortions are compensated on the reconstruction stage as a result of interference of the rays in the plane of the photographic plate.

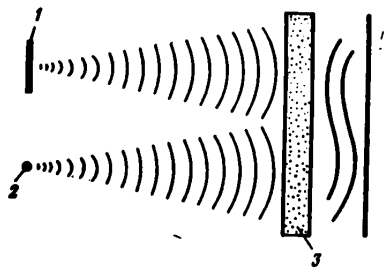

Fig. 6.9. Diagram of holography through a distorting medium: 1--object; 2--reference object; 3--distorting medium; 4--photographic plate

Let us evaluate the resolution of the reconstructed image. Let ϕ_0 be phase distortions in the reference beam, and let $\phi(x)$ be the phase distortions of the wave reflected by some point of the object. In reconstruction, the field distribution in the light beam that constructs the real image takes the form

$$uu_0^* \exp[i(\varphi - \varphi_0)], \qquad (6.20)$$

where u and u_0 are the field distributions on the hologram produced by a point of the object and by the point reference source. We can see from expression (6.20) that compensation of phase distortions takes place with satisfaction of the equality $\exp i\phi \cong \exp i\phi_0$, or according to the Rayleigh criterion, the condition $\phi - \phi_0 \leqslant \pi/2$.

This circumstance imposes a restriction on the dimensions of observable objects for a certain strength of perturbations.

Ref. 134 gives a detailed analysis of imaging of two-dimensional objects based on this method. Let us limit ourselves to consideration of media such that the logarithm of amplitude and phase fluctuations of the wave front incident on the entrance pupil can be considered a locally steady process describable by a Gauss statistic. Atmospheric fluctuations conform to such conditions [Ref. 126].

The long-exposure case is analyzed, where intensity on the hologram is averaged over all values of the random function that characterizes fluctuations of the atmosphere, and also the short-exposure case, where inhomogeneity of the atmosphere leads to shifting (blurring) of the diffraction pattern in the plane of the hologram, and intensity averaging takes place over the field of the set of reconstructed images.

It is found for a long exposure that the influence of the inhomogeneous medium boils down to a reduction in brightness of the reconstructed image with increasing distance between the object and the reference source. As long as the brightness of the reconstructed image exceeds the noise threshold of the detector, the sought object is observed with good resolution.

In the second case, there is a loss of resolution over the entire field of the image. If the distance between object and reference source is small, the reconstructed pattern contains the sought image with superimposed noise that depends only on the amplitude of variations of the incident wave front.

Experimental results on determining the possibilities of the method are given in Ref. 139. Lensless Fourier holograms were formed in the presence of atmospheric interference. A Q-switched ruby laser was used as the emission source. Beam divergence was ≅200 rad. An object was imaged that consisted of a set of reflecting plates fastened on a board. A corner reflector was mounted on the edge of the board to form the reference background. The scattered radiation was collected by a newtonian telescope system with mirror diameter of 1.2 m and focused on a photographic emulsion. The size of the holograms was ≅7.5 mm and the distance between the object and the reception part was 12 km. Distance between the axis of propagation of the beam and ground terrain ranged from 35 to 800 m. Quality of the reconstructed images depended considerably on the nature of atmospheric perturbations. In particular, under conditions of good visibility a hologram was obtained for mirror objects situated at a distance of 100 and 12 cm from the corner reflector. Resolution of the reconstructed images was ≅0.5', which was approximately 1/5 of the diffraction limit of the telescope. Imaging was also done on more complicated objects. The reconstructed images were of poor quality. One of the most important factors leading to image distortion was the presence of a large range of reference wave intensity fluctuations. Because of this, some regions of the hologram had long exposure, while in other regions the exposure was below the limits of sensitivity of the photographic emulsion. Thus only a part of the working aperture of the hologram participated in image formation. It is proposed that an alternative solution to this problem would be to use electronic detectors such as orthicons or multilayered photographic emulsions.

Let us take up the advantages and disadvantages of the given holographic methods.

The method of optical matched filtration enables differentiation of the sought signal against a noise background. To do this, it is necessary to know the parameters of the signal itself or of the interference. Depending on the problem, the coordinates of an object are sought or its image is reconstructed. The method has been most extensively used for posterior processing of optical

images. These may be compound transparencies with a set of patterns, images taken from radar screens, photographs of objects in the presence of atmospheric distortions or aberrations of forming systems. On the current stage of development, the technique of making holographic filters is complicated, and the operation of installing them is time-consuming. This situation impedes the practical introduction of the method for high-speed signal processing. Furthermore, it cannot be used to detect unknown targets or to suppress unknown interference.

The technique of subtracting optical signals has the same disadvantages. The method of compensation when a reconstructed complex-conjugate wave front passes through an inhomogeneous medium has been successfully used for suppressing phase interference. Knowledge of interference parameters is not mandatory for its realization. It has been put to extensive use in eliminating lens aberrations and diffraction distortions.

A peculiarity of this method is that on the stage of hologram reconstruction the wave front passes through an inhomogeneity that causes distortion of the sought signal during recording. Thus the speed of the system must be at least the same as the characteristic time of fluctuations of parameters of the inhomogeneity.

From this standpoint, a more promising method is averaging of optical signals by fixing statistically independent realizations of wave fronts on different detectors or with accumulation of holograms on the same light-sensitive medium.

When an object that sets up a reference perturbation is close to the sought target, the process of suppressing distortions is relatively simple. It is sufficient to fix one realization of the wave front and to use the technique of optical Fourier transformation on the reconstruction stage. Imaging with long and short exposures is possible during recording. This fact is of particular importance for observing moving objects.

These properties determine the tremendous outlook of this method for detecting and recognizing objects through the atmosphere.

The most important advantage of optical systems over electronic analogs is their capability for handling enormous amounts of information over a short time interval -- at the limit, over the time of light propagation in the system. Operating in terms of communication theory, we can state that optical systems have a large value of the product of input signal area multiplied by the square of the maximum linear frequency included in the signal.

For example, consider the linear operation of filtration (see Fig. 6.2). Let the input signal have area S and limiting resolution R, and let the filter have area S' and resolution R. For every element at the input, the optical system performs $S'R^2$ operations of multiplication, and $S'R^2$ operations of subtraction. These operations are done SR^2 times simultaneously. On the whole, $SS'R^4$ operations are needed to get the necessary signal at the output. If we assume that $S = 10^4$ mm^2, $S' = 4$ mm^2 and $R = 100$ lines/mm (values that are easily attainable at present), then the number of operations is $4 \cdot 10^{12}$. Let

us assume that it is necessary to process a signal in this way in 1/30 s (the usual scanning time in television systems) by an electronic system. Its passband must be at least $12 \cdot 10^{12}$ Hz, and this is for the case of processing only a single signal. In optical systems, several filters can be placed simultaneously in the filtration plane, i. e. a large number of two-dimensional signals can be processed at the same time. Thus with a data input-output time of 1/30 s in optical systems, we get an operator speed much greater than in electronics.

At the same time, optical data processing systems have a number of peculiarities that prevent extensive application in place of electronic systems. To handle radio signals, an electrical signal must be preconverted to optical form, and so far we have not developed any adequately convenient and rapid methods for doing such operations. Light-sensitive media that are used for recording optical signals require considerable time for processing or have low resolution.

Nonetheless, even considering these specifics, the field of application of optical data processing methods is quite extensive. Optical systems are used for high-resolution spectral analysis, correlation analysis of functions and fields in space and time, distinguishing signals on a background of noise and interference, the operation of matched filtration and for handling other jobs in radio astronomy, engineering, medicine, geophysics and acoustics.

6.2. Using Holography Without a Reference Beam

Methods of holography in which a coherent reference beam is used have found wide application in various kinds of research [Ref. 33, 26, 71, 65, 127].

However, the conditions that ensure the necessary requirements impose limitations on the class of solvable problems. Among these is rigidity of the geometry of recording holograms, coherence of sources of radiation and high resolution of light-sensitive materials. These difficulties can be eliminated by using the technique of holography without a reference beam [Ref. 2, 4].

Image reconstruction is realized if a wave scattered by part of the object is used as a reference wave [Ref. 80, 82, 175].

Having a known part of the signal in form

$$u_0(x) = A_0(x) \exp[i\varphi_0(x)],$$

we define the amplitude transmission of the hologram t(x) as

$$t(x) \sim |A_0(x) e^{i\varphi_0(x)} + A_1(x) e^{i\varphi_1(x)}|^2 = |u_1(x)|^2 + |u_0(x)|^2 + u_1^*(x) u_0(x) + u_1(x) u_0^*(x),$$

where $u_1(x) = A_1(x)e^{i\phi(x)}$ is the unknown wave perturbation.

The deficient information on the object is contained in the last two terms of the given expression. To reconstruct it, the spectral component corresponding to one of these terms is isolated and divided by the signal $u_0(x)[u_0^*(x)]$. This is done by forming an additional hologram and transparency with amplitude transmissions $t_1(x)$ and $t_2(x)$ respectively:

$$t_1(x)=|e^{iv_0x}+u_0(x)|^2=1+|u_0(x)|^2+u_0(x)e^{-iv_0x}+u_0^*(x)e^{iv_0x};$$
$$t_2(x)=\frac{1}{u_0(x)u_0^*(x)}=\frac{1}{|u_0(x)|^2}.$$

The coefficient $v_0 = 2\pi\alpha/\lambda$ determines the phase distribution of the field in the plane of the hologram, which sets up a reference wave with wavelength λ that propagates at angle α to the optical axis. Transparency $t_2(x)$ is made by recording signal $u_0(x)$ on a photographic plate and processing to coefficient of contrast $\gamma = 2$. After adding the three transparencies $t(x)$, $t_1(x)$ and $t_2(x)$, they are illuminated with a plane monochromatic wave. In the direction of light beam propagation $-\alpha$, we get the field distribution in the form

$$u(x)=e^{-iv_0x}\left\{u_0(x)+\frac{|u_1(x)|^2}{|u_0(x)|^2}u_0(x)+u_1(x)+\frac{u_0(x)u_0(x)}{|u_0(x)|^2}u_1^*(x)\right\}.$$

The last two terms of this expression give the sought image and its conjugate. The spurious effect of their superposition is eliminated by special selection of the geometry of recording hologram $t(x)$. To do this, the part of the object that scatters wave $u_0(x)$ is situated to the side or at a different depth from the object of observation $u_1(x)$. Then the reconstructed images are localized in different regions of space [Ref. 67].

The procedure of reconstructing a hologram without a reference beam is simplified if it is illuminated by a wave that coincides in localization and phase with a wave scattered by part of the object [Ref. 50]. Let there be a hologram on which an object is fixed that consists of a discrete set of N points. Its transmission at some fixed point is written as

$$\sum_1^N \frac{A_g}{r_g}e^{-ikr_g}\sum_1^N \frac{A_p^*}{r_p}e^{ikr_p},$$

where A_g, A_p are the complex amplitudes of the sources that are points of the object; r_g, r_p are distances from points of the object to a point on the hologram; $k = 2\pi/\lambda$; g, p = 1, 2,..., N are the subscripts of points of the object.

On the reconstruction stage, the hologram is illuminated by a spherical wave of form $\frac{A_n}{r_n}e^{ikr_n}$ emitted by a point source. If it coincides in localization with one of the points of the object, the following set of images is reproduced:

an image corresponding to the initial object (p = n):

$$\frac{1}{2}\frac{|A_n|^2}{r_n^2}\sum_1^N \frac{A_g}{r_g}e^{-ikr_g}, \qquad (6.20)$$

its conjugate image (g = n)

$$\frac{1}{2}\frac{|A_n|^2}{r_n^2}e^{-ir_kr_n}\sum_1^N \frac{A_p^*}{r_p}e^{ikr_p},$$

and N - 1 more pairs of images (g, p ≠ N)

$$\frac{1}{2}\left\{\frac{A_n A_p^*}{r_n r_p} e^{-ik(r_n - r_p)} \sum_1^N \frac{A_g}{r_g} e^{-ikr_g} + \right.$$
$$\left. + \frac{A_n A_g}{r_n r_g} e^{ik(r_n - r_g)} \sum_1^N \frac{A_p^*}{r_p} e^{ikr_p} \right\}.$$

With an increase in the number of point sources coinciding with points of the object, there is an increase in the number of reconstructed images. In this connection, images (6.20) that correspond to the object are superimposed with respect to localization and phase, whereas such superposition does not occur for the other images. Thus when a hologram is reconstructed by a wave from some part of the object, the useful image stands out in intensity, and all other images form a comparatively faint background. Unfortunately, it should be noted that reconstruction of the missing part of the object necessitates availability of considerable a priori information about it. For example in experiments done by the authors on reconstructing an object consisting of four points, it was necessary to illuminate the hologram with a wave formed by three points of the object.

Reconstruction of unknown information about the object is realized by using Fourier holograms [Ref. 161]. To do this, the wave scattered by the object is focused in the plane of the light-sensitive medium. If $t_a(x)$ is the transmission function of the unknown part of the object, and $t_b(x)$ is the transmission function of the known part, then the recorded intensity distribution is written as

$$I(v) = |\Phi\{t_a(x)\} + \Phi\{t_b(x)\}|^2 = |T_a(v) + T_b(v)|^2,$$

where $\Phi\{\ \}$ denotes the operation of Fourier transformation.

When such a hologram is reconstructed by a wave of form $T_b(v)$, we get the field distribution

$$U(v) = T_b(v)[T_a(v) + T_b(v)][T_a^*(v) + T_b^*(v)].$$

Let us note that $T_b(v)$ is the spatial spectrum of perturbation $t_b(x)$. Thus for reconstruction we can use a wave diffracted from the corresponding part of the object. By optical realization of inverse Fourier transformation, we get the following field distribution in the plane of observation:

$$u(x) = [t_a(x) + t_b(x)] * t_b(x) * [t_a^*(-x) + t_b^*(-x)],$$

where * denotes convolution.

When the condition

$$t_b(x) * [t_a^*(-x) + t_b^*(-x)] \simeq \delta(x) \qquad (6.21)$$

is met, we get the reconstructed image $t_a(x) + t_b(x)$. The condition (6.21) is realized if the field of perturbation from the object has random phase

distribution in space. The other case of image reconstruction is realized if distribution $t_b(x)$ has sufficiently large amplitude, i. e. an object is holographed with an exceptionally bright point [Ref. 4, 5, 6].

One variety of holography without a reference beam is holography with a local reference wave [Ref. 112], which has found wide application in interference studies. Part of the radiation scattered by the object is used on the stage of forming the hologram. This radiation is passed through a spatial filter to form a reference wave with a simple wave front -- spherical or planar [Ref. 110, 111]. The procedure of reconstructing the image from such a hologram is no different from that of reconstructing conventional holograms with side (oblique) reference beam.

It is well known that holography of a focused image is insensitive to the shape of the reconstruction wave front [Ref. 173]. Therefore, by using part of the radiation not diffracted by the object, we can get an image with rather good resolution [Ref. 49, 104].

Extensive possibilities are opened up by using three-dimensional light-sensitive media for making holograms without a reference beam. Three-dimensional holograms can be treated as a set of two-dimensional holograms. In reconstruction, each of them will form the above-mentioned images, with the useful images being added in phase and intensified. In this case, we can get by with fewer "reading points." And in fact reconstruction of a two-dimensional object from a three-dimensional hologram is realized by using a single point source [Ref. 5, 7].

If during recording the entire holographic scene is focused in a given volume of the light-sensitive medium, then in reconstructing one of the rays emanating from the object, we reconstruct the entire system of rays that produce its image. A three-dimensional focused image of the object can be observed behind the hologram in the region that is free of the direct beam [Ref. 7, 45].

An interesting possibility opens up for studying various processes associated with change in phase of the light wave when diffractograms are formed by diffracting elements and reconstructed as holograms without a reference beam [Ref. 2].

Consider the optical arrangement diagrammed on Fig. 6.10. A ray from coherent light source 1 (Fig. 6.10a) is shaped by lenses 2 into a parallel beam that passes through the investigated object 3 and diffaction grating 4 and is incident on plate 5. The intensity pattern formed by diffraction of the plane wave by the grating, and the pattern distorted by the object are sequentially fixed on the photographic emulsion. On the reconstruction stage (see Fig. 6.10b) the diffractogram 5 is illuminated by a parallel monochromatic light beam passing through lens 6. Several diffraction orders

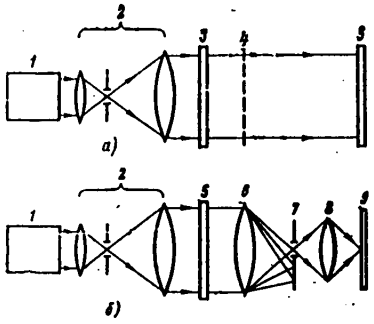

Fig. 6.10. Diagram of recording with diffraction grating: a--recording; b--reconstruction

with intensity that decreases with increasing distance from the optical axis are focused in the focal plane of lens 6. The reconstructed image is observed in one of the orders by supplemental lens 8. Slit disphragm 7 isolates the corresponding diffraction order and suppresses the spurious background.

The operation of the arrangement is described as follows. if $I(x)=\sum_n \delta(x-nx_0)$ is intensity distribution in the plane of the photographic plate as determined by a grating with period x_0, and f(x) is a function that characterizes the intensity redistribution introduced by the object, then for case $f(x) < x$ the distribution of blackening on the photographic emulsion takes the form $I(x) + f(x) = I(x) + I'(x)f(x)$.

The transmission of the photographic plate is written as

$$I_0 - I(x) - I'(x) f(x) = C - I(x) - I(x) f'(x).$$

When such a hologram is reconstructed in the focal plane of lens 6, the amplitude distribution that depends on x will be

$$\int_{-\infty}^{\infty} I(x) f'(x) e^{ixv} dx = \sum_n \delta(v - nv_0) * F(v) = \sum_n F(v - nv_0),$$

where F(v) is the Fourier transform of function f'(x).

We can see from the resultant expression that in reconstruction of holograms by Fourier transformation, there is a Fourier spectrum of the first derivative of function f(x) in each interference order.

Let us note that information with predetermined field intensity in the plane of the diffraction element can be transmitted by such a method. Let us assume that the transmission function of the grating takes the form

$$t(x) = \sum_{n=-\infty}^{\infty} \delta(x - nx_0).$$

If a plane monochromatic wave is normally incident on the grating, then at a distance $z = 2x_0^2 n/\lambda$, n = 1, 2, 3,... away from the grating, the field is equal except for a constant coefficient to the field distribution immediately behind the grating:

$$u_1(z; x) = \sum_{n=-\infty}^{\infty} \delta(x - nx_0).$$

Using the relation

$$\Phi\left\{\sum_{n=-\infty}^{\infty} \delta(x - nx_0)\right\} = \frac{2\pi}{x_0} \sum_{n=-\infty}^{\infty} \delta(v - nv_0) = v_0 \sum_{n=-\infty}^{\infty} \delta(v - nv_0),$$

we write the recorded intensity distribution as

$$I_1(z, x) = \Phi\left\{v_0^2 \left[\sum_{n=-\infty}^{\infty} \delta(v - nv_0) * \sum_{n=-\infty}^{\infty} \delta(v - nv_0)\right]\right\},$$

where $\divideontimes$ denotes the operation of autocorrelation.

In filtration plane 7 we have

$$U'_{\Phi}(v)\simeq v_0^2\left[\sum_{n=-\infty}^{\infty}\delta(v-nv_0)\divideontimes\sum_{n=-\infty}^{\infty}\delta(v-nv_0)\right]=v_0^2\sum_{n=-\infty}^{\infty}\delta(v-nv_0).$$

Isolating the first diffraction order $v_0\delta(v-v_0)$, we get the following field distribution in observation plane 9:

$$\Phi\{U'_{\Phi}(v)\}=Ce^{iv_0x}. \qquad (6.22)$$

When the object is inserted immediately in front of the grating, the field distribution behind it takes the form

$$u_2(x)=f(x)\sum_{n=-\infty}^{\infty}\delta(x-nx_0).$$

The corresponding intensity distribution fixed on the diffractogram is

$$I_2(z;\ x)=\Phi\left\{v_0^2\left|\sum_{n=-\infty}^{\infty}F(v-nv_0)\divideontimes\sum_{n=-\infty}^{\infty}F^*(v-nv_0)\right|\right\},$$

where

$$F(v)=\Phi\{f(x)\}.$$

If the spatial spectrum of the investigated object fits into the gap between diffraction orders of the grating spectrum, then a signal can be isolated in the filtration plane characterized by autocorrelation function $F\divideontimes F^*$.

Then for the filtered first order, we get

$$U_{\Phi}^2(v)=v_0^2[F(v-v_0)\divideontimes F^*(v-v_0)]=$$
$$=v_0^2\{[F(v)\divideontimes F^*(v)]\divideontimes\delta(v-v_0)\}.$$

This implies that the field in plane (9) takes the form

$$\Phi\{u_{\Phi}^2(v)\}=|f(x)|^2e^{iv_0x}.$$

Fig. 6.11a [photo not reproduced] shows a diffractogram and reconstructed image (Fig. 6.11b [photo not reproduced]) of a candle flame taken by the method described above. The reconstructed picture is a shadowgram of an inhomogeneity. An OKR-11 laser source was used in the experiment. The object was placed immediately in front of the grating, and the diffractogram was recorded in the plane where a clear image of the line structure of the grating was observed. The diffraction grating was made by winding metal wire on a frame with pitch of 0.5 mm and diameter of 0.4 mm.

One of the possible elements that introduces the phase modulation necessary for forming diffractograms is space itself.

As an example, consider an arrangement for recording the diffractogram of a phase object (Fig. 6.12). A parallel monochromatic light beam illuminates

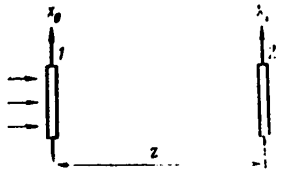

Fig. 6.12. Diagram of recording phase objects: 1--object; 2--photographic plate

the object placed in plane x_0. The diffraction pattern is fixed on the photographic plate in plane x_1.

Let us write the transmission function of an object that has phase characteristic $\phi(x_0)$,

$$t(x_0)=e^{-i\varphi(x_0)}.$$

Let us denote the field immediately behind the object by $u_0(x_0)$. The field distribution in plane x_1 is defined as

$$u_1(x_1)=u_0(x_1)\divideontimes h_0(x_1).$$

The spatial spectrum of the field $u_1(x)$ is

$$\Phi(u_1(x_1))=C_1[\Phi(u_0(x_1))\exp(iv^2/4b)]. \qquad (6.23)$$

Here $b=k/2z$, C_i are constant coefficients, $i=1, 2,\ldots, n$. Since for real objects there is an interval of spatial frequencies $(-v_0, v_0)$ in which most of the energy of signal $u_1(x_1)$ is concentrated, we can select the condition of observation

$$\frac{v_0^2}{4b}=\frac{v_0^2z\lambda}{4\pi}\ll 1. \qquad (6.24)$$

Performing the operation of inverse Fourier transformation in expression (6.23) and taking (6.24) into consideration, we have

$$u_1(x_1)\sim u_0(x_1)-\frac{i}{4b}\frac{d^2u_0(x)}{dx_1^2}.$$

Substituting the value of the field $a_0(x_0)$, we get

$$u_1(x_1)=C_2e^{-i\varphi(x_1)}\left\{1+\frac{i}{4b}[\varphi'(x_1)]^2-\frac{1}{4b}\varphi''(x_1)\right\}.$$

The corresponding intensity distribution is written as

$$I(x_2)=u_1(x_1)u_1^*(x_1)=C_2^2\left\{1-\frac{1}{2b}\varphi''(x_1)+\frac{1}{16b^2}[\varphi''(x_1)]^2-\right.$$
$$\left.-\frac{1}{16b^2}[\varphi'(x_1)]^4\right\}\simeq C_2^2\left[1-\frac{1}{2b}\varphi''(x_1)\right].$$

Thus when condition (6.24) is met, the recorded diffraction pattern contains information on the second derivative of the phase distribution function on the object.

Decoding (reconstruction) of such a diffractogram is done in the optical system presented on Fig. 6.13. A parallel monochromatic light beam shaped by collimator 2 illuminates diffractogram 3 located in the rear focal plane of

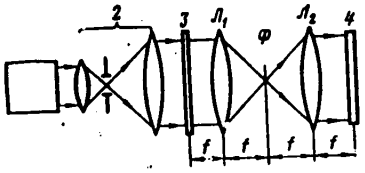

Fig. 6.13. Diagram of phase object visualization: 1--laser; 2--collimator; $Л_1$, $Л_2$--focusing lenses; Φ--filter; 4--visualization plane

lens $Л_1$. Lenses $Л_1$ and $Л_2$ are for filtration of spatial frequencies. Filter Φ is located in the plane of conjugation and foci. The field distribution in the filter plane takes the form

$$\Phi\{1-\varphi''(x)\}=C[\delta(v)+v^2\Phi\{\varphi(x)\}].$$

If a transparency is placed here that suppresses the zero order of radiation component δ(v) and has a transmission function inversely proportional to the square of the distance from the optical axis in the remaining region [$t_\phi \cong 1/v^2$], then as a result of the operation of secondary Fourier transformation realized by lens $Л_2$, a field is reconstructed in the plane of observation that is determined by real function φ(x). By observing the condition of linear recording of intensity φ(x) on the photographic emulsion and then bleaching it, we get a transparency with transmission

$$t_1(x)=e^{i\beta\varphi(x)}.$$

Coefficient β describes the relation between phase shift and intensity of the wave incident on the photographic emulsion. When the transparency is illuminated by a plane monochromatic wave, a field is reconstructed that reproduces the wave front scattered by the investigated object.

In order to solve some problems, it is sufficient to have information on the object in the form of an autocorrelation function of scattering (transmission) of the investigated object. In this case, holography without a reference beam is a simple means of isolating optical signals against a noise background.

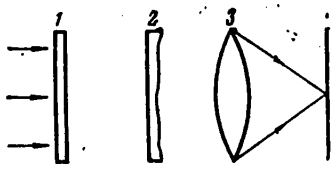

Fig. 6.14. Diagram of holography through an inhomogeneous medium: 1--object; 2--inhomogeneous medium; 3--focusing lens; 4--photographic plate

Fig. 6.14 shows one of the arrangements of recording holograms that is used for observing objects through an inhomogeneous medium. Object 1 is illuminated by monochromatic coherent radiation. The wave front distorted by inhomogeneity 2 is focused by lens 3. The hologram is recorded on photographic plate 4 in the focal plane of the lens. Subsequent reconstruction is accomplished by the method of optical Fourier transformation.

The hologram in this case is in fact a difractogram that contains information on the observed object.

The process of recording and reconstructing such holograms (diffractograms) is described as follows. Let $u_1(x, y)$ be the distribution of the field on

the object; $u_2(x, y)$ -- the field distribution on the entrance pupil of the lens. Field $u_1(x, y)$ is related to field $U(u, v)$ in the focal plane of the lens by Fourier transformation

$$U(u, v)=C_1\Phi\{u_1(x, y)\},$$

where $\Phi\{\ \}$ denotes Fourier transformation with respect to spatial frequencies $u = kx/f$; $v = ky/f$; f is focal length; C is a constant coefficient.

Intensity $I(u, v) = C_2U(u, v)U^*(u, v)$ is recorded on a photographic plate in the rear focal plane.

In reconstruction, inverse Fourier transformation is realized with respect to the same spatial frequencies as in recording. We have the following field distribution in the observation plane:

$$u(x, y)=\Phi^{-1}\{I(u, v)\}=u_1(x, y)\ast u_1^*(-x, -y).$$

If there is no inhomogeneous medium on the stage of hologram formation, the response function of free space $H_0(x, y)$ is determined by the relation

$$H_0(x, y)=C\exp\left[i\frac{k}{2z}(x^2+y^2)\right], \qquad (6.25)$$

where z is the distance from the object to the entrance pupil of the lens. We have $u_2(x, y) = u_1(x, y)\ast h_0(x, y)$. From this and expression (6.25) we get

$$u(x, y)=u_1(x, y)\ast u_1^*(-x, -y),$$

since $$h_0(x, y)\ast h_0^*(-x, -y)=\delta(x, y).$$

Thus the field distribution in the plane of observation is determined by the autocorrelation function of the field distribution on the object.

In the presence of a distorting medium, field $u_2(x, y)$ is written as integral

$$u_2(x_2, y_2)=\int_{-\infty}^{\infty}\int u_1(x_1, y_1)h_1(x_2, y_2, x_1, y_1)dx_1dy_1.$$

For an isotropic medium, the response function $h_1(x_2, y_2, x_1, y_1)$ depends only on coordinate difference $x_2 - x_1$; y_2-y_1. In this case, field $u_2(x_2, y_2)$ is written as

$$u(x, y)=u_1(x, y)\ast u_1^*(-x, -y)\ast h_1(x, y)\ast h^*(-x, -y).$$

and the reconstructed pattern takes the form

$$u_2(x_2, y_2)=u_0(x_2, y_2)\ast h_1(x_2, y_2),$$

If the spatial spectra of object and inhomogeneity differ from one another, then the distortions introduced will be insignificant. In the special case

of white noise $h_1(x, y) \ast h_1(-x. -y) \to \delta(x, y)$, the autocorrelation function of the field distribution function on the object is observed just as in the absence of interference.

In the experiment, the object was a transparency of the letter "H" with spectrum in the region of low spatial frequencies. The object was illuminated by a plane wave. The light source was a helium-neon laser operating in the multimode state. For effective resolution of low spatial frequencies, the focus of the lens was taken as ~1.5 m, and the hologram was recorded on MIKRAT-300 photographic emulsion. A frosted plate was used as the inhomogeneous medium. The frosted screen was rotated during exposure to simulate fluctuations of the elements of inhomogeneity. The same optical system was used on the reconstruction stage as in recording. In this case the frosted screen was removed.

Fig. 6.15, 6.16 show photographs [not reproduced] of holograms and reconstructed images for objects taken through stationary and rotating frosted screens. For comparison, Fig. 6.17 [photo not reproduced] shows a hologram and reconstructed image of the same object produced in the absence of an inhomogeneous medium. We can see from the given photographs that distortions introduced by the medium completely change the nature of the spatial spectrum recorded on the hologram. However, the general form of the reconstructed outline determined by the autocorrelation function of field distribution on the object is the same.

When the above described method is used for recognizing objects against a noise background, the problem arises of uniqueness of the signal representation at the output of the optical system in the form of an autocorrelation function [Ref. 2, 172].

It is known that a single autocorrelation function may correspond to a broad set of signals with the same duration constraint [Ref. 39, 141]. However, only one signal out of this whole set is formed by a system with limited transmission spectrum. Any optical system is just such a system. Therefore the autocorrelation pattern will correspond to a unique object that can be recorded by the given optical device.

Regarding the method of holography, it should be noted that it is one of the possible versions of solution of a more general phase problem, i. e. the problem of finding the signal phase from its amplitude [Ref. 39, 2].

The necessity for mandatory introduction of a reference beam has usually been justified by the fact that in registering a signal

$$u(x) = A(x)e^{i\varphi(x)}$$

on a square-law detector, we get a distribution equal to

$$u(x)u^*(x) = A^2(x),$$

in which there is no function that characterizes phase. However, even in the first research on holography it was noted that the scattered wave is formed

in accordance with the Huygens-Fresnel principle, i. e. the amplitude at each observation point is determined by the sum of amplitudes taken with their phase from each point of the object. Therefore the problem has been reduced to methods of recording both information components in explicit form. The same goal is pursued by the so-called methods of holography without reference beam.

The general formulation of the problem is correct if signal u(x) is defined as a signal of arbitrary nature. However, we are dealing with electromagnetic radiation, and are treating the object as some boundary condition that influences the nature of distribution of the scattered field. In the far zone that realizes Fourier transformation of a spatially limited function, we have a distribution that is described by analytical functions. Thanks to this circumstance, an additional equation arises that relates the amplitude and phase of the sought distribution and is defined by the theory of functions of a complex variable. And this means that a single-beam hologram (diffractogram) carries complete information on the amplitude and phase of the light wave scattered from the object.

6.3. Reconstruction of Object Image From Modulus of Autocorrelation Function

The problem of finding the image of an object from the modulus of the autocorrelation function consists in the following. Knowing the modulus of the autocorrelation function, it is necessary to find its phase, and then by using the resultant amplitude-phase information to determine the function corresponding to this autocorrelation function.

This problem arose for the first time in connection with finding the intensity distribution of an incoherent light source.

It is known that the image of a remote incoherent light source can be reconstructed if the second-order optical correlation function is known [Ref. 159, 160]. The correlation function is usually determined from interferometric measurements, for example by using a Michelson stellar interferometer. The phase of the correlation function is related to the position of the interference bands, and its modulus is related to the luminosity function.

Since technical difficulties preclude sufficient accuracy in determining the displacement and position of the bands, experimenters frequently run up against the problem of reconstructing the unknown function from its modulus.

An analogous problem arises in x-ray crystallography, where the phase of the wave signal is usually unknown, in the theory of particle scattering when determining the scattering cross section, and in other problems [Ref. 89, 136].

Some scientists have discussed the loss of phase information from the standpoint of the limitations stemming from the analytical properties of the correlation function [Ref. 39, 122, 123, 141, 165, 195]. Superposition of the reference light beam with the field carrying information on the source of radiation has been suggested [Ref. 157]. This method is analogous in nature to the holographic method of recording amplitude-phase information [Ref. 137].

Another method of finding the phase was suggested in Ref. 156. In this case, exponential filters are used for analytical continuation of the correlation function into the complex region. If the modulus of the complex correlation function is known outisde the real axis, then its phase is determined from the modulus by integrating Cauchy-Riemann differential equations.

The last two methods of finding phase information have been experimentally studied [Ref. 149]. The correlation function $\Gamma(x)$ in the far zone of diffraction, which is related to intensity distribution of the light source by the formula

$$\Gamma(x)=C\int_{-\infty}^{\infty} S(u)\exp(-ik_0xu/R)\,du, \qquad (6.26)$$

was measured by a prism interferometer (Fig. 6.18). Here R is the distance from the source to the plane of registration, x is the displacement of the interfering rays, C is a constant coefficient, $k_0 = 2\pi/\lambda_0$, λ_0 is mean wavelength.

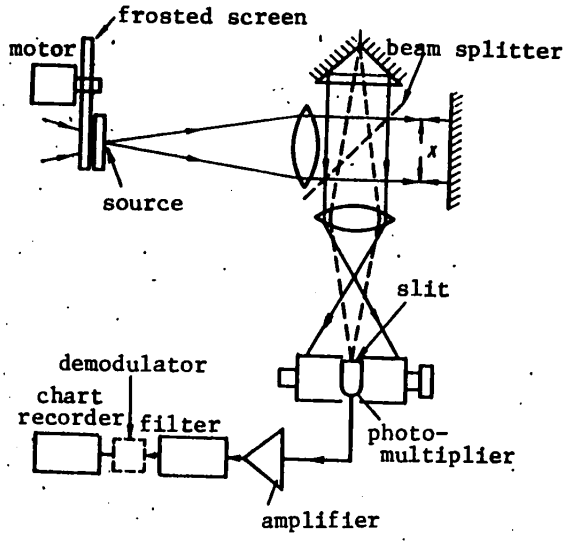

Fig. 6.18. Diagram of facility for making correlation measurements

The interference pattern is described by the relation

$$|\Gamma(x)|\cos[vx+\arg\Gamma(x)]+\text{const},$$

where v is the average spatial frequency.

A scanning photoelectric detector was used in recording the interference pattern. The x-coordinate is proportional to scanning time t, i. e. the signal at the detector output is

$$|\Gamma(\beta t)|\cos[v\beta t+\arg\Gamma(\beta t)]+\text{const}.$$

The signal from the detector output went to an amplifier and filter that did not pass the constant component. A chart recorder was used for registration of the interference pattern. The recorded pattern contained information on the modulus and phase of $\Gamma(x)$. A helium-neon laser and rotating frosted glass were used to simulate an incoherent source.

The first method of finding phase information is analogous to the use of a reference beam in holography.

Using the formula of inverse Fourier transformation, we write

$$A(u)=\int_{-\infty}^{\infty} S(u')S(u'+u)\,du'=(k_0/2\pi C^2R)\int_{-\infty}^{\infty}|\Gamma(x)|^2\exp(ixuk_0/R)\,dx. \tag{6.27}$$

Let us assume that the unknown source S(u) has limited dimensions $a<u<b$, and G(u) is a reference source situated at distance $b-a$ from source S(u). Then we have

$$O(u)=S(u)+C_1\delta(u-u_0),$$

where C_1 is a constant corresponding to the intensity of the reference source. Now expression (6.27) takes the form

$$(k_0/2\pi CR)\int_{-\infty}^{\infty}|\Gamma(x)|^2\exp(ixuk_0/R)\,dx+C_1^2\delta(u)+$$

$$+\int_{-\infty}^{\infty}S(u')S(u'+u)\,du'+C_1S(u+u_0)+C_1S(u_0-u). \tag{6.28}$$

The third and fourth terms of this expression correspond to the real and imaginary (mirror) images of the source. The uniqueness of the reconstruction is determined from the a priori information on the position of the reference source relative to the object.

In principle, there is no need for the reference source to be situated at distance $b-a$ from the object, but in this case, two measurements are required: one with the reference source and one without it. The interferometric device shown on Fig. 6.18 was used to form the interference bands. The measurement source was modified as shown in Fig. 6.19.

Fig. 6.20 shows the reconstructed image obtained by Fourier transformation of function $|\Gamma(x)|^2$ in accordance with expression (6.28). The object was a 95 μm slit.

Reconstructed images of more complicated objects are shown on Fig. 6.21.

Let us consider the method of determining phase by exponential filters. Following Ref. 156, we get the analytical continuation of the correlation function by replacing the real variable with the complex variable $z=x+iy$, where x and y are real quantities. We have

$$\Gamma(x+iy)=C\int_{-\infty}^{\infty}S(u)\exp(k_0uy/R)\exp(-ik_0ux/R)\,du. \tag{6.29}$$

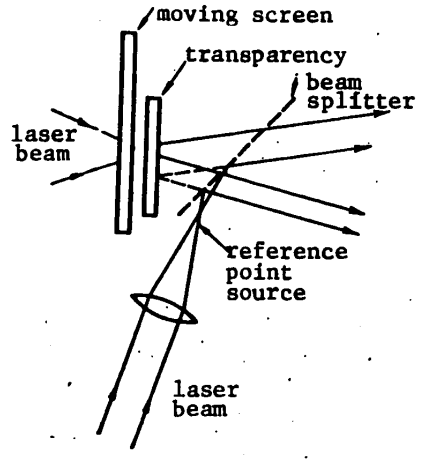

Fig. 6.19. Diagram of formation of source image

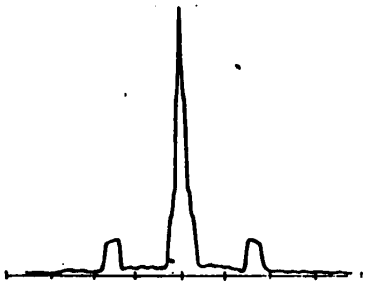

reconstructed image of slit

Fig. 6.20. Reconstructed image of 95 μm slit. The central peak corresponds to the first two terms of equation (6.28). The image is situated symmetrically relative to the central peak

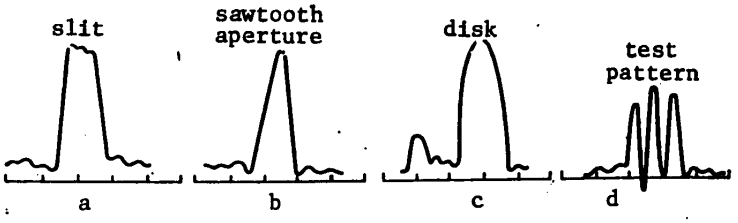

Fig. 6.21. Reconstructed images: a--95 μm slit; b--sawtooth radiation source 95 μm wide; c--two disks with diameters of 58 and 116 μm; d--test pattern of three lines of 19 μm size spaced 38 μm apart

If $\Gamma(x+iy)$ is treated as a function of the real variable x, then (6.29) has the same form as formula (6.26) when S(u) is replaced by $S(u)\exp(k_0uy/R)$. The new source can be constructed by placing the filter close to source S(u), the filter transmission varying according to an exponential law relative to y In cases where it is physically possible to locate such a filter directly behind source S(u), measurements of $\Gamma(x+iy)$ with and without the filter will give information on analytical continuation of the correlation function into the complex plane. Such measurements enable us to determine the derivative $\partial|\Gamma(x+iy)|/dy$.

It is known that correlation function $\Gamma(z)$ is regular in the lower half-plane of complex plane z. Therefore the modulus and argument of $\Gamma(z)$ are related by Cauchy-Riemman relations:

$$\frac{\partial|\Gamma(x+iy)|}{\partial x}=|\Gamma(x+iy)|\frac{\partial\varphi(x+iy)}{\partial y};\qquad(6.30)$$
$$\frac{\partial|\Gamma(x+iy)|}{\partial y}=-|\Gamma(x+iy)|\frac{\partial\varphi(x+iy)}{\partial x},$$

where $\Gamma(x+iy)=|\Gamma(x+iy)|\exp[i\varphi(x+iy)]$. Integrating expression (6.30), we have

$$\varphi(x+iy)-f(y)=-\int_0^x \frac{1}{|\Gamma(x'+iy)|}\frac{\partial|\Gamma(x'+iy)|}{\partial y}dx',$$

where f(y) is some function of y. From this we get

$$\varphi(x)=\frac{\partial}{\partial y}\int_0^x \ln|\Gamma(x'+iy)|dx'. \qquad (6.31)$$

Thus in principle we have a procedure for determining the phase of the correlation function from measurement of its modulus. If we need to know $\Gamma(x+iy)$ only in the neighborhood of $y=0$, the exponential function can be approximated by a straight line, i. e. the exponential filter can be replaced by a linear filter.

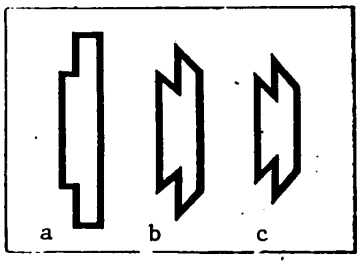

Fig. 6.22. Shapes of sources used for method of reconstruction with exponential filters: a--initial source; b--source modified by exponential function with damping duration of 1232 μm; c--source modified by exponential function with damping duration of 616 μm

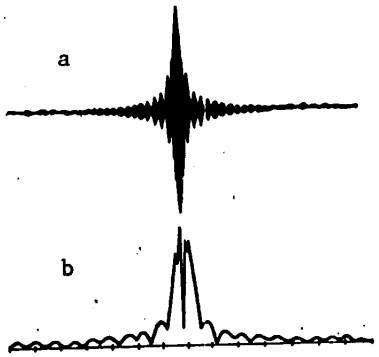

Fig. 6.23. Machine recording of interferograms: a--typical interferogram fixed on chart recorder; b--graph of $|\Gamma(x)|$ produced by using the given interferogram. The source was the transparency of Fig. 6.22a

The experiment used the interferometer shown on Fig. 6.18. The function of source S(u) was simulated by a slit mask with height corresponding to the selected function. The exponential modification was realized by changing the shape of the mask (see Fig. 6.22). Fig. 6.23 shows interferograms recorded on a strip chart, and a graph of the modulus of the autocorrelation function calculated by computer. Fig. 6.24 shows the same autocorrelation function obtained after filtration, and the phase calculated by equation (6.3). The source was reconstructed by calculating the Fourier transform of function $\Gamma(z)$ and the phase obtained from equation (6.31).

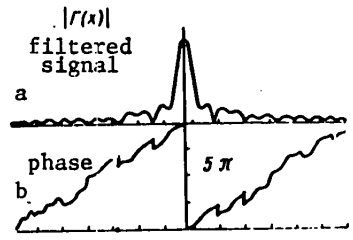

Fig. 6.24. Correlation function obtained by filtration: a--modulus of $\Gamma(x)$; b--phase of $\Gamma(x)$

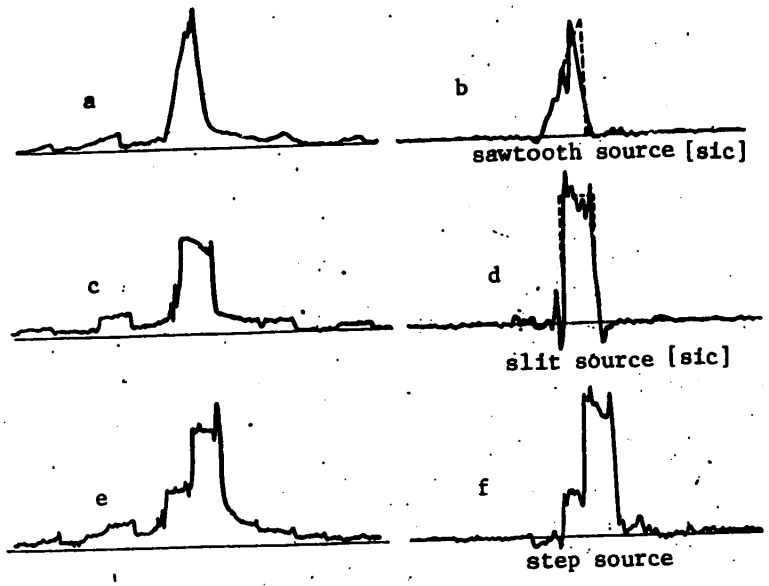

Fig. 6.25. Reconstructed images of sources: a--398 μm slit reconstructed from measurement of function $\Gamma(x)$; b--reconstructed from function $|\Gamma(x)|$ with (broken line) and without (solid line) exponential filter; c--sawtooth source 398 μm wide reconstructed from measurement of function $\Gamma(x)$; d--reconstructed from measurement of $|\Gamma(x)|$ with (broken line) and without (solid line) exponential filter; e--source in the form of a double step 616 μm wide reconstructed from measurement of function $\Gamma(x)$; f--reconstructed from measurement of function $|\Gamma(x)|$ with (broken line) and without (solid line) exponential filter

The reconstructed images for three shapes of sources are shown on Fig. 6.25.

The resultant experimental data effectively demonstrate the feasibility of determining the shape of a source and the phase of the correlation function from its modulus.

It should be noted that the given methods of finding the phase of an optical signal from its modulus are not the only solutions of the phase problem. As has already been pointed out (see chapter 1), all optical signals belong to the class of signals with finite spectrum. Therefore (see section 1.4), the phase can be represented as

$$\varphi(z)=\frac{1}{\pi}P\int_{-\infty}^{\infty}\frac{\log|A(z)|}{z'-z}dz+\sum_{i}\arg\frac{z-z_i}{z-z_i^*},$$

where A(z) is the amplitude of the optical signal analytically continued into the complex plane, and z_i is the value of zeros in the complex plane. By

TABLE 6.1

Prerequisite	Recording	Conclusion	References
Signal. Square-law reception.	$u = Ae^{i\varphi}$ $I = Ae^{i\varphi}Ae^{-i\varphi} = A^2$	Ambiguous relation between $\|A\|$ and ϕ.	
Analyticity $f(z) = a(z) + ib(z)$ $b = \frac{1}{\pi} P \int \frac{a(z')}{z'-z} dz'$ $a = \frac{1}{\pi} P \int \frac{b(z')}{z'-z} dz'$	$\ln u = \lg \|A\| + i\varphi$ $\varphi(z) = \frac{1}{\pi} P \int_{-\infty}^{\infty} \frac{\log \|A(z')\|}{z'-z} dz' +$ $+ \sum \arg \frac{z-z_i}{z-z_i^*}$	Ambiguous relation between $\|A\|$ and ϕ. Physical meaning of zeros not clear.	[171]
Miniphase systems. Fermat principle. Optical systems without sources $\delta\phi(z) = 0$. Zeros on real axis	$\varphi(z) = \frac{1}{\pi} P \int_{-\infty}^{\infty} \frac{\log \|A(z')\|}{z'-z} dz'$	One-to-one correspondence between $\|A\|$ and $\pm\phi$. One-beam holography.	[2, 32, 80]
Differentiability $\frac{\partial a}{\partial x} = \frac{\partial b}{\partial y}$ $\frac{\partial a}{\partial y} = \frac{\partial b}{\partial x}$	$\frac{\partial A(x,y)}{\partial x} = -A(x,y) \frac{d\varphi(x,y)}{\partial y}$ $\frac{\partial A(x,y)}{\partial y} = A(x,y) \frac{d\varphi(x,y)}{\partial x}$ $A(x,y) = \int_0^{\infty} U(u) e^{2\pi i y u} e^{-i2\pi x^2 du}$	One-to-one correspondence between $\|A\|$ and $\pm\phi$.	[149, 156]
Reference wave $A_0(x)$	$\overline{A}(x) = A(x) + A_0(x)$ $\|\overline{A}(x)\|^2 = \|A(x)\|^2 + \|A_0(x)\|^2 +$ $+ 2\|A(x)\|\|A(x)\| \cos(\varphi(x) - \varphi_0(x))$	One-to-one correspondence between $\|A\|$ and $\pm\phi$. Two-beam holography.	[39, 149, 157]

imposing an additional condition on the optical signals, namely the Fermat principle $\delta\phi(z) = 0$, we get

$$\varphi(z)=\frac{1}{\pi}P\int_{-\infty}^{\infty}\frac{\log|A(z')|}{z-z'}dz. \qquad (6.32)$$

Thus, optical signals that are formed by passive optical systems (systems without sources) contain zeros only on the real axis. Therefore the phase of the optical signal is uniquely determined by its modulus.

The diffraction pattern obtained in coherent light contains complete amplitude-phase information on the optical signal, and in this sense we can speak of holography without a reference beam (one-beam holography).

Let us note that phase reconstruction from such a hologram is possible not only analytically in accordance with expression (6.32), but also in a coherent optical system that realizes Hilbert transformation. The method proposed in Ref. 140 can be used to get a transparency with transmission that varies according to a logarithmic law.

In conclusion, the methods of solving the phase problem are summarized in Table 6.1.

6.4. Phase Problem in Radio Astronomy

The phase problem as initially formulated in optics has analogous treatment in other regions of the spectrum, and particularly in the x-ray and radio bands. The problem is closely related to use of the luminosity function first introduced by Michelson in optical interferometry, and subsequently generalized by Wolf, who saw it as a "complex function of mutual coherence." Let us look more closely at the formulation of the problem and some possible ways of solving it as applied to radio astronomical research.

It is known that one of the major problems of radio astronomy is determination of the distribution of radio brightness over a source of space radiation. The distribution of radio brightness B is related via inverse Fourier transformation to the complex luminosity function U of the lobe structure of the radio interferometer as measured on different bases, which in the one-dimensional case is represented as

$$B(\xi)=\int_{-\infty}^{\infty}U(u_x)e^{iu_x\xi}du_x, \qquad (6.33)$$

where $u_x = 2\pi D_x/\lambda$ is spatial frequency; D_x is the base of the interferometer with respect to coordinate x; λ is working frequency. The complex luminosity function can be represented as

$$U(u_x)=|U(u_x)|e^{-i\varphi(u_x)}. \qquad (6.34)$$

In principle, experiment can give us the modulus and phase of luminosity:

$$|U(u_x)|=\frac{P_{max}-P_{min}}{P_{max}+P_{min}};$$
$$\varphi(u_x)=2\pi\Delta t/t_0,$$

where P_{max}, P_{min} are the maximum and minimum values of the main lobe of the interferometer relative to the zero value; Δt is the time of delay of the maximum of the envelope relative to the calculated interference maximum; t_0 is the time interval between adjacent maxima, i. e. the period of the interferogram [Ref. 68].

While it is easy to measure the modulus (see for example Ref. 24), there are a number of difficulties in determining the phase. Nonetheless, knowledge of the phase of the luminosity function is considered necessary for determining the distribution of radio brightness.

Thus the formulated problem reduces to determination of the phase of the complex luminosity function followed by substitution in (6.33) and (6.34).

The key to solving the phase problem is use of the analytical properties of the investigated functions, enabling reciprocally single-valued determination of their real and imaginary parts on the basis of Hilbert transforms.

In application to our problem, we note that functions $U(u_X)$

$$\ln U(u_x)=\ln U(u_x)-i\varphi(u_x) \qquad (6.35)$$

are analytical in the lower half-plane J_- of the complex plane. Expression (6.35) gives the possibility of determining phase $\phi(u_X)$, which in general form is written as [Ref. 181]

$$\varphi(u_x)=\varphi_m(u_x)+\varphi_b(u_x), \qquad (6.36)$$

where
$$\varphi_m(u_x)=-\frac{1}{\pi}P\int_{-\infty}^{\infty}\frac{\ln U(u'_x)}{u'_x-u_x}du'_x; \qquad (6.37)$$

$$\varphi_b(u_x)=\sum_i \arg\frac{u_x-u_{xi}}{u_x-u^*_{xi}}. \qquad (6.38)$$

The first term $\phi_m(u_X)$ is the value of the minimum phase that in the absence of zeros in J_- uniquely relates the phase and modulus $U(u_X)$ through Hilbert transformation.

The second term $\phi_b(u_X)$ is the Blaschke factor that evaluates the contribution of zeros of u_{xi} in J_-. Summation extends to all zeros of the function $U(u_X)$ in J_-.

Thus phase $\phi(u_X)$ is determined from knowledge of the modulus of function $U(u_X)$ and the position of its zeros in J_-. We should take note of the importance of this statement, as until recently it had been assumed according to Rayleigh that the amplitude (modulus) and position of interference lobes (phase) are mutually independent quantities, and that both measurements (space and time) have to be made separately to reconstruct the spectra [Ref. 24].

The problem of the influence that the Blaschke factor has on reconstruction was considered by Wolf [Ref. 195], who concluded that in the case of consideration of the function of time coherence $U(\tau)$ the differences in the curves of the reconstructed spectra in the "miniphase" solution (with consideration of ϕ_m alone) and in the complete solution ($\phi_m - \phi_b$) do not exceed a few percent with respect to major parameters.

Examples can be given of spectra that do not have zeros in J_ [Ref. 122].

Furthermore, for the two extreme cases that are of interest for radio astronomy, namely ideal blackbody radiation and monochromatic emission, the phase problem has been considered and a solution has been found in the research.

Thus we can make a general recommendation that the simple and elegant miniphase solution in form (6.35) be used to get information on the phase in the first approximation, and that the question of sufficiency of the resultant solution that is associated with the presence and influence of zeros be determined separately in each individual case.

In accordance with this, we arrive at the following "skeleton" of a solution for the problem of reconstructing radio brightness from experimental recordings of W:

$$W(t)=|U(u_x)|\overset{H}{\leftarrow}\varphi(u_x)\rightarrow U(u_x)\overset{\Phi}{\rightleftarrows}B(\xi), \qquad (6.39)$$

where the symbols H and Φ denote the Hilbert and Fourier transforms respectively.

As has been noted, determination of the modulus U from W presents no difficulties, and therefore, writing out (6.33) we get

$$B(\xi)=\int_0^\infty U(u_x)\,e^{-i(\varphi_m+\varphi_b+u_x\xi)}du_x, \qquad (6.40)$$

where

$$\varphi_m=\lim_{\varepsilon\to 0}\left[\int_{-\infty}^{u_x-\varepsilon}\frac{\ln U(u'_x)}{u'_x-u_x}du'_x+\int_{u_x+\varepsilon}^{\infty}\frac{\ln U(u'_x)}{u'_x-u_x}du'_x\right] \qquad (6.41)$$

is the principal value of the Cauchy integral.

As we can see, analytical Fourier transform (6.40) differs from conventional Fourier transform (6.33) in the change of limits of integration and the inclusion of Hilbert transformation as an internal operation.

Denoting the analytical Fourier operator by symbol $\tilde{\Phi}$, we can write (6.40) as

$$B(\xi)\overset{\tilde{\Phi}}{\rightleftarrows}U(u_x). \qquad (6.42)$$

Let us note that expressions (6.40)-(6.42) are the fundamental solution of the problem for a symmetric interferometer without consideration of issues of practical realization relating to the influence of the inhomogeneous medium, smoothing effects of antennas, inequality of interferometer arms, etc. The

solution has been obtained for asymmetric inhomogeneous distributions $B(\xi)$. for symmetric [distributions] relative to the center of gravity ξ_0 of the source, expression (6.40) is simplified:

$$B(\xi)=\int_0^{\infty} U(u_x)\cos \nu_x \xi_0 du_x. \qquad (6.43)$$

A solution of form (6.43) can be extended to time frequencies as well, thus giving time spectra of the radiation sources.

In this case we have

$$O(\omega)\overset{\tilde{\Phi}}{\rightleftarrows} U(\tau), \qquad (6.44)$$

where operator $\tilde{\Phi}$, being extended to time frequencies, has the above-mentioned meaning, and τ is time delay introduced into the arms of the interferometer.

Radio astronomical interferometry experimentally realizes both kinds of coherence: spatial (SC) and temporal (TC). The former is realized due to a change in base of the interferometer, and the latter is due to rotation of the earth. In this sense, we have an analog of the Michelson and Young optical interferometers [Ref. 18]. Thus we find that the complex luminosity function reflects the concepts of SC and TC and completely determines the characteristics of radiation from cosmic sources arriving at the earth, which in the final analysis gives information about the morphology of the sources, and about the nature of processes occurring in them. This is reflected in the following transcription of the solution found in the most general form:

$$E(\xi, \omega)\overset{\tilde{\Phi}}{\rightleftarrows} U(u_x, \tau), \qquad (6.45)$$

where $E(\xi, \omega)$ denotes the distribution of radiation energy of the source with respect to spatial coordinates ξ and temporal frequencies ω.

Assuming in (6.45) $\tau = \text{const}$, i. e. singling out the spatial frequencies, we get the spatial spectrum of the source ("static one-dimensional portrait" of the source) that reveals its morphological features.

Setting $\omega = \text{const}$ in (6.45), the interferometer is contracted to a point, which is equivalent to recording on an isolated antenna, i. e. by isolating the time frequencies we get the time spectrum of the source. This gives information on the dynamics of processes that take place in the source and on the nature of its radiation, i. e. we get a "dynamic portrait" of the source.

It should be noted that in the general case, spatial and temporal coherence are not independent, conforming to the two-wave equations [Ref. 18]:

$$\nabla^2_{1,2} U(u_x, \tau)=\frac{1}{c^2}\left[\frac{\partial^2 U(u_x, \tau)}{\partial \tau^2}\right], \qquad (6.46)$$

where $\nabla^2_{1,2}$ is the laplacian with respect to coordinates of the end points of the base in predetermined direction x; c is the velocity of light in vacuum.

In essence, solution (6.46) is the well-known Van Zittert-Zernike theorem which in the most general form is represented by expression (6.45). Thus even from (6.46) we get in case $U(u_X, \tau_0)$ the spatial spectrum corresponding to SC, and in case $U(u_0, \tau)$ -- the temporal spectrum of the source corresponding to TC, if u_0, τ_0 are constant parameters.

For spectrally pure processes, the so-called "reduction formula" is applicable [Ref. 24]:

$$U(u_x, \tau)=U(u_x, \tau_0)U(u_x, \tau-\tau_0),$$

where the first factor in the right-hand member denotes spatial coherence, and the second denotes temporal coherence.

Let us note that the resultant solution of the phase problem is applicable not only in interferometry where the informer is the function of coherence as the correlation of emission at two points of the wave front, but also in the case of signal registration at one point on an isolated antenna (here the meaning of "point" is arbitrary).

In the latter case the signal can be considered as the resultant of elementary interferometers with different bases fitting in the aperture of the antenna.

In principle, any point of the wave front contains information about all details of the emitting object.

A certain analog in classical holography is the well-known fact of reconstruction of the wave image of an object from a fragment of a hologram.

Aperture synthesis, which has come into extensive use in radio astronomy, can be considered as a spatial radio hologram, and with appropriate recording and processing, e. g. for the radiation of cosmic sources -- "space masers" (spectral atomic and molecular lines of H, OH, NH_3, H_2O and so on) -- we can reconstruct a "portrait" of the emitting regions.

Correlation processing of signals recorded by elements of aperture synthesis can be done both with respect to high frequency and with respect to the envelope. In the latter case we get the analog of the so-called "intensity interferometer", where the informer is the square of the modulus of the luminosity function. Even in this case, after elementary conversion, the phase of the complex luminosity function is reconstructed from the known modulus, i. e. there are no losses of information on phases of high-frequency signals.

6.5. Systems Approach to the Optical Cavity Problem

The use of systems theory gives new possibilities for analyzing and synthesizing open cavities [Ref. 1, 14].

The essence of the systems approach to the optical cavity problem consists in the following. Some distribution of the electromagnetic field is taken as the input signal simulating the open cavity, and the field distribution in the same plane produced by the input action as a result of its repeated

propagation from one grain to another is taken as the output signal. Such a system is completely described by the space-frequency characteristic. Besides, the inverse Fourier transform of the frequency response gives the response of the system to the input signal described by a delta function, or else gives the Green's function of the optical cavity problem. Knowledge of the Green's function enables us to find the modes of the open cavity, since it is the sum of the eigenfunctions (modes) of the given problem.

In most solutions of electrodynamic problems, finding the Green's functions presents serious difficulties. The simplicity of the elements that comprise the optical cavity (mirrors or generators of frequency-modulated waveforms, space as a linear phase filter [Ref. 14]), enable us to construct a model of the optical cavity as a linear system with feedback [Ref. 14], to determine the space-frequency characteristic of such a system, and by carrying out its Fourier transformation to get a pulse response, i. e. the Green's function of the optical cavity problem.

The general space-frequency characteristic of the open cavity is found in the following way. Let H(u) be the space-frequency characteristic of the system that describes one circuit of the cavity by an electromagnetic perturbation.

After each circuit of the cavity, the electromagnetic perturbation of a certain plane is again incident on this plane, in virtue of which the cavity is a system with feedback, and its general space-frequency characteristic has the form

$$H_0(u)=\frac{P_{u_0}(u)}{1-H(u)},$$

where $P_{u_0}(u)=\begin{cases}1, \text{for } |u|\leqslant u_0\\ 0, \text{for } |u|>u_0\end{cases}$ is the pupil function that determines the band of transmitted space frequencies. Here use is made of the property of the pupil function

Within the framework of idealization that uses the Huygens-Fresnel principle:

$$H_0(u)=\frac{P_{u_0}(u)}{1-r_1r_2\exp i\left[-\left(\frac{1}{4(2\alpha-\beta_1)}+\frac{1}{4(2\alpha-\beta_2)}\right)u^2-(\beta_1+\beta_2)x^2\right.}, \quad (6.47)$$

where r_1, r_2 are the mirror reflectivities, $\alpha=k/2L$; $k=2\pi/\lambda$ is the wave number; L is the distance between mirrors; $\beta=k/2f$; f is the focal length of the mirror.

Inverse transformation of the Fourier characteristic gives the pulse response of the system

$$h_0(x)=\frac{1}{2\pi}\int_{-\infty}^{\infty}H_0(u)e^{iux}du.$$

Let us represent this integral in the form of the convolution of Fourier transforms of the cofactors $P_{u_0}(u)$ and $\frac{1}{1-H(u)}$ of function $H_0(u)$

$$h_0(x)=\Phi\{P_{u_0}(u)\} \ast \Phi\left\{\frac{1}{1-H(u)}\right\}, \qquad (6.48)$$

that defines the Green's function of the cavity problem. (Here $\ast$ dnotes convolution of the two functions.) The first function in convolution (6.48) is $\sin u_0 x/\pi x$, and accounts for finiteness of the mirror dimensions. The second function defines the solution of the problem of modes with infinite mirrors, and is expressed in form $\Sigma e^{iu_m x}$, where

$$u_m=\sqrt{-\frac{4(\beta_1+\beta_2)(2\alpha-\beta_1)(2\alpha-\beta_2)}{4\alpha-(\beta_1+\beta_2)}x^2+\frac{2(2\alpha-\beta_1)(2\alpha-\beta_2)}{4\alpha-(\beta_1+\beta_2)}(2\pi m-\ln r_1 r_2)}.$$

Thus the general solution is written as integral

$$h_0(x)\sim\sum_m\int_{-\infty}^{\infty}e^{iu_m x}\frac{\sin u_0(x-\xi)}{x-\xi}d\xi.$$

As an example we consider a cavity with identical infinite mirrors ($R_1=R_2=R$) and we find the set of eigenfunctions that correspond to subscript $m=0$. We restrict ourselves to the approximation of real mirrors, i. e. we set $r_1=r_2=1$. We have

$$u_0=ix\frac{2\pi}{\lambda L}\sqrt{2\nu-\nu^2},\quad \nu=\beta/\alpha=L/R,$$

implying $\psi_0(x)=e^{iu_0x}=e^{-\frac{2\pi}{L\lambda}\sqrt{2\nu-\nu^2}x^2}$.

Under these conditions, in the case of infinite plane-parallel mirrors ($\beta_1=\beta_2=L/2R=0$) the optical cavity is a spatially invariant system and its general space-frequency characteristic will be in accordance with (6.47)

$$H_0(u)=\frac{1}{1-\exp i(-Lu^2/k)}.$$

The pulse response of such a system will be equal to

$$h_0(x)=\frac{1}{2\pi}\int_{-\infty}^{\infty}\frac{1}{1-\exp\left(-i\frac{L}{k}u^2\right)}e^{iux}du. \qquad (6.49)$$

The integrand has first-order poles at points

$$u_m=\pm\sqrt{2\pi mk/L},$$

and a second-order pole at point $u=0$. The residue at point $u=0$ is zero. The residue at point u_m is $e^{iu_m x}/2\frac{L}{k}u_m$. Thus the pulse response of the cavity will take the form of the sum

$$h_0(x)=\sum\frac{\cos(u_m x)}{Lu_m/k}.$$

For a planar cavity we get a solution in the form of cosines with argument that includes the distance between mirrors. The latter circumstance enables us to find the solution of a cavity with a mirror that has periodically spaced apertures.

Let us consider a cavity in which one of the plane-parallel mirrors has a periodic structure that consists of alternating reflecting and transparent strips of identical width $x_0/2$.

The space frequency characteristic of the system that describes the process of propagation between two planes separated by distance z takes the form [Ref. 33]

$$H_z(u)=\exp\left\{i2\pi\frac{z}{\lambda}\sqrt{1-\left(\frac{\lambda u}{2\pi}\right)^2}\right\}. \qquad (6.50)$$

Let us limit ourselves to consideration of the case of two spatial harmonics (m = 0, 1). Then the output signal of the system will have a spectrum defined by the expression

$$F_{\text{вых}}(u)=F_{\text{вх}}(u)\sum_{m=0,1}H(m2\pi/x_0)\delta(u+m2\pi/x_0)=$$
$$=F_{\text{вх}}(0)H(0)+F_{\text{вх}}(2\pi/x_0)H(2\pi/x_0).$$

[Russian subscripts вых = output; вх = input]

In the case of optical systems, the function $F_{\text{вых}}(u)$ is equal to the amplitude of the field in the exit pupil. In the given case it is equal to the amplitude of the field in plane z. The intensity of this field is

$$F_{\text{вых}}(u)F^*_{\text{вых}}(u)=|F_{\text{вх}}(0)|^2+|F_{\text{вх}}(2\pi/x_0)|^2+$$
$$+2|F_{\text{вх}}(0)||F_{\text{вх}}(2\pi/x_0)|\cos[\varphi(0)-\varphi(2\pi/x_0)],$$

where $\phi(u)$ is the phase of frequency response (6.50).

With consideration of expression (6.50), the intensity in plane z is represented in the following form:

$$F_{\text{вых}}(u)F^*_{\text{вых}}(u)=|F_{\text{вх}}(0)|^2+|F_{\text{вх}}(2\pi/x_0)|^2+$$
$$+2|F_{\text{вх}}(0)||F_{\text{вх}}(2\pi/x_0)|\cos\left[2\pi z/\lambda-2\pi z/\lambda\sqrt{1-(\lambda/x_0)^2}\right].$$

This implies that the intensity of bands formed in plane z is maximum if the distance to this plane is

$$z_M=\frac{M\lambda}{1-\sqrt{1-(\lambda/x_0)^2}},\quad M=1,2,...$$

If period $x_0>>\lambda$, we get the relation

$$z_M=2Mx_0^2/\lambda.$$

The resultant relations coincide with the known Rayleigh relations [Ref. 74]. It was Rayleigh who called attention to this effect of lattice reproduction

in coherent light. Subsequently, the effect was experimentally verified and a number of papers were devoted to it, e. g. Ref. 38, 125. Space-frequency analysis of an open optical cavity gave the capability of determining the form of the natural oscillations of the resonant cavity -- periodic modes -- a phenomenon similar in nature to the lattice reproduction described by Rayleigh.

In the general case for a cavity with mirrors having radii of curvature R_1 and R_2, we get the condition of existence of periodic modes from the expression that defines the Green's function:

$$\left[\lambda L-\frac{\lambda L^2}{4}\left(\frac{1}{R_1}+\frac{1}{R_2}\right)\right]=Nx_0,$$

where N = 1, 2, 3...

Fresnel Sandwich as Optical Cavity

The Fresnel sandwich is a device in which the distribution of the field of electromagnetic radiation repeats itself.

Finding the conditions of self-reproduction of the field is the problem of mode determination.

Consequently, if we make the reflectivity of one of the mirrors vary like a Fresnel function (which is reproduced in the sandwith), then under certain conditions the distribution of the field reflected from this mirror will reproduce itself after each pass through the cavity, and the Fresnel sandwich can be used as an optical cavity. According to Ref. 58, a Fresnel sandwich made up of three Fresnel zone plates (Fig. 6.26 realizes Fourier transformation at certain parameters so that its action is described by the following equation:

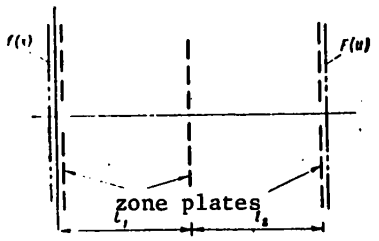

Fig. 6.26. Fresnel sandwich

$$F(u)=z_0^*(x)\{[f(x)Z_0^*(x)\ast Z_0(x)]\}(u), \qquad (6.51)$$

where f(x) is the initial function to be transformed by the Fresnel sandwich. This function may be the amplitude distribution of the electromagnetic field in plane z = 0, i. e. in direct proximity to the first Fresnel zone plate (see Fig. 6.26):

$Z_0(x)=u_0\sqrt{2}\exp(iu_0^2x^2)$ is the Fresnel function.

Here we are considering one-dimensional distribution of the electromagnetic field f(x). The results of such consideration are easily extended to the case of real two-dimensional distribution f(x, y).

Transformation of the image f(x) via the Fresnel sandwich leads to the Fourier transform of the initial function. For this purpose it is necessary that the

zone plate in plane $z = l_1$ be reduced with respect to zone plates in planes $z = 0$ and $z = l_1 + l_2$ by a factor of $l_1/l_1 + l_2$, and that the parameter of the Fresnel function $Z_0^*(x)$ satisfy equality $u^2 = 1/2$. The Fourier image of the initial function is formed in the plane directly behind the third zone plate, i. e. in plane $z = (l_1 + l_2)$.

Now let the surfaces of the plane-parallel mirrors that comprise the open optical cavity have reflectivity that varies as the transmission function of the Fresnel zone plate, and let the corresponding zone plate be placed between such mirrors in plane $z_1 = l_1$. The action of such a cavity, like the Fresnel sandwich, is described by equation (6.51), i. e. at certain parameters such a cavity realizes Fourier transformation of the electromagnetic field distribution after one pass from one mirror to another.

The first multiplication $f(x)Z_0^*(x)$ in the right-hand part of equation (6.51) takes place upon reflection of the electromagnetic wave from the first mirror in plane $z = 0$. The operation of convolution is also realized just as in the Fresnel sandwich as a result of light transmission through the zone plate located in plane $z = l_1$. The last multiplication is realized upon reflection of light from the second mirror located in plane $z=(l_1 + l_2)$. The Fourier image of function $f(x)$ is formed in plane $z = (l_1 + l_2)$ -- in direct proximity to the surface of the second mirror.

In virtue of symmetry, its eigenfunctions will be defined by the equation

$$\lambda_k \psi_k(x) = \int_{-a}^{a} \psi_k(\xi) e^{-ikx} d\xi, \qquad (6.52)$$

where λ_k are eigenvalues corresponding to eigenfunction $\psi_k(x)$, and a is the transverse dimension of the mirror.

Equation (6.52) for the modes of the described cavity coincides with the equation that defines the eigenfunctions of a confocal cavity. These functions are proportional to spheroidal wave functions, and they have a number of properties that are useful for applications. For example $\psi(x)$ has the maximum possible energy on interval $|x| \leqslant a$, which dictates minimum possible diffraction losses in the optical cavity. In addition to this property of the eigenfunctions of the Fresnel sandwich, the feasibility of using it as the optical cavity in a laser is due to the capability of coupling electromagnetic energy out through apertures in the zone-plate mirrors, the influence on output beam parameters (reduction of divergence as a consequence of an increase in spot diameter on the mirror), and more complete utilization of the active substance of the laser due to diffraction by the zone structures of such a cavity.

6.6. Holographic and Integrated Optics

A certain number of optical devices are used to transform the amplitudes, phases and polarization characteristics of light beams: mirrors, prisms, lenses, birefringent and phase plates, polarizers, various kinds of gyrators and diffraction gratings. Optical components of this type are usually cumbersome and expensive, and their capabilities for handling light beams are limited.

This has given rise to the problem of developing compact optical equivalents of known optical components and devices that have new properties. These problems have been studied in a number of papers [Ref. 22, 36, 61, 62, 113, 114, 145].

Holographic methods enable us to produce holograms that are analogs of conventional optical components and that in addition have a number of interesting peculiarities [Ref. 62]. The capability of superimposed holograms to act independently allows the development of complex combinations of such components and even creation of new devices that have no analogs in classical optics.

The new field of application of holographic methods of producing and proliferating both elementary and complex optical components is developing rapidly.

Hologram-Mirrors. The simplest optical component is a flat mirror (total internal reflection prism) -- an optical device that changes the direction of a light beam. Its principal characteristic is reflectivity; multilayered dielectric coatings are used to increase this parameter. Such mirrors are essentially artificial holograms adapted for operation in monochromatic light. With appropriate production they can alter the nature of polarization of reflected light beams in a predetermined way. Extensive use is made of multilayered coatings that do not change the nature of polarization of light that is incident on them at a certain angle. Sometimes such hologram-mirrors can be used as light filters and polarizers. Such components are characterized by less irregular scattering of light than conventional optical mirrors.

Hologram-Lenses and Holographic Objectives. The diffraction analog of a lens is the zone plate. A zone plate forms an image of an extended object in the same manner as a conventional lens, and its resolution at the focus is equal to that of an ideal lens of the same aperture. The main disadvantage of the zone plate (both phase and amplitude plates) is the presence of a series of focal lengths corresponding to real and imaginary foci that depend on the wavelength of light. In contrast to an ideal lens, the zone plate is not tautochromic. In imaging objects that are a finite distance away or off the optical axis, the light reaches the end zones and the center at different times, leading to dephasing of waves in the focal plane.

An important advantage of zone plates is their two-dimensionality and their capability for focusing infrared, ultraviolet and soft x-rays. This property is used in making compact light equipment for space research [Ref. 113, 11].

Zone plates are made most precisely and simply by a holographic method. Zone plates can be recorded on both sides of a thick photographic emulsion by Yu. N. Denisyuk's technique [Ref. 36] with subsequent reconstruction by white light with selection of one wavelength. Such zone plates give only the real image. When a zone plate is recorded in the light of three lasers operating on different wavelengths, it can be used to get a color image.

Holographic recording of zone plates in the off-axis arrangements gives plates with spatial separation of the principal real and imaginary foci from each other and from the zero diffraction order. Such a recording scheme almost completely eliminates background and considerably improves image quality.

In addition to the classical zone plate, a hologram-lens can be made that is formed by two point sources producing diverging spherical waves. High-quality objective lenses have been recorded on holograms in this arrangement. The resultant holograms are the analogs of the objective lenses. The use of a hologram-lens for recording an image to produce focused-image holograms enables simultaneous production of both the focused image and a reference beam in the form of undiffracted light.

Computers can be used to improve the diffraction efficiency of hologram-lenses made on photographic emulsions. In this case, the calculated relief is applied to a large surface, then reproduced by precision optics. The diffraction efficiency of such hologram-lenses (kinoforms) reaches 90% [Ref. 145].

The strong chromatic aberration of the hologram-lens can be used in spectral instruments. The hologram-lens can serve as a dispersing component, replacing expensive concave diffraction gratings.

An important advantage of diffraction optics is the capability of producing complex optical components. One of these is the holographic image multiplier on which the Fourier transform of a set of point sources is recorded. Such a device produces multiplied images with resolution of 6 μm on a 5 x 5 cm field.

Holographic Diffraction Gratings. These are made in sizes up to 150 mm, band frequency 3000 lines/mm, resolution of the order of 1 Å. The holographic method produces gratings that give forward diffraction of a wave of given shape, enabling correction of aberrations of optical systems of spectral instruments.

Holograms as independent optical elements produce a real image of an object without using additional lenses and objectives. Holographic methods that permit recording of several holograms on a single photographic plate open up new possibilities for making light and compact optical devices capable of performing the functions of several components simultaneously [Ref. 22].

One of the important jobs on the road to development of holographic optics is to work out a method of getting holograms that have high diffraction efficiency, i. e. low losses [Ref. 107, 108]. Obviously these must be phase holograms since amplitude holograms inevitably absorb part of the energy passing through them.

The development, standardization and classification of artificial optical components enables us to make optical devices in accordance with principles analogous to those in electronic systems.

Optical effects in thin-film waveguides can be used for optical and optoelectronic data processing. Thin-film dielectric waveguides can be used as a basis for miniature laser devices, optical modulators, filters, parametric generators and other components for communication systems with large information capacity, high-speed computers and for optical data processing systems. The production of thin-film optical components on a flat dielectric backing opens up the serious possibility of integrated optical circuits [Ref. 145].

Integrated optics sprang up as a result of studying the principal properties of optical waveguides on a dielectric backing, development of the method of input and extraction of light through a waveguide surface based on the optical tunnel effect, and accomplishment of laser frequency conversion in a nonlinear thin-film waveguide.

One of the problems of integrated optics is creation of passive optical components (lenses, prisms, diffraction gratings) in film. Just as prisms and lenses are formed in conventional optics by appropriately shaping the surfaces of transparent dielectrics, so components that act as prisms or lenses can be formed in thin films by appropriately shaping the boundaries of a region of change in the index of refraction. For practical purposes, this can be done by a local change in thickness of the film. In another technique, prisms and lenses are formed by introducing a suitably shaped layer with high index of refraction into a waveguide film or substrate. Film prisms can be used to analyze the frequency spectrum of a waveguide light beam in any mode, or for spatial separation of the light of different modes on the same frequency. Thin-film lenses for a surface wave are formed by shaping a curved boundary of the region with changed film thickness.

An important part in making prisms and lenses in thin-film optics is played by dispersion of the index of refraction, which is readily altered over a wide range by selecting film thickness. It should be noted that we can have refraction on the boundary of two regions without dispersion, which is important for making achromatic prisms and lenses.

In addition to prisms and lenses, diffraction gratings can be made in two-dimensional optics by applying closely spaced depressions on film surfaces, or by applying dielectric strips with low index of refraction. The constant of propagation of the surface wave in such a structure undergoes periodic variations, leading to diffraction effects similar to light scattering on a standing acoustic wave in a volumetric medium. These phenomena can be used in a number of thin-film devices of the spectral filter and mode selector type. Material with high saborption applied instead of a dielectric on the film surface causes rapid attenuation of the optical surface wave. This effect can be used to create thin-film equivalents of amplitude masks, spatial filters, gratings and lenses of the Fresnel zone plate type.

Dielectric films with thickness of the order of a wavelength of light or less are important in integrated optics. Critical film thicknesses corresponding to low-order surface waves lie in this range. At the minimum effective thickness of the waveguide, the maximum gradient of the effective index of refraction is reached. The optical tunnel effect based on a prism is used for coupling the radiation into and out of thin-film waveguides. It is a complicated job to get the optimum profiles of the film and gap that ensure total input of a given light beam into a predetermined mode of a thin-film waveguide.

In addition to tunnel input of radiation, it is highly effective to excite surface waves by a phase diffraction grating applied on the surface of the waveguide film. The input devices use both planar and volumetric diffraction gratings that are applied directly on the wavetuide film. Radiation can be coupled in and out through a tapering edge of waveguide film.

The waveguide film may consist of dielectric layers of optically nonlinear material. The properties of nonlinear optical waveguides can be used to excite radiation on combination frequencies of the initial waves, and also to get the second harmonic. Thin-film optical waveguides can be used for spatial scanning of surface waves. Of greatest promise here is an acoustic method--interaction of light with elastic waves propagating in the film. The capability for getting high concentrations of optical and acoustic energy in thin films allows creation of efficient thin-film spatial modulators. The acoustic method of converting surface wave modes is not unique. It is possible to convert optical modes in films with anisotropic and gyrotropic backings and boundary interfaces.

At the present time, a number of active components have been suggested and realized in thin-film waveguides. An investigation has been made of stimulated emission of gelatin films of different thicknesses and under different pumping conditions. In addition to the capability for single-frequency lasing in a film 14 μm thick, the possibility has been noted of multifrequency lasing with strong pumping and in thicker films. The multifrequency nature of the radiation is associated with stimulated emission of different modes of the gelatin film. A change in the period of spatial modulation of the index of refraction or gain gives the capability of tuning laser wavelength with distributed feedback. For these purposes we can use the property of an organic dye solution to change gain and index of refraction upon absorption of intense optical radiation. Creation of a thin-film ring laser in which strong feedback is set up by the simplest method enables expansion of the class of thin-film lasers by using media with moderate gain. The thin-film ring laser can be quite simply joined to a flat film on a backing, and is used for coupling radiation into the film.

Electroluminescent and semiconductor lasers can be used as thin-film active elements, and have a fine outlook in integrated optics in view of their small size, high efficiency and other advantages over lasers of different types.

In recent years, integrated optics has reached a level of development where its capabilities revealed in laboratory studies are finding ever wider application for optical and optoelectronic data processing.

6610
CSO: 1862/163

PLASMA PHYSICS

UDC 533.9.01

NONEQUILIBRIUM LOW-TEMPERATURE PLASMA KINETICS

Moscow KINETIKA NERAVNOVESNOY NIZKOTEMPERATURNOY PLAZMY in Russian 1982 (signed to press 10 Dec 81) pp 2-5, 373-375

[Annotation, preface and table of contents from book "Nonequilibrium Low-Temperature Plasma Kinetics", by Leon Mikhaylovich Biberman, Vladimir Sergeyevich Vorob'yev and Igor' Tevfikovich Yakubov, Institute of Low Temperature Physics, USSR Academy of Sciences, Izdatel'stvo "Nauka", 2350 copies, 376 pages]

[Text] This book is the first to cover a wide class of problems in nonequilibrium low-temperature plasma kinetics. Data are given on collisional and radiative elementary processes. Radiative transfer of excitation is considered. Criteria of equilibrium under a variety of experimental conditions are discussed. Nonequilibrium distributions of atoms by levels are described as well as electron energy distributions. Methods are outlined for calculating coefficients of ionization and recombination. Unsteady processes are discussed. Some questions of kinetics in a molecular plasma are considered.

The book is intended for scientists and engineers working in the fields of plasma physics and plasma chemistry, electric discharge in gases, physical electronics, and also for graduate students and upperclassmen majoring in physical and technical fields. Figures 128, tables 44, references 490.

Preface

The first plasma research was done in connection with studying electric discharge in gases. Physicists had been concentrating on partly ionized plasma with kinetics determined by various collisional and radiative processes. This trend of research was determined to a considerable extent by practical problems that were urgent at the time: developing gas-discharge light sources, rectifiers, inverters.

Since the early fifties, interest in plasma physics has taken a sharp upturn. This applies primarily to the investigation of completely ionized plasma with its various collective phenomena, instabilities, interesting and at times unexpected effects associated with propagation of electromagnetic waves in such a plasma and the action of external electric and magnetic fields on the plasma. Interest in hot plasma has been stimulated not only by the variety and novelty of physical processes and effects, but also by problems that have arisen in connection with controlled nuclear fusion.

The appearance of new technical fields in the early sixties, such as gas-discharge lasers, magnetohydrodynamic generators, thermoemission converters, plasma chemistry, plasma engines, various methods of plasma technology and the like, rekindled interest in weakly ionized low-temperature plasma. This applies primarily to nonequilibrium plasma that is distinguished by extraordinary diversity of states and properties. It is in a weakly ionized nonequilibrium plasma that population inversion of excited states of atoms and ions is realized, high electrical conductivity of low-enthalpy gas flows is attained that is necessary for installations of direct energy conversion, and selective excitation of individual states of atoms is realized that ensures efficiency of plasma-chemical reactions. Specific oscillations and instabilities that originate in nonequilibrium low-temperature plasma are of considerable physical interest.

Low-temperature plasma kinetics is determined by a combination of a large number of elementary processes, among which we mention inelastic collisions of electrons with excited and unexcited atoms, inelastic collisions of atoms and ions, processes of associative ionization and dissociative recombination and many others that are absent or of little significance in a hot plasma. Processes of radiative excitation transfer play an appreciable part. As a result, the kinetics of low-temperature plasma is in some sense also more complicated and varied than the kinetics of a completely ionized plasma, largely due to the presence of atoms and molecules with their numerous excited states.

Despite the considerable advances that have been made in recent decades, low-temperature plasma kinetics has not yet been duly reflected in monographs devoted to plasma physics. The widely known series "Problems of Plasma Theory" edited by M. A. Leontovich, and books by L. A. Artsimovich and R. Z. Sagdeyev "Plasma Physics for Physicists", I. Shkarovskiy, T. Johnston and M. Bachinskiy "Kinetics of Plasma Particles", N. Kroll and A. Trayvelpis "Fundamentals of Plasma Physics" and others have dealt primarily with other problems. In this book the authors have attempted to fill this gap. Major emphasis has been given to kinetics of ionization, excitation, recombination, energy distribution among plasma components and individual degrees of freedom of these components, energy exchange between plasma and ambient medium. The plasma is treated as an interrelated system of electrons, ions and atoms in different energy states. Interaction among particles in the presence of external perturbations gives rise to compromised nonequilibrium states. A more detailed exposition of some problems can be found in other publications. The state of a plasma in magnetic fields is described in the series "Problems of Plasma Theory". The book by A. V. Yeletskiy, L. A. Palkina and B. M. Smirnov "Transport Phenomena in Weakly Ionized Plasma" contains a fairly complete exposition of the physics of transport phenomena in low-temperature plasma. Instability problems are covered in a series of surveys by Ye. P. Velikhov et al., and also in the book by A. V. Nedospasov and V. D. Khait "Oscillations and Instabilities of Low-Temperature Plasma". There is a series of monographs dealing with problems of kinetics that arise in connection with development of specific applied devices: MHD generators, lasers and the like. In our monograph we cover problems that are in some measure common to all these applied studies. Nonequilibrium plasma theory is presented simultaneously with numerous experimental results.

Chapter 1 outlines the region of parameters corresponding to low-temperature plasma, giving the major concepts of plasma physics necessary for further exposition.

Chapter 2 is devoted to elementary collisional and radiative processes. It is a reference chapter that provides the minimum required information on probabilities of elastic and inelastic collisions and radiative transitions. Considerable attention is given to approximate and semiempirical relations for probabilities of various elementary processes.

Radiative excitation transfer plays a rather important part in nonequilibrium plasma kinetics. This question is treated in Chapter 3.

The authors have deemed it necessary to set forth the criteria of arisal of various kinds of nonequilibria individually in the fourth chapter. Research results given in this chapter are presented on the basis of physical considerations, and can be used without studying the subsequent chapters where they are more rigorously substantiated.

Chapter 5 examines the distribution of atoms with respect to excited states. This topic is of interest not only from the standpoint of the optical properties of plasma and its diagnosis. Excited atoms play a quite important part in the kinetics of ionization and recombination, being as it were the rungs of a ladder over which the electron passes from the bound to the free state and back.

Chapter 6 outlines the kinetics of ionization and recombination. Various mechanisms of ionization and recombination are discussed, methods are given for calculating coefficients of ionization and recombination, and also reference data. Nonequilibrium ionization in a plasma is considered.

Chapter 7 is devoted to the velocity distribution of electrons, and to the energy balance of an electron gas. Considerable attention is given to the influence of inelastic collisions on energy distribution of electrons, and to the relation between nonequilibrium electron energy distribution and the distribution of atoms by excited states.

In chapter 8 we consider some questions of an unsteady nonequilibrium plasma; primarily the rather important criteria of quasisteadiness, problems of ionization relaxation, distribution of atoms by excited states and the electron energy distribution function. Also discussed are some problems of low-temperature plasma instability that are closely related to the kinetics presented above.

Molecular plasma kinetics is much more complicated, and at the present time has been less developed than the kinetics of atomic plasma. Some questions of molecular plasma kinetics are discussed in chapter 9. With a view mainly to gas lasers, we briefly consider the kinetics of population of vibrational states of molecules. This section of chapter 9 was written by A. A. Likal'ter, who has the authors' sincere gratitude.

Abbreviated notation is used in tables: e. g. 6.37^{-2} means $6.37 \cdot 10^{-2}$.

Contents

6610
CSO: 1862/166

UDC 533.92

DYNAMICS AND RADIATION OF OPEN (VACUUM) PLASMA-DYNAMIC DISCHARGES OF 'PLASMA FOCUS' TYPE: SURVEY

Moscow TEPLOFIZIKA VYSOKIKH TEMPERATUR in Russian Vol 20, No 2, Mar-Apr 82 (manuscript received 25 Feb 80) pp 359-375

[Article by A. S. Kamrukov, N. P. Kozlov and Yu. S. Protasov, Moscow Higher Technical Academy imeni N. E. Bauman]

[Text] The paper gives the results of an experimental study and analysis of the dynamics, space-time structure and emission properties in the range of energies of quanta of 2-350 eV for open (vacuum) intense plasma-dynamic discharges of the "plasma focus" type. A method is described for comprehensive investigation of the radiation properties of intense emitting discharges in the spectral region from the visible to the extreme ultraviolet (XUV). It is shown that the emission spectrum of a plasma focus is sharply different from planckian, and is due mainly to the recombination continuum of typical groups of ions that determine the properties of plasma at a given temperature and density, 70-90% of the emitted energy belonging to the XUV region of the spectrum.

The authors consider possibilities of effective control of the emission spectrum over a wide range of energies of quanta (influence of macrostructure of hypersonic flow, chemical composition, etc.) and attainment of high brightnesses in the XUV. Brightness temperatures exceeding 5 eV have been reached for the first time in the region beyond the helium ionization potential.

Recent years have seen a considerable upsurge of interest in development of powerful sources of radiation with high brightness temperature in the extreme ultraviolet region. This is due to expansion of the sphere of scientific and applied problems whose solution in large measure depends on development of such sources. In the first rank among such problems are promising developments in design of powerful lasers for the visible and near ultraviolet region for which the absorption bands of working media are in the XUV region (lasers that use allowed electron transitions of molecules [Ref. 1], excimer

photodissociation lasers [Ref. 2]), and also research on the possibilities of developing new types of coherent radiators (photoionization lasers [Ref. 3]). Furthermore, such sources can be used for other purposes as well, e. g. for studying photochemical reactions, processes of interaction of radiant high-density fluxes with condensed media, etc.

The outlook for developing high-intensity plasma sources in the XUV region is determined in large measure by the capabilities of getting sufficiently large volumes of dense ($N_e = 10^{17}$-10^{19} cm^{-3}) plasma with temperature T_e = 2-10 eV, for which a considerable part of the radiation may be in the extreme ultraviolet and associated with photorecombination of electrons to the ground states of double, triple and higher-multiple ions. High selectivity of the emission spectrum of such a plasma, which is important for example for excitation of active laser media, can be attained at fairly small optical thickness of the plasma, where recombination maxima show up in the emission spectrum and have appreciable intensity.

Attracting the most attention among methods of getting a dense radiating plasma is an electric-discharge method with plasma containment by the magnetic self-field of the discharge current. However, in developing XUV radiation sources based on intense self-compressed discharges of the z-pinch type, fundamental difficulties arise that are associated with shielding of short-wave radiation by layers of cool plasma expanding at thermal velocity (vacuum discharges in metal vapor [Ref. 5]), or with arisal of an ionization wave that stabilizes the brightness temperature of the radiating surface on a level of 2-3 eV (discharges in inert gases [Ref. 6]). In contrast to the mentioned sources of radiation, conditions may be realized in the intense plasma-dynamic discharges of a magnetoplasma compressor of the "plasma focus" type [Ref. 7] under which shielding of short-wave radiation of the hot plasma is excluded in principle [Ref. 8]. As is known [Ref. 7], a characteristic feature of self-compressed discharges of magnetoplasma compressors is the high average mass velocities of the radiating plasma ($v_\parallel \sim 50$ km/s), considerably exceeding its thermal velocities (Mach number in the flow $M \sim 5$-10 [Ref. 9]). Thus even in a quasi-steady state of flow, an optically dense shielding layer is not formed due to satisfaction of the condition $v_\parallel >> v_\perp \sim v_{therm}$ ($v_\perp$ is the velocity component perpendicular to the axis of flow).

Of interest in connection with this is a detailed study of the space-time structure and peculiarities of spectral distribution of emission of open plasma-dynamic discharges for the purpose of determining capabilities for effective control of the emission spectrum over a wide range of quantum energies $h\nu \sim 5$-100 eV, and attainment of high brightness characteristics in the extreme ultraviolet.

1. Experimental Conditions and Research Method. Studies of dynamic and radiation properties of open (vacuum) intense plasma-dynamic discharges were done on a facility consisting of a steel discharge chamber 0.8 m in diameter and 3 m long pumped out by a high-capacity vacuum system to a pressure of 10^{-3} Pa, a capacitive energy storage device, a charging module with initiation unit, and also measurement and diagnostic instrumentation.

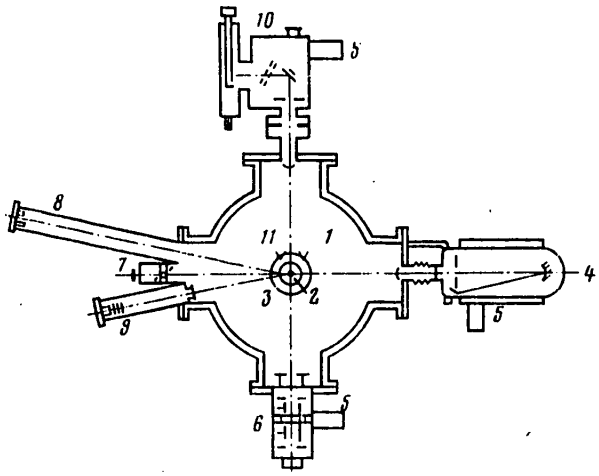

Fig. 1. Diagram of experiment: 1--vacuum section; 2--magnetoplasma compressor; 3--quartz (glass) calorimeter; 4--DFS-29 diffraction spectrometer; 5--differential high-vacuum pumping units; 6--open ionization chamber; 7--vacuum standard based on KRIS; 8--bolometric section; 9--photoelectric sensor with M-foils; 10--scintillation spectrometer; 11--Xr-Co thermocouples

The plasma sources in the described experiments were magnetoplasma compressors of erosion type comprising a coaxial system of cylindrical or specially shaped electrodes separated by a dielectric sleeve. The plasma-forming substances were products of erosion of the electrodes and/or products of ablation of the separating sleeve. The chemical composition of the electric-discharge plasma was controlled by appropriate choice of the construction materials of the magnetoplasma compressor. For example, to get a discharge in metal vapor, heat-resistant dielectrics were used as the material for the separating sleeve (boron carbonitride BNC, zirconium dioxide ZrO_2 or alundum Al_2O_3), and the electrodes of the magnetoplasma compressor were made of the appropriate metal (Cu, Cd, Al, Mo). The main yield of metal in the discharge came from the central electrode (cathode); the partial fraction of erosion of the outer electrode was less than 10%, and did not significantly change the chemical composition of the plasma. When a separating sleeve of ablatable material was used (fluorocarbon plastic $(C_2F_4)_n$, polyformaldehyde $(CH_2O)_n$, cesium iodide CsI, etc.) with electrodes of erosion-resistant metals (Mo, W, Cu), the plasma composition was determined mainly by the products of dissociation and ablation of the dielectric.

Magnetoplasma compressors were used in the experiments with geometry of the electrode system similar to that described in Ref. 10; diameters of the outer electrode were varied over a range of 30-80 mm. The magnetoplasma compressor models were installed on the dielectric end flanges of the discharge chamber, and the investigated discharges were observed and diagnosed through optical side windows in the chamber. All experiments were done with negative polarity of the central electrode in the first half-period of the discharge current.

The electric energy accumulator was a bank of low-inductance IMM-5-150 capacitors connected in parallel. Maximum capacitance of the bank in the described experiments was C = 750 μF, maximum charging voltage was U_0 = 5 kV.

The electrotechnical parameters of the discharge were measured by a standard technique, using calibrated Rogowski loops and compensated RC voltage dividers. The discharge was periodic in nature with strong damping. As a rule, a current pulse contained two or three half-periods with duration varying over a range of 17-20 μs for different models. Maximum current was reached in 6-8 μs of the discharge, and in operation on a fluorocarbon plasma at C_0 = 750 μF was ~420-460 kA (at a rise time dI/dt up to $0.8 \cdot 10^{11}$ A/s). Current damping factor was $\sim 7.7 \cdot 10^4$ s^{-1}. The total inductance and impedance of the discharge circuit together with the magnetoplasma compressor as calculated from the electrical engineering equation for the current in the RLC tank were ~40 nH and $\sim(3\text{-}5) \cdot 10^{-3}$ Ω respectively.

The energy input to the discharge was determined in each specific experiment from oscillograms of the current and voltage, and at C_0 = 750 μF was ~75-85% of the energy stored in the capacitor bank, about 90-95% of the invested energy being introduced during the first half-period of the discharge. Typical values of peak electric powers were ~0.8 GW.

The space-time development of open plasma-dynamic discharges was studied by SFR-2M high-speed cameras operating in single-frame and slit-scan modes. The density of flows and the time-integrated radiation output in individual spectral intervals of the optical band were determined by light-filtered photocells calibrated by the EV-45 reference source. Recording of the time-scanned radiation spectrum was done with an ISP-30 quartz spectrograph equipped with disk slit chronograph. The space-time distribution of brightness temperature T_{br} of the radiation in the visible region was studied by methods of monochromic photometric comparison of densities of blackening of negatives of the slit scans of the discharge and the EV-45 reference source, and the spectral distribution of T_{br} was determined by the method of photoelectric comparison of radiation intensities.

The brightness temperatures of discharges in the XUV range were measured by double open ionization chambers, the integrated energy output of short-wave radiation was determined from heating of a quartz calorimeter and by bolometric methods, the relative distribution of radiation over the spectrum was studied by a photoemission-scintillation spectrum, the XUV spectrum was recorded by the DFS-29 vacuum spectrograph. Fig. 1 shows a diagram of an experimental setup for studying the emission characteristics of plasma-dynamic discharges in the extreme ultraviolet.

2. Dynamics of Open Self-Compressed Plasma-Dynamic Discharges. Fig. 2 [photos not reproduced] shows typical photochronograms that illustrate the dynamics of development of an open plasma-dynamic discharge. The discharge was ignited by a high-voltage (20-50 kV) ignition pulse to the third auxiliary electrode installed in the dielectric sleeve in the middle of the discharge gap in the central electrodes of the magnetoplasma compressor.

The plasma of the ignition discharge initiates a powerful streamer discharge over the surface of the dielectric, leading to intense vaporization and ionization of the working substance. Streamer formation as a contracted current channel (Fig. 2) causes amplitude inhomogeneity of the plasma flow on the initial stage of the discharge ($\tau = 2$-4 μs).

The plasma in the interelectrode gap gives rise to volumetric electric current whose radial component j_r upon interaction with the azimuthal magnetic self-field B_ϕ sets up a longitudinal component of ampere force $F_z = j_r B_\phi$ that accelerates the plasma. The process of plasma acceleration is accompanied by electromagnetic cumulation of flow along the axis of the system and formation of a compressed zone -- the plasma focus -- beyond the tip of the magnetoplasma compressor (Fig. 2a). The mechanism of electromagnetic cumulation reduces to a two-stage process that shows up as Hall compression of the flow toward the central electrode (cathode) in the interelectrode gap, and collapsing of the plasma due to the pinch effect in the entrained streams beyond the tip of the magnetoplasma compressor [Ref. 7].

The region of compression is localized in space, and is a macroscopically stable formation, i. e. a fairly clear outline of a quiescent jet is observed over nearly the entire first half-period of the discharge. Maximum compression occurs 1-2 μs after attainment of the maximum current in cross sections 1.5-3 cm away from the tip of the magnetoplasma compressor. The transverse size of the flow in this case is a few mm, length of the compression zone is 7-15 cm, divergence of the jet is 12-16°.

The plasma flow in the compression zone is contained by the magnetic field of the discharge. Estimates of the ratio of magnetic pressure p_M and gasdynamic pressure p_r

$$\frac{p_M}{p_r} = \frac{\mu_0 H^2/2}{\left(N_e + \sum N_i\right) kT} = \frac{2 \cdot 10^{-7} I^2/\pi d^2}{N(1+\bar{z})\, kT}$$

show that for typical plasma parameters (see below) the concentration of heavy particles $N \sim 10^{19}$ cm^{-3}, average charge of ions $\bar{z} = N_e/\Sigma N_i \sim 2$, temperature $kT \sim 5$ eV, diameter of the plasma column $d \sim 0.6$ cm, magnetic forces predominate over gasdynamic forces even at currents greater than ~40 kA.

An important characteristic of the magnetoplasma compressor as a device for producing dense high-velocity plasma flows is the coefficient of utilization of the working substance $\eta_{w.s}$, which is the ratio of the amount of material flowing through the zone of the plasma focus to the total consumption of mass over the discharge pulse. In its physical sense, this parameter characterizes the macroscopic structure of the plasma flow discharged from the magnetoplasma compressor. At high values of $\eta_{w.s} \sim (0.9$-$0.95)$ (Fig. 3a, c [photos not reproduced]) the flow is a dense magnetohydrodynamically formed plasma jet with small angular divergence. A reduction of $\eta_{w.s}$ (Fig. 3b [photo not reproduced]) results in a considerable part of the erosion mass not flowing through the focus zone, and being discharged from the magnetoplasma compressor as a supersonic jet that is practically not contained by the magnetic field of the discharge and expands freely into the vacuum. Capabilities for controlling $\eta_{w.s}$

and consequently the macrostructure of the flow in discharge systems based on magnetoplasma compressors of erosion type involve appropriate choice of energy conditions, the geometry of the discharge gap, thermophysical properties and the method of introducing the plasma-forming substances into the discharge. As will be demonstrated below, the macroscopic structure of the flow has a considerable effect on the radiation properties and spectral distribution of emission energy of an open plasma-dynamic discharge.

The microscopic structure of the plasma jet escaping from the magnetoplasma compressor is revealed on photochronograms of the discharge taken with high space-time resolution. Fig. 2c [photo not reproduced] shows a slit scan of a discharge across a fluorocarbon plasma obtained with orientation of the slit along the axis of the flow. The formed magnetoplasma compressor flow is characterized by a discrete structure observed on the photochronograms in the form of alternating dark and light bands. The characteristic dimension of inhomogeneities in the direction of the axis of flow and the recurrence rate were determined by photometry of the negatives of the scans, and are 0.2-0.5 cm and 5-10 MHz respectively. It is known that the interrupted flow structure observed in a number of papers [Ref. 11-17] in the investigation of pulsed accelerators of gas-discharge and erosion plasma is due to the existence of individual microplasmoids [Ref. 17]. Investigation of the nature of erosion destruction of the surface of electrodes and dielectric inserts of magnetoplasma compressors and comparison with the results obtained on other erosion plasma systems [Ref. 17] shows that the formation of individual microplasmoids is due to the discrete nature of arrival of the mass of plasma-forming material in the discharge, which is caused by space-time inhomogeneity of energy release on the surface of the electrodes and dielectric inserts.

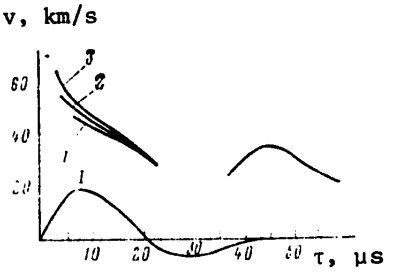

Fig. 4. Velocity of plasma in free jet at distance L = 10 cm from the tip of the magnetoplasma compressor (C = 750 μF, C_2F_4 plasma) at U_0: 1--3 kV; 2--4 kV; 3--5 kV

If the inhomogeneities are detached plasmoids, the velocity of their propagation (which can be determined from slit scans that are x-t diagrams) will be the velocity of the flow. The results of processing slit scans obtained at different initial voltages U_0 of the discharge are shown on Fig. 4. Typical of the initial discharge stage is considerable time inhomogeneity of velocities. With increasing U_0, inhomogeneity increases rapidly. The average mass velocities of the plasma flow are ~40-50 km/s. The resultant distribution of velocities agrees with the results of measurements of the dynamic characteristics of the discharge by using double electrostatic probes [Ref. 18].

The transverse structure of the flow in the compression zone was studied by slit scans obtained with the slit of the streak camera normal to the discharge axis. Fig. 2d [photo not reproduced] shows a typical photochronogram corresponding to the cross section at distance L = 2.5 cm from the tip of the magnetoplasma compressor. It can be seen that the plasma column preserves

its dimensions and position in space practically throughout the first half-period of the discharge, i. e. force instabilities of the type of pinches, kinks and the like that are typical of intense self-compressed discharges are absent [Ref. 4, 19]. At the same time, the initial stage of the discharge shows azimuthal inhomogeneity due to streamer formation and subsequent propagation of the ionization front over the surface of the dielectric leads to development of a helical instability with characteristic frequencies of oscillations that vary over a range of 200-300 kHz. Four microseconds after supply of the initiating pulse the corkscrew instability becomes small-scale. A peculiarity of the structure of the plasma flow in the compression zone is also the presence of transverse small-scale high-frequency oscillations ("noises") with characteristic frequencies of ~10 MHz. Let us note that small-scale structures of this kind are also observed in the region of compression of a gas-discharge magnetoplasma compressor [Ref. 20].

3. Space-Time and Spectral Characteristics of open Plasma-Dynamic Discharges in the Quantum Energy Region of $h\nu \sim 2$-350 eV. Ref. 7, 21, 22 devoted to the investigation of radiation properties of a dense plasma focus give data that reflect the integrated emission characteristics of open plasma-chemical discharges, i. e. that characterize the spectral distributions of energy densities and radiated power averaged over the entire emitting surface of the discharge. At the same time, knowledge of the local parameters of the radiation, their space-time and spectral distributions, is necessary for a more complete idea of the potential capabilities of the discharge as a source of radiation, as well as to determine the mechanism of radiation and the nature of the emission spectrum of the plasma.

The space-time distribution of brightness temperature (spectral brightness of radiation) of an open plasma-dynamic discharge was studied by the method of photometric comparison of the blackening densities of photographic film with time scanning of luminescence of a plasma focus and a reference light source on the SFR-2M high-speed camera. Photometry was done on films of the slit scans of the plasma focus taken with orientation of the camera slit both along and across the discharge axis. The measurements were made in the blue region of the spectrum on an effective wavelength of $\lambda_{ef} = 430 \pm 20$ nm isolated by a set of light filters (SS4 + SZS-22 + ZhS-11). An EV-45 pulsed light source was used as the reference. In photographing the reference source, a nine-step neutral optical wedge [Ref. 23, 24] was installed on the focal arc of the SFR-2M; this enabled coverage of the entire optical range of photographic densities of the film anticipated in photographing the plasma focus. The position of the rotating mirror of the camera was synchronized with the flash of the EV-45 source in such a way as to expose the photographic film behind the optical step wedge in the time period when the brightness of the reference standard was constant.

Identity of exposure conditions in photographing the marks of the reference standard and the investigated effect does not require the use of reciprocity law in determining temperature [Ref. 23-26], thus eliminating possible concomitant errors. The films of each series of experiments and the photographs of the reference sources were developed concurrently to eliminate the effect of photochemical processing on measurement results.

The use of a source with brightness temperature close to that being measured (see below) as the comparison standard reduces the error of the method. The error in relative measurement of energy brightness does not exceed ±5% (error of the method), and the error in absolute measurement of energy brightness (error of the method and reference) does not exceed ±15% for the visible region [Ref. 23]. The corresponding accuracy of brightness temperature measurement is ±5-10%.

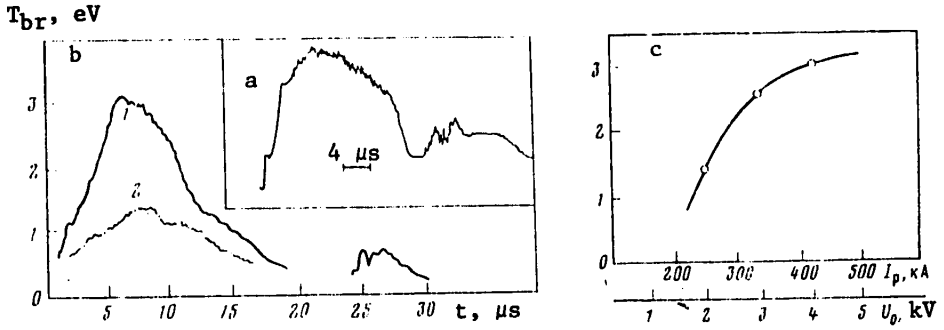

Fig. 5. Results of photographic measurements (C_2F_4 plasma, $C_0 = 750$ μF) in the center of a plasma focus (L = 25 mm): a--typical densitometer plot of the discharge ($W_0 = 9.4$ kJ); b--time dependence of brightness temperature of the discharge: 1--$U_0 = 5$ kV; 2--2 kV; c--dependence of maximum brightness temperature on the electrotechnical parameters of the discharge

Fig. 5a shows a typical densitometer plot of the discharge obtained by microphotometry along the time axis of a slit scan of the central zone of the plasma focus in the cross section at a distance L = 25 mm from the tip of the magnetoplasma compressor (slit oriented across the flow), and Fig. 5b shows the results of measurement processing. At stored energy $W_0 = 9.4$ kJ the maximum brightness temperature in the zone of the plasma focus is ~3 eV (~35,000 K). Maximum temperature is reached on the 6-8th microsecond of the discharge, and corresponds in brightness to the instant of maximum compression of the flow. Dependence of the maximum brightness temperature on electrotechnical parameters of the discharge is shown in Fig. 5c. With increasing discharge energy the brightness temperature of the zone of maximum compression of the flow shows a tendency to stabilize. Comparison of this result with the power-law dependence of spectral brightness $B_{\nu, av}$ averaged over the lateral surface (spectral density of radiation energy E_ν), $B_{\nu, av} \sim E_\nu \sim U^{3-4}$ [Ref. 10] shows an increase in effective radiating surface of the discharge with increasing energy input.

The space-time distribution of brightness temperature of an open plasma-dynamic discharge is shown in Fig. 6a, b. The region of plasma compression with radiation brightness temperature greater than 20,000 K has average dimensions of ~50 mm in the axial direction, and ~6 mm in the radial direction. Maximum brightness temperatures are reached on the axis of the flow at distances of 20-30 mm from the tip of the magnetoplasma compressor.

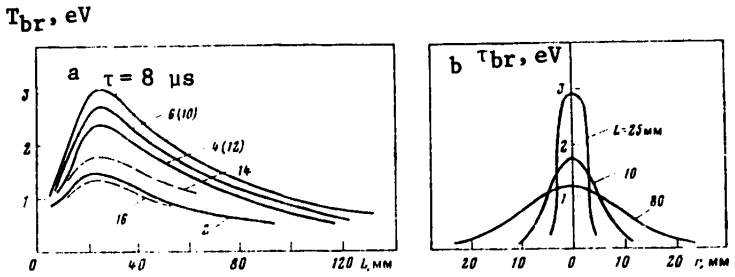

Fig. 6. Distribution of brightness temperature along the discharge axis at different times (a) and in different cross sections of the jet at the instant of maximum current (b) (C_2F_4 plasma, $W_0 = 9.4$ kJ, $U_0 = 5$ kV)

The spectral dependence of brightness of radiation and brightness temperature of the plasma in the zone of maximum flow compression was determined by the method of photoelectric comparison of the emission intensity of the plasma focus and the EV-45 reference source in the visible and near-ultraviolet regions of the spectrum [Ref. 27]. Measurements were made both on individual wavelengths by using an FEU-39A photomultiplier crossed with a DMR-4 double quartz monochromator as the radiation receiver, and over a fairly broad spectral range $\Delta h\nu \sim 1$ eV by using photocells with optical filters: F1 photocell with ZhS-3 filter, F1 with UFS-2 filter, and F7 with UFS-1. Both the photocells and photomultiplier were equipped with cathode followers to preserve the necessary time resolution ($\Delta\tau \sim 1$ μs).

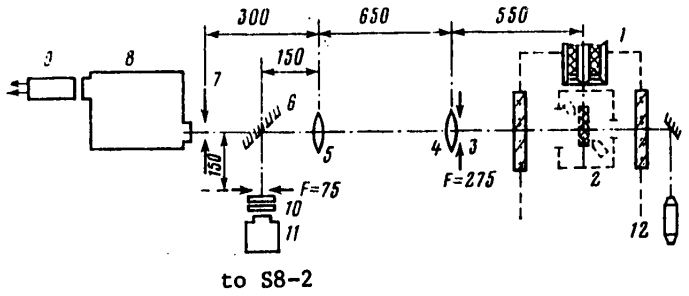

Fig. 7. Diagram of optical measurements: 1--magnetoplasma compressor; 2--EV-45; 3, 7, 10--diaphragms; 4, 5--achromatic objective lenses; 6--mirror; 8--DMR-4 monochromator; 9--FEU-39A; 11--photocell; 12--alignment laser

A diagram of the optical measurements is shown on Fig. 7. An optical system made up of quartz achromatic objectives 4 and 5 projects a triply magnified image of capillary 2 (or of the central zone of the plasma focus) on diaphragm 7 or through rotating aluminized mirror 6 onto diaphragm 10.

Diaphragms 7 and 10 isolate the central part of the capillary and determine the size of the area on the surface of the plasma focus from which light is incident on the photocell. Diaphragm 3 limits the solid angle in which radiation is registered.

Measurements on each wavelength or in a separate spectral interval were made in two stages. On the first stage, a reference source was used to calibrate the optical channel, the axis of the capillary being aligned by a reference laser beam with coordinates corresponding to the coordinates of the zone of maximum compression of the plasma flow. On the second stage, after setting up the magnetoplasma compressor model and evacuating the discharge chamber, measurements were made. To reduce statistical scatter ($\sigma_{\bar{x}} = \sqrt{\Sigma(x - \bar{x})^2/n(n-1)}$) the measurements on each wavelength were repeated at least 5-6 times. The advantage of this method of measuring the spectral brightness of radiation is that the ratio of the signals from the reference and the investigated sources depends only on their brightness temperatures, while the influence of geometry and transmission of the optical system is completely eliminated. The absolute accuracy of the given method of measuring brightness temperature is determined mainly by the accuracy of calibrating the reference source, and is equal to ±7 in the visible region of the spectrum and ±10% in the ultraviolet [Ref. 27].

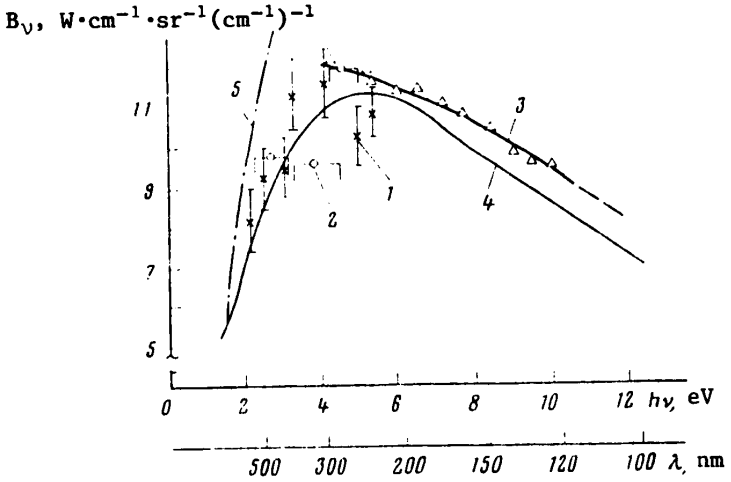

Fig. 8. Spectral brightness of central zone of plasma focus (L = 25 cm, C_2F_4 plasma, W_0 = 9.4 kJ, U_0 = 5 eV): 1--measurements by photomultiplier; 2--measurements by photocells; 3--photographic measurements; 4--theoretical emission spectrum; 5--ideal blackbody isotherm with T = 4.5 eV

Results of optical measurements are shown on Fig. 8. Photoelectric measurements made by photocells and by a photomultiplier crossed with a monochromator give similar values of spectral brightnesses, and agree well (~10%) with the results of photometric measurements of the brightness temperature on effective wavelength of λ_{ef} = 430 nm ($h\nu_{ef} \approx 2.9$ eV). The results show that as quantum energy increases, the brightness temperature of plasma focus emission drops off. In the visible region, the brightness temperature is 3-3.5 eV, and in the near ultraviolet ~2.3 eV. The reduction in brightness temperature is due to spectral dependence of the coefficient of continuous absorption of the plasma. To confirm this, and also to determine the nature of the observed

radiation spectrum, the authors calculated the coefficients of continuous absorption and the emission spectrum of a fluorocarbon plasma.

In the general case, calculation of the coefficient of absorption is an extremely difficult problem since it requires accounting for different kinds of transitions, including free-bound and bound-bound transitions, whose calculation requires knowledge of exact wave functions of atoms and ions. However, under conditions of high densities and temperatures (and it is just such conditions that are of interest in developing high-intensity light sources, and that are realized in high-current radiating discharges), due to the strong interaction of plasma particles with each other and with radiation it is sufficient to consider only continuous emission either in the hydrogen-like approximation of atoms and ions [Ref. 4, 28], or with consideration of the individual structure of terms, by introducing additional correcting functions or coefficients [Ref. 29].

Coefficients of decelerating and photoionization absorption were calculated by the approximate theory of Ref. 29 based on the quantum defect method [Ref. 30, 31]. In this case, the photoionization cross sections for upper excited states were determined by integrating the Burgess-Seaton equation [Ref. 32-35], while calculation of the coefficients of decelerating absorption utilized matrix elements obtained by extrapolating the matrix elements of bound-free transitions with consideration of the specifics of free-free transitions to the field of multiply charged ions [Ref. 36, 37].

The overall coefficient of bound-free absorption by z-tuple ions and free-free absorption in the field of z+1-ions takes the form

$$\varkappa_{\nu,T} = C\frac{U_{z+1}}{U_z}T\exp\left(\frac{\nu - I_z + \Delta\nu}{T}\right)(z+1)^2\xi_z(\nu)\nu^{-3}N_z, \qquad (1)$$

where $C=16\pi^2c^{-3}/3\sqrt{3}ch = \text{const}$, U_Z and U_{Z+1} is the statistical sum of the initial and final ion, I_Z is the potential in eV of the z-tuple ion, $\Delta\nu$ is the displacement of the photoionization potential due to interaction of particles in the plasma in eV, N_Z is the concentration of the z-tuple ion in cm^{-3}, $\xi_Z(\nu)$ is a function that accounts for the specific structure of terms of the z-ion (i. e. the deviation from the hydrogen-like approximation).

Formulas for calculating $\xi_Z(\nu)$ are given in Ref. 29, 32. For most elements the function $\xi_Z(\nu)$ is weakly dependent on plasma temperature (or completely independent) and has a value of the order of unity. Values of the function $\xi(\nu)$ for atoms and ions of carbon and fluorine are given in Ref. 38. Formula (1) is valid for frequencies less than the cutoff frequency ν_g equal to the maximum threshold frequency of the photoelectric effect for excited states that are accounted for integrally. For frequencies $\nu > \nu_g$ the coefficient of continuous absorption is calculated by the formula

$$\varkappa_{\nu,T} = \varkappa(\nu_g, T)\frac{\xi(\nu)}{\xi(\nu_g)}\left(\frac{\nu_g}{\nu}\right)^3 + \sum \varkappa_{nl}(\nu, T), \qquad (2)$$

where $\nu_{n,l}$ is the coefficient of photoionization absorption from a single level with quantum numbers n and l.

Using the Saha formula, the coefficient of continuous absorption can be written as

$$\varkappa_\nu = 2{,}45\cdot10^{-37} N_e N_{z+1} (z+1)^2 \exp\left(\frac{\Delta\nu_z - \Delta I_z}{T}\right) \xi_z(\nu) \frac{\exp(\nu/T)}{T^{1/2}\nu^3}. \qquad (3)$$

For a plasma of complex composition that contains ions of various multiplicity, the absorption coefficient takes the form

$$\varkappa_{\nu,T} = \sum_{k,z} \varkappa(\nu, T)_{k,z} =$$
$$= 2{,}45\cdot10^{-37} N_e \frac{\exp(\nu/T)}{T^{1/2}\nu^3} \sum_{k,z} \exp\left(\frac{\Delta\nu_{z-1} - \Delta I_{z-1}}{T}\right) \xi_{z-1}(\nu) N_{zk} z_k^2, \qquad (4)$$

where k is the index of the chemical element, and summation is done with respect to k and z. Quantities N_z, ν_g and $\xi(\nu)$ depend on k and z, while $\Delta\nu$ and ΔI are assumed to depend only on z.

The coefficient of absorption with consideration of stimulated emission is determined by the experession

$$\varkappa_{\nu T}' = \varkappa_{\nu T}[1 - \exp(-\nu/T)]. \qquad (5)$$

By using formulas for the coefficient of decelerating and photoionization absorption, we can evaluate the concentration of the electronic component in the zone of magnetohydrodynamic compression of the flow from the experimentally measured density of continuous radiation and plasma temperature.

The magnitude of the factor for deviation from the hydrogen-like approximation $\xi(\nu)$, as already pointed out above, differs insignificantly from unity[1]; estimates of the factor $\exp[(\Delta\nu_{z-1} - \Delta I_{z-1})/T]$ show that over a wide range of plasma parameters in the compression zone its value changes only slightly, being ~1.1-1.25. Therefore in a first approximation these cofactors can be disregarded in the formula for the coefficient of absorption. Then the expression for the coefficient of overall absorption with consideration of stimulated emission can be represented as

$$\varkappa_{\nu,T}' \approx \frac{2{,}45\cdot10^{-37} N_e^2}{T^{1/2}} f\left(\frac{\nu}{T}\right) \sum_{k,z} \left(\frac{N_{z,k}}{N_e}\right) z_k^2, \qquad (6)$$

$$f\left(\frac{\nu}{T}\right) \approx \frac{\exp(\nu/T) - 1}{(\nu/T)^3}, \qquad \sum_{k,z} \left(\frac{N_{z,k}}{N_e}\right) z_k^2 = \tilde{z},$$

where $\tilde{z}$ is the effective atomic number of the ions. The quantity $\tilde{z}$ was determined from calculating the composition of the fluorocarbon plasma [Ref. 39].

[1]For ions of fluorine and carbon, $\xi(\nu)$ at $\nu = 3$ eV varies over a range of 0.8-1.0 [Ref. 39].

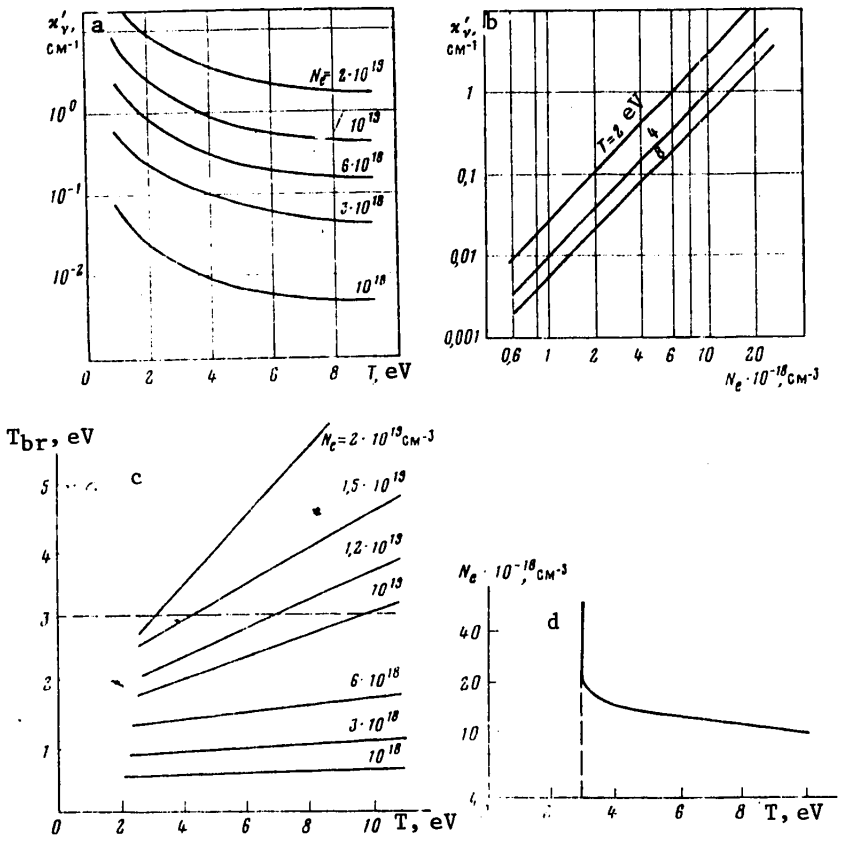

Fig. 9. Coefficient of continuous absorption of a fluorocarbon plasma as a function of temperature (a) and electron concentration (b); c--brightness temperature of a plane layer of fluorocarbon plasma with thickness of $\delta = 0.5$ cm; d--region of plasma parameters that ensure a brightness temperature of the layer equal to 3 eV at thickness $\delta = 0.5$ cm

Results of calculations of the coefficients of continuous absorption for quantum energy $h\nu = 3$ eV in the temperature range of 1-10 eV and electron concentration of 10^{18}-$2 \cdot 10^{19}$ cm^{-3} are shown on Fig. 9a and b.

The spectral density of radiation intensity (or brightness) for a plane homogeneous plasma layer in the direction along the normal to its surface is

$$B_\nu = B_{\nu p}[1 - \exp(-\varkappa_\nu' l)], \tag{7}$$

where

$$B_{\nu p} = \frac{2h\nu^3}{c^2} \frac{1}{\exp(\nu/T) - 1} = \frac{0{,}624\nu^3}{\exp(\nu/T) - 1}, \quad [\text{W}/(\text{cm}^2 \cdot \text{sr} \cdot \text{cm}^{-1})] \tag{8}$$

is the equilibrium intensity of radiation (ν and T are expressed in eV), l is the thickness of the layer. For cylindrical plasma formations, the equivalent thickness of a plane layer is determined by the formula $l = \pi D/4$.

Fig. 9c shows the results of calculation of the brightness temperature of emission of a plane layer of fluorocarbon plasma of thickness $l = 0.5$ cm corresponding to the average thickness of the discharge in the compression zone, where $\nu = 3$ eV at different plasma temperatures and electron concentrations. The temperatures of the plasma focus experimentally observed on these frequencies are ~3 eV and at the anticipated plasma temperatures in the compression zone ($T < 10$ eV) can be realized only at electron concentrations of greater than 10^{19} cm^{-3}. The region of plasma parameters N_e and T_e that ensure a brightnes temperature of radiation greater than 3 eV at the given thickness of the plasma formation ($l = 0.5$ cm) and on the given frequency ($\nu = 3$ eV) lies above the curve shown on Fig. 9d. Experimental data on the plasma temperature in the compression of a magnetoplasma compressor operating on a fluorocarbon plasma are given in Ref. 7, 40. The electron temperature determined by the method of self-inversion of spectral lines [Ref. 40] is $T_e = 3.5$-5 eV, and it is noted that with increasing energy input to the discharge this temperature is stabilized at a level of 4.5-5 eV due to intense radiation cooling of the plasma. Measurement of ion temperature by Doppler broadening of lines [Ref. 40] and by registration of Mach reflection on a thin plate [Ref. 9] as well as estimation of relaxation times have shown that maxwellization of the plasma occurs in the zone of the focus along with equalization of the electron-ion temperature. Existence of local thermodynamic equilibrium in the vicinity of the plasma focus was established in Ref. 40.

Taking the plasma temperature in the zone of the focus as $T_e = 3.5$-5 eV, we get (Fig. 9c) the electron concentration in the plasma: $(1.2\text{-}2)\cdot 10^{19}$ cm^{-3}. Let us note that this is a lower estimate since consideration was not taken of the radial distribution of electron density and temperature in the focus zone.

The emission spectrum of a fluorocarbon plasma in the quantum energy range of $\Delta\nu = 0$-60 eV was calculated at typical parameters of the compression zone $T_e = 4.5$ eV and $N_e = 1.5\cdot 10^{19}$ cm^{-3}. The plasma composition was determined from solution of a system of Saha equations for sequential stages of ionization together with equations of quasineutrality and constancy of composition [Ref. 39]. Reduction of ionization energy in the plasma was accounted for in accordance with the Debye-Huckel theory [Ref. 42]. The values of statistical sums and ionization energies necessary for the calculation were taken from Ref. 42, and the missing data were calculated by the approximate method of Ref. 43. Displacement of the photoionization threshold was accounted for by the approximate Ingliss-Teller theory [Ref. 44, 45]

$$\Delta\nu_{zi} = 8{,}05\cdot 10^{-6}(z_i+1)^{0.8}N_e^{0.267}, \text{ eV}. \qquad (9)$$

The photoionization cross sections for individually considered levels were calculated by the Kramers formula [Ref. 28]

$$\sigma_{n,i} = 7{,}9\cdot 10^{-18}\frac{n}{(z+1)^2}\left(\frac{\nu_n}{\nu}\right)^3 \qquad (10)$$

where n is the principal quantum number of the level, ν_n is the minimum energy of a quantum capable of ionizing an atom or ion that is in the n-excited state. The coefficient of absorption is determined by the expression

$$\varkappa_{z,n}(\nu) = N_z \sum \alpha_{z,n}\sigma_{z,n}(\nu), \tag{11}$$

Here $\alpha_{z,n}$ is the relative concentration of ions of multiplicity z on level with number n determined in the case of boltzmannian distribution by the formula

$$\alpha_{z,n} = \frac{g_{n,z}}{U_z(T, \Delta I_z)} \exp\left(-\frac{I_z - I_{n,z}}{T}\right), \tag{12}$$

where $g_{n,z}$, $I_{n,z}$ are the statistical weight and ionization energy of a z-tuple ion from level n, $U_z(T, \Delta I_z)$ is the statistical sum of the ion.

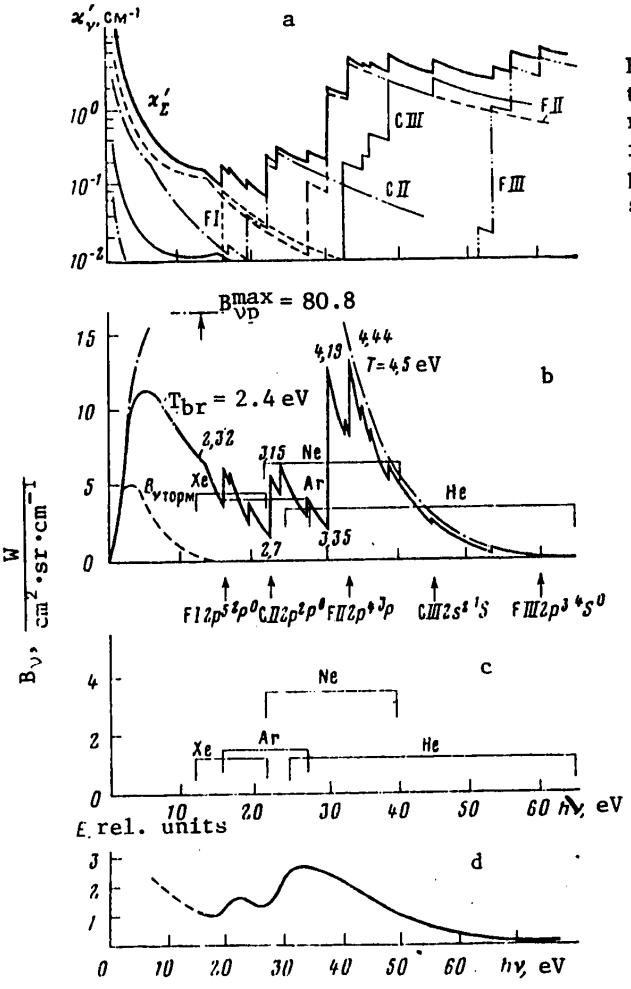

Fig. 10. Coefficients of continuous absorption (a), theoretical (b) and measured (by ionization chambers (c) and photoemission-scintillation spectrometer (d)) emission spectra of fluorocarbon plasma

The results of calculation of coefficients of continuous absorption and the resultant radiation spectrum of a fluorocarbon plasma are shown on Fig. 10a. The partial fraction of ions of different multiplicity in the overall coefficient of continuous absorption varies depending on the spectral range being considered. In the infrared, visible and near-ultraviolet regions of the spectrum the maximum contribution is from singly charged ions of fluorine and carbon (~60 and ~36% respectively). In the far ultraviolet, an appreciable role is played by double ions. The radiation spectrum of a fluorocarbon plasma with characteristic dimension of the plasma formation $l = 0.5$ cm is considerably different from planckian at a temperature equal to that of the plasma, which is due to optical transparency of the plasma in the region of quantum energies $2.7 < \nu < 31$ eV (optical thickness $\tau_\nu = \kappa'_\nu l < 1$).

The theoretical radiation spectrum is compared with the results of optical measurements in the visible and near-ultraviolet region on Fig. 8. Values of spectral brightness of the plasma focus measured both on individual wavelengths and in wide spectral intervals agree fairly well (about 20%) with calculated radiative characteristics. The reduction in brightness temperature of emission of the focus with transition from the visible to the near-ultraviolet region is due to reduction in the optical thickness of the plasma. In the region of quantum energies $\nu \sim T$, continuous radiation of the plasma is due to decelerating and photorecombination mechanisms. The contribution of decelerating processes for the given plasma parameters in the resultant radiation spectrum is shown on Fig. 10b. Even in the near-ultraviolet region of the spectrum the recombination mechanisms predominate, and the plasma radiation spectrum is determined mainly by photorecombination of electrons to the upper excited states of singly ionized ions.

In the quantum energy region of $5 < \nu < 10$ eV, the distribution of radiation is measured by a photographic method using the DFS-29 parallel-incidence vacuum spectrograph. To eliminate the influence of self-sensitivity of the photographic material to hard photons, the XUV spectra of plasma focus radiation were registed on type ML-2 photographic film sensitized with sodium salicylate, which has a constant quantum yield (in a range of 10-15%) in the spectral region of 340-40 nm [Ref. 46, 47]. The sensitivity of the spectrograph-photomaterial system in relative units was determined by a pulsed continuous-spectrum source made in exact accordance with the recommendations of Ref. 48 and calibrated with respect to brightness in the extreme ultraviolet. The reference source is based on a pulsed electric discharge through a capillary in vacuum. In this case, the source of the continuous spectrum in the XUV is a Lyman continuum produced by radiation of a high-pressure plasma formed from the material of the capillary walls (polyformaldehyde) when an intense discharge current pulse passes through the capillary. Upon satisfaction of conditions with respect to current ($I_{max} = 10$ kA, $\tau_{pulse} \sim 5$ μs) and capillary geometry (diameter $d_c = 3.5$ mm, length $l_c = 30$ mm), according to the results of Ref. 48 the central zone of the capillary 2.5 mm in diameter is homogeneous (with accuracy of 10%) as a light source that emits in the XUV region of the spectrum up to $\lambda = 120$ mm as an ideal blackbody with temperature $T = 37{,}000 \pm 3{,}000$ K.[2]

[2]Using the EV-39 standard, we predetermined the brightness temperature of the capillary in the region $\lambda = 250 \pm 20$ nm: $T_\lambda = 37{,}000 \pm 10\%$ K, which agrees well with data of Ref. 48.

In determining the relative spectral distribution of plasma focus emission in the XUV from the known (as a result of calibrating the reference source) sensitivity of the optical system of registration, deviation from reciprocity law was disregarded since the difference in the duration of the emission pulse of the light sources being compared is small. For example, the calibrated source had an effective duration of continuous radiation of ~5 μs, while the investigated discharges had $\tau \sim 15$-20 μs. It is known [Ref. 49-51] that in this exposure time range the iso-opaque line of the photographic material has a constant section, and deviations from reciprocity law are practically unobserved.

Absolute calibration of spectral distribution was done with respect to the emission brightness of the central zone of the plasma focus in the region $\Delta\nu = 4.35$-5.0 eV registered by photoelectric methods. Fig. 11 [photo not reproduced] shows typical XUV spectrograms of the plasma focus for various experimental conditions,[3] and Fig. 8 shows the distribution of emission brightness in the near vacuum ultraviolet obtained by spectral measurements for a plasma-dynamic discharge on a fluorocarbon plasma. The spectra of the plasma focus in the XUV region consist of intense cw emission and radiation lines that belong mainly to single, double or triple ions of the material of the dielectric washer of the magnetoplasma compressor; lines of elements of the electrode materials are weakly represented in the resultant spectra. When processing the densitometric plots of the spectra, consideration was taken of only the continuous radiation of the plasma since the contribution to the total emitted energy by lines in region $\lambda > 120$ nm is small. The experimental spectrum in the quantum energy range $\Delta\nu = 5$-10 eV obtained by the photographic method correlates well with the calculated spectrum; the brightness temperature of the central zone of the plasma focus in region $\lambda = 150$ nm is ~27,000 K. The drop in intensity of radiation in the short-wave region is due to the reduction in optical density of the plasma, which is also confirmed by the increase in the relative fraction of line emission in the overall discharge emission spectrum.

The spectral density of radiation intensity of the plasma focus in the extreme ultraviolet region was measured by open double ionization chambers filled with spectrally pure inert gases [Ref. 22]. The region of spectral sensitivity of the ionization chamber is determined on the long-wave boundary by the ionization potential, and on the short-wave boundary by a fall-off in the photoionization cross section of the filler gas. By using inert gases, the spectral region from 12 to 65 eV was broken down into four partly overlapping intervals: 12.1-22 eV (Xe), 15.8-28 eV (Ar), 21.6-40 eV (Ne) and 24.6-65 eV (He). Results of measurements of the spectral brightness of the central zone of the plasma focus in the extreme ultraviolet are shown on Fig. 10c. The experimental conditions are similar to those used for optical measurements in the visible and near-ultraviolet regions of the spectrum (Fig. 8).

To compare experimental results with the calculated emission spectrum of a fluorocarbon plasma, the authors calculated the average values of brightness

[3]The emission spectra of discharges in the XUV region were taken by S. G. Shashkovskiy and A. G. Opekan.

in spectral intervals corresponding to regions of sensitivity of the chamber with different fillers

$$B_{\text{sep}} = \frac{1}{\nu_2 - \nu_1} \int_{\nu_1}^{\nu_2} B_\nu \, d\nu.$$

Values of brightness averaged over the calculated spectrum are shown on Fig. 10b.

Comparison of the calculated emission spectrum of the fluorocarbon plasma (Fig. 10b) with that measured by ionization chambers (Fig. 10c) shows fairly good qualitative agreement between calculation and experiment.

In contrast to measurements in the visible and near-ultraviolet regions, the experimental values of spectral brightnesses in the extreme ultraviolet were lower than the calculated levels. This is due to the difference in spatial resolution of the ionization chamber used ($\Delta x \sim 6$ mm) from that of the arrangement for optical measurements in the visible and near-ultraviolet regions ($\Delta x \cong 1.5$ mm), resulting in averaging of brightness in the extreme ultraviolet over a larger area of the radiating surface of the plasma focus.

Measurements by ionization chambers showed an increase in the brightness temperature in the short-wave region of the spectrum, which may be evidence of the presence of recombination maxima in the emission spectrum of the plasma focus. However, the width of regions of spectral sensitivity of the chamber does not permit registration of the position of individual emission maxima, or determination of the specific form of spectral distribution of emission energy in the extreme ultraviolet. For this purpose, a photoemission-scintillation spectrometer was used to measure the relative distribution of radiation of the plasma focus in the range of quantum energies from 10 to 350 eV. The method used was based on registration and analysis of the spectrum of photoelectrons knocked out of the photocathode by direct radiation of the plasma [Ref. 52, 53]. The method of measurements and the experimental facility are described in detail in Ref. 54. The form of the spectral distribution of radiation obtained by the photoemission-scintillation spectrometer is shown on Fig. 10d. The nature of the measured spectrum, the amplitude of maxima and their shape (with consideration of the spectral resolution of the instrument $\Delta\nu \sim 5$ eV) correspond fairly well to the calculated recombination continuum, and also to the distribution of emission brightness measured by ionization chambers.

A maximum of focus emission in the region of 30-35 eV is due mainly to photorecombination to the ground state ^3P and to the lower excited state ^1D of the first fluorine ion FII; a second maximum in the region of 20-25 eV is due to recombination to the ground level $^2P^0$ and to a group of lower mixed terms ^4P, ^2D, ^2S of the carbon ion CII. Recombination maxima of the second ions CIII and in the region $\nu \sim 45$ and 60 eV did not show up in the measured spectrum which may be due to the appreciable optical thickness of the plasma in this range of quantum energies. The increase in optical density of the plasma in the short-wave region of the spectrum is also associated with the increase in brightness temperature registered by the ionization chambers in the absorption bands of neon ($T_{br}^{ex} \sim 3.9$ eV) and helium ($T_{br}^{ex} \sim 4.2$ eV). A

distinguishing feature of the emission spectrum of the plasma focus is the presence of a hard radiation component in the region of 100-350 eV ("super-planckian" for $T_e \sim 5$ eV) registered in measurements by spectrometer [Ref. 54] and bismuth bolometers [Ref. 7]. The nature of this radiation is possibly associated with microinhomogeneities that are typical of the initial unsteady stage of discharge in the magnetoplasma compressor.

Thus these studies show that radiation of the plasma focus is due mainly to the recombination continuum of characteristic groups of ions that determine the properties of the plasma, the percentage of XUV emission in the overall spectrum of the plasma-dynamic discharge being ~70-90% as evaluated from the results of integrated measurements by a quartz calorimeter and bolometers [Ref. 21, 55]. By appropriately altering the chemical and ionizational compositions and parameters of the plasma in the zone of MHD compression, we can realize fairly effective control of the radiation spectrum of a plasma focus, which enables creation of selective sources of radiation in the far ultraviolet.

The spectral distribution of plasma-dynamic discharge radiation energy may be profoundly influenced by the macroscopic structure of the plasma flow emanating from the magnetoplasma compressor. This flow structure depends on the configuration of the discharge gap, the energy conditions of operation and the conditions of introducing the plasma-forming substance into the discharge. The structural influence shows up in varying degrees of shielding of the short-wave radiation of the plasma focus by peripheral layers of cool erosion products that are not captured by the magnetic field of the discharge current. Depending on the chemical composition and particle density in the peripheral annular layer that surrounds the hot zone of the discharge, the shielding may be in the nature of either filtration of short-wave radiation in individual spectral intervals that as a rule are fairly narrow, or in lines, or else an abrupt reduction (by a factor of several tens) in the magnitude of emission intensity of the plasma focus, beginning at some cutoff wavelength, with a simultaneous increase in the luminous output of the discharge in the visible and near-ultraviolet regions of the spectrum. The latter is due to rapid heating, ionization and radiation of the products of erosion as a result of their broad-band absorption of high-energy XUV radiation of the plasma focus. Since the radiating surface of the peripheral layer is larger than the surface of the focus, the balance of the radiation and the absorption in it sets in at a lower temperature, i. e. conditions are realized for transformation of short-wave radiation to emission in the visible and near-UV bands.

The XUV spectrograms of the plasma focus shown on Fig. 11 [photo not reproduced] that were obtained under different experimental conditions, illustrate the influence that macrostructure of the plasma-dynamic discharge has on spectral distribution of radiation energy in the short-wave region. Microphotometric analysis of spectra shows that discharges on fluorocarbon and polyformaldehyde plasmas (Fig. 11b and c [photos not reproduced]) characterized by approximately the same coefficient of utilization of material ($\eta_{w.s} \sim 0.94$) have similar emission characteristics in the XUV region, but differ considerably with respect to the nature of spectral distribution of radiation from discharge in CsI vapor (Fig. 11d), in which the coefficient of utilization of working

substance for the given magnetoplasma compressor model and the selected energy conditions are considerably lower than in discharges on $(CH_2O)_n$ and $(C_2F_4)_n$ plasmas (Fig. 11b, c).

According to spectroscopic measurements in the region of quantum energies $\Delta\nu = 4$-8 eV, the CsI discharge is characterized by higher (by ~4-5 times) energy yield of radiation than discharges on fluorocarbon and polyformaldehyde plasmas; however, in the region of $\nu > 8$ eV ($\lambda < 150$ nm) the intensity of continuous emission of the cesium iodide plasma is insufficient for exposure of the photographic emulsion during a single discharge pulse. These data agree well with the results of photoelectric measurements of the integrated energy yield of radiation of open discharges in the near ultraviolet region ($\Delta\nu = 4.35$-5 eV) [Ref. 10] and also with measurements in the range of $\Delta\nu = 12$-45 eV made by ionization chambers, according to which the spectral brightness of the CSI discharge decreases in the indicated region by 30-50 times compared with the discharge on fluoroplastic [Ref. 22].

Thus the assurance of high coefficients of utilization of working substance is a necessary condition for eliminating effects of shielding short-wave radiation and attainment of high brightness temperatures of the plasma focus in the XUV region of the spectrum. When this condition is met, the brightness temperature of the discharge is limited from above only by the true temperature of the plasma in the zone of the focus, which can be increased by increasing the degree of magnetohydrodynamic compression of the plasma flow as the density of electromagnetic energy in the interelectrode gap and the zone of entrained currents of the magnetoplasma compressor is increased. Thus, as a result of optimizing the geometry of the discharge gap in the magnetoplasma compressor, the energy conditions of operation and the conditions of introducing the plasma-forming substance in the discharge, it has been possible for the first time to reach brightness temperatures of radiation exceeding 60,000 K [Ref. 56] in the spectral region beyond the helium ionization potential ($\Delta\nu = 24.6$-65 eV). Let us also note that such flux densities in the far XUV region have so far been reached only on facilities of synchrotron type [Ref. 41]. Fig. 11a shows the emission spectrum of an optimized plasma-dynamic discharge. The steep drop in the intensity of continuous radiation on the short-wave boundary ($\lambda < 90$ nm) recorded on the spectrogram is apparently due to an abrupt increase in the coefficient of reflection of the aluminum coating of the diffraction grating of the spectrograph [Ref. 46].

Let us point out one more possibility for controlling the spectral properties of open plasma-dynamic discharges, which consists in producing plasma layers of a given chemical composition surrounding the zone of MHD compression (in the general case, a chemical composition differing from that of the radiating plasma of the focus), and with given density, and hence having certain predetermined optical characteristics. These layers may act as plasma filters that have "transparency windows" in individual (defined for the specific problem) spectral intervals, or totally blocking the hard radiation of the plasma focus beginning at some quantum energy that is undesirable or even harmful for the selected application. Technically, the realization of such layers may be accomplished by using ablating separative sleeves in the magnetoplasma compressor with chemical composition profiled along the radius in the zone of the deflagration current layer.

The authors thank P. A. Ovchinnikov and A. G. Opekan for assisting with the research.

REFERENCES

1. Borovich, B. L., "Feasibility of Making Optically Pumped Gas Lasers Using Allowed Electronic Transitions of Molecules", ZHURNAL EKSPERIMENTAL'NOY I TEORETICHESKOY FIZIKI, Vol 61, 1971, p 2293.

2. Mikheyev, L. D., "Gas Lasers With Wide-Band Optical Pumping", KVANTOVAYA ELEKTRONIKA, Vol 5, 1978, p 1189.

3. Rozanov, V. B., "Feasibility of Producing Inverse Medium by Photoionizing Inner-Shell Electrons in Atoms", PIS'MA V ZHURNAL EKSPERIMENTAL'NOY I TEORETICHESKOY FIZIKI, Vol 12, 1970, p 486.

4. Aleksandrov, A. F., Rukhadze, A. A., "Fizika sil'notochnykh elektrorazryadnykh istochnikov sveta" [Physics of Intense Electric-Discharge Light Sources], Moscow, Atomizdat, 1976.

5. Pukhov, A. M., "Exploding Wire Vapor Shielding of Pulse Discharge XUV Radiation", ZHURNAL PRIKLADNOY SPEKTROSKOPII, Vol 22, 1975, p 922.

6. Zvorykin, V. D., Klementov, A. D., Rozanov, V. B., "Characteristics of Intense Discharge in Neon at High Pressure", KVANTOVAYA ELEKTRONIKA, Vol 4, 1973, p 43.

7. Kozlov, N. P., Leskov, L. V., Protasov, Yu. S., Khvesyuk, V. I., "Experimental Investigation of Plasma Focus in Erosion Plasma Accelerators: I", ZHURNAL TEKHNICHESKOY FIZIKI, Vol 43, 1973, p 730; "II: Energy Characteristics of Dense Plasma Focus", ZHURNAL TEKHNICHESKOY FIZIKI, Vol 44, 1974, p 2519.

8. Kamrukov, A. S., Kashnikov, G. N., Kozlov, N. P. et al., "Feasibility of Making High-Brightness Sources in the Far Ultraviolet Based on Hypersonic Flows of Dense Plasma", PIS'MA V ZHURNAL TEKHNICHESKOY FIZIKI, Vol 2, 1976, p 447.

9. Kozlov, N. P., Leskov, L. V., Protasov, Yu. S. et al., "Measurement of Mach Number in Plasma Jets", TEPLOFIZIKA VYSOKIKH TEMPERATUR, Vol 12, 1974, p 697.

10. Kamrukov, A. S., Kozlov, N. P., Malashchenko, V. A., Protasov, Yu. S., "Experimental Investigation of Plasma Focus in Erosion Plasma Accelerators: III. Radiation Properties of Dense Plasma Focus", ZHURNAL TEKHNICHESKOY FIZIKI, Vol 47, 1977, p 1673.

11. Kvartskhava, I. F., Meladze, R. F., Suladze, K. V., "Experiments on Electrodynamic Plasma Acceleration", ZHURNAL TEKHNICHESKOY FIZIKI, Vol 30, 1960, p 289.

12. Skvortsov, Yu. V., Komel'kov, V. S., Tserevitinov, S. S., "Structure of Magnetic Fields in Plasma Jet With Self-Currents", ZHURNAL TEKHNICHESKOY FIZIKI, Vol 34, 1964, p 965.

13. Grigor'yev, V. N., "Plasmoid Structure in Electrodynamic Accelerator", ZHURNAL PRIKLADNOY MEKHANIKI I TEKHNICHESKOY FIZIKI, Vol 2, 1965, p 35; "'Pinches' Observed in Rail Plasma Accelerators", ZHURNAL PRIKLADNOY MEKHANIKI I TEKHNICHESKOY FIZIKI, Vol 4, 1965, p 146.

14. Osadin, V. A., "Energy Release in Intense Plasma Discharge", ZHURNAL TEKHNICHESKOY FIZIKI, Vol 35, 1965, p 1230; "Problem of Clot Formation in Pulsed Plasma Accelerators", ZHURNAL TEKHNICHESKOY FIZIKI, Vol 35, 1965, p 1327.

15. Derevshchikov, V. A., "Measuring Velocities of Plasma Components by High-Speed Photography in Monochromatic Light", ZHURNAL TEKHNICHESKOY FIZIKI, Vol 37, 1967, p 315.

16. Rushaylo, A. M., "Flow Inhomogeneities in Pulsed Electromagnetic Accelerator", ZHURNAL PRIKLADNOY MEKHANIKI I TEKHNICHESKOY FIZIKI, Vol 4, 1970, p 165.

17. Min'ko, L. Ya., "Polucheniye i issledovaniye impul'snykh plazmennykh potokov" [Producing and Studying Pulsed Plasma Flows], Minsk, Nauka i tekhnika, 1970.

18. Gubarev, V. Ya., Kozlov, N. P., Leskov, L. V. et al., "Experimental Determination of Velocity Characteristics of Pulsed Erosion Accelerator" in: "Plazmennyye uskoriteli" [Plasma Accelerators], Moscow, Mashinostroyeniye, 1973.

19. Aleksandrov, A. F., Zosimov, V. V., Rukhadze, A. A. et al., "Study of Equilibrium and Stability of Self-Compressed Discharges in Optically Dense Plasma", ZHURNAL EKSPERIMENTAL'NOY I TEORETICHESKOY FIZIKI, Vol 64, 1973, p 1568.

20. Kovrov, P. Ye., Morozov, A. I., "Structure of Compression Region in Magnetoplasma Compressor", ZHURNAL TEKHNICHESKOY FIZIKI, Vol 46, 1976, p 2508.

21. Zvorykin V. D., Kashnikov, G. N., Klementov, A. D. et al., "Radiation of Plasma Focus of Magnetoplasma Compressor in Visible and Ultraviolet Regions of the Spectrum", KVANTOVAYA ELEKTRONIKA, Vol 2, 1975, p 2416.

22. Zvorykin, V. D., Kamrukov, A. S., Klementov, A. D. et al., "Investigation of Plasma Focus Emission in the XUV Region by Ionization Chambers", KVANTOVAYA ELEKTRONIKA, Vol 4, 1977, p 290.

23. Zatsepin, Yu. A., Popov, Ye. G., Tsikulin, M. A., "Brightness of Shock Wave Front in Some Gases", ZHURNAL EKSPERIMENTAL'NOY I TEORETICHESKOY FIZIKI, Vol 54, 1968, p 112.

24. Tsikulin, M. A., Popov, Ye. G., "Izluchatel'nyye svoystva udarnykh voln v gazakh" [Radiative Properties of Shock Waves in Gases], Moscow, Nauka, 1977.

25. Model', I. Sh., "Measuring High Temperatures in Intense Shock Waves in Gases", ZHURNAL EKSPERIMENTAL'NOY I TEORETICHESKOY FIZIKI, Vol 32, 1957, p 714.

26. Dubovik, A. S., "Fotograficheskaya registratsiya bystroprotekayushchikh protsessov" [Photographic Recording of High-Speed Processes], Moscow, Nauka, 1967.

27. Basov, N. G., Borovich, B. L., Zuyev, V. S. et al., "Intense Discharge in Gases: I. Experimental Study of Luminosity and Energy Characteristics of Powerful Discharge in Air", ZHURNAL TEKHNICHESKOY FIZIKI, Vol 40, 1970, p 516.

28. Zel'dovidh, Ya. B., Rayzer, Yu. P., "Fizika udarnykh voln i vysokotemperaturnykh gidrodinamicheskikh yavleniy" [Physics of Shock Waves and High-Temperature Hydrodynamic Phenomena], Moscow, Nauka, 1966.

29. Biberman, L. M., Norman, G. E., "Continuous Spectra of Atomic Gases and Plasma", USPEKHI FIZICHESKIKH NAUK, Vol 91, 1967, p 193.

30. Seaton, M. J., "Method of Quantum Defect", MON. NOT. ROY. ASTRON. SOC., Vol 118, 1958, p 504.

31. Norman, G. E., "Substantiating the Quantum Defect Method", OPTIKA I SPEKTROSKOPIYA, Vol 12, 1962, p 333.

32. Burgess, A., Seaton, M. J., "Cross Sections for Photoionization From Valence Electron States", REV. MOD. PHYS., Vol 30, 1958, p 992.

33. Biberman, L. M., Norman, G. E., "Plasma Recombination Emission and Bremsstrahlung", J. QUANT. SPECTROSC. RAD. TRANSFER, Vol 3, 1963, p 221.

34. Biberman, L. M., Norman, G. E., "Calculating Photoionization Absorption", OPTIKA I SPEKTROSKOPIYA, Vol 8, 1960, p 433.

35. Biberman, L. M., Norman, G. E., Ul'yanov, K. N., "Photoionization of Excited Many-Electron Atoms and Ions", ASTRONOMICHESKIY ZHURNAL, Vol 39, 1962, p 107.

36. Norman, G. E., "Free-Free Electron Transitions in Ion Field", OPTIKA I SPEKTROSKOPIYA, Vol 14, 1963, p 521.

37. Norman, G. E., "Photoionization Cross Sections of Lower Excited States, and Oscillator Strengths of Some Lines of Carbon and Nitrogen Atoms", OPTIKA I SPEKTROSKOPIYA, Vol 14, No 5, 1963, p 593.

38. Bondar', V. A., Kiselevskiy, L. I., Trukhan, Ye. P., "Using Pulse Discharge With Restricted Channel Cross Section in Experimental Spectroscopy", ZHURNAL PRIKLADNOY SPEKTROSKOPII, Vol 9, 1968, p 792; Vol 9, 1968, p 928.

39. Ablekov, V. K., Kashnikov, G. N., Kozlov, N. P. et al., "Raschet sostava plotnykh mnogokomponentnykh plazm" [Calculating Composition of Dense

Multicomponent Plasmas] in: "Teplofizicheskiye svoystva nizkotemperaturnoy plazmy" [Thermophysical Properties of Low-Temperature Plasma], Moscow, Nauka, 1976.

40. Kozlov, N. P., Malashchenko, V. A., Protasov, Yu. S., "Interferometry of Dense Plasma Flows", ZHURNAL PRIKLADNOY SPEKTROSKOPII, Vol 22, 1975, p 210.

41. "Sinkhrotronnoye izlucheniye" [Synchrotron Radiation], TRUDY FIZICHESKOGO INSTITUTA IMENI P. N. LEBEDEVA, Moscow, Nauka, Vol 80, 1980.

42. Darwin, H. W., Felenbok, P., "Data for Plasmas in LTE", Paris, 1965.

43. Traving, G., Bachec, B., Holveger, H., "Zur Berechnung von zugtand Summen", Abhandl. Hamburger Sternwarte, 1966.

44. Ingliss, D. R., Teller, E., "Ionic Depression of Series Limits in One-Electron Spectra", ASTROPHYS. J., Vol 90, 1939, p 439.

45. Grim, G., "Spektroskopiya plazmy" [Plasma Spectroscopy], Moscow, Atomizdat, 1969.

46. Zaydel', A. N., Shreyder, Ye. Ya., "Spektroskopiya vakuumnogo ul'trafioleta" [Extreme Ultraviolet Spectroscopy], Moscow, Nauka, 1967.

47. Samson, J. A. R., "Techniques of Vacuum Ultraviolet Spectroscopy", New York, London, 1967.

48. Podmoshenskiy, I. V., Pukhov, A. M., Yakovleva, A. V., "Pulse Continuous-Spectrum Sources Calibrated With Respect to Brightness in the Extreme Ultraviolet", ZHURNAL PRIKLADNOY SPEKTROSKOPII, Vol 16, 1972, p 415.

49. Kartuzhanskiy, A. L., "Violation of Photochemical Reciprocity Law for Photographic Layers", USPEKHI FIZICHESKIKH NAUK, Vol 51, 1953, p 161.

50. Ryabtsev, A. N., Sukhodrev, N. K., "Investigation of Deviations From Reciprocity Law in Photographic Layers in the Extreme Ultraviolet Region of the Spectrum", ZHURNAL NAUCHNOY I PRIKLADNOY FOTOGRAFII I KINEMATOGRAFII, Vol 15, 1970, p 167.

51. Zatsepin, Yu. A., "Investigation of Deviations From Reciprocity Law at Exposure Times of 10^{-5}-10^{-8} s" ZHURNAL NAUCHNOY I PRIKLADNOY FOTOGRAFII I KINEMATOGRAFII, Vol 5, 1960, p 60.

52. Vekhov, A. A., Nikolayev, F. A., Rozanov, V. B., "Photoemission-Scintillation Spectrometer for Studying Plasma Emission in the Extreme Ultraviolet", PRIBORY I TEKHNIKA EKSPERIMENTA, Vol 6, 1974, p 198.

53. Vekhov, A. A., Nikolayev, F. A., Rozanov, V. B., "Investigating Radiation of Intense Pulsed Discharges in Metal Vapor in the Vacuum Ultraviolet", PIS'MA V ZHURNAL EKSPERIMENTAL'NOY I TEORETICHESKOY FIZIKI, Vol 17, 1973, p 750.

54. Vekhov, A. A., Kamrukov, A. S., Kozlov, N. P. et al., "Emission Spectrum of Plasma Focus in 10-350 eV Region", ZHURNAL TEKHNICHESKOY FIZIKI, Vol 3, 1977, p 661.

55. Kozlov, N. P., Protasov, Yu. S., "Radiation Properties of Dense Plasma Focus", TEPLOFIZIKA VYSOKIKH TEMPERATUR, Vol 10, 1972, p 1319.

56. Kamrukov, A. S., Kozlov, N. P., Protasov, Yu. S., "Emission Spectrum of Plasma Focus in Quantum Energy Region of 0.64-350 eV", DOKLADY AKADEMII NAUK SSSR, Vol 237, 1977, p 1334.

6610
CSO: 1862/183

- END -